Large-scale characterization of exposure to downlink radiofrequencies

Yanis Boussad

UNIVERSITÉ CÔTE D'AZUR

ÉCOLE DOCTORALE
SCIENCES ET TECHNOLOGIES DE L'INFORMATION ET DE LA COMMUNICATION

THÈSE DE DOCTORAT

Caractérisation à grande échelle de l'exposition aux ondes radiofréquences descendantes

Yanis BOUSSAD

Inria

Présentée en vue de l'obtention du grade de docteur en Informatique **d'**Université Côte d'Azur
Dirigée par : Arnaud Legout
Co-encadrée par : Leonardo Lizzi
Soutenue le : 30/09/2021

Devant le jury, composé de :
Jean-Yves Dauvignac, Professeur, LEAT,
Navid Nikaein, Professeur, Eurecom
Shyam Gollakota, Professeur, Université de Washington
Joe Wiart, Professeur, Telecom ParisTech
Arnaud Legout, Directeur de recherche, Inria,
Leonardo Lizzi, Professeur, LEAT, CNRS

Inria

LEAT
LABORATOIRE D'ELECTRONIQUE ANTENNES ET TELECOMMUNICATIONS

Caractérisation à grande échelle de l'exposition aux ondes radiofréquences descendantes

Jury:

Président du jury:
Jean-Yves Dauvignac, Professeur, LEAT, Université Côte d'Azur.

Rapporteurs:
Navid Nikaein, Professeur, Eurecom
Shyam Gollakota, Professeur, Université de Washington

Examinateur:
Joe Wiart, Professeur, Telecom ParisTech

Directeur de thèse:
Arnaud Legout, Directeur de recherche, Inria, Université Côte d'Azur
Co-encadrant:
Leonardo Lizzi, Professeur, LEAT, CNRS, Université Côte d'Azur

Résumé

La prolifération des technologies sans fil ces deux dernières décennies, telles que le cellulaire, le Wi-Fi et le Bluetooth, a engendré une utilisation intensive des ondes radiofréquences. Cela a causé beaucoup d'inquiétudes concernant l'exposition des gens à ces ondes. En 2011, le Centre International de Recherche sur le Cancer (CIRC), un organisme de l'Organisation Mondiale de la Santé (OMS), a classé les ondes radiofréquences comme "possiblement" cancérogènes pour l'homme (Groupe 2B). Cette classification signifie qu'« il existe des études montrant que ces radiations peuvent provoquer un cancer chez l'homme mais qu'à l'heure actuelle, c'est loin d'être concluant". Une façon de répondre à cette question est de mener des études épidémiologiques scientifiquement solides. Cependant, toutes les études sont confrontées à la difficulté d'évaluer avec précision l'exposition de la population à ces ondes radiofréquences. L'étude de l'exposition de la population aux ondes radiofréquence est extrêmement difficile, nécessitant beaucoup de données sur une large population, et sur une longue période de temps.

Parallèlement aux progrès des technologies sans fil, les smartphones ont évolué pour devenir des appareils riches en fonctionnalités à des prix très abordables, capables de mesurer les ondes radiofréquences. Ils embarquent divers capteurs et antennes. Cela les rend d'une très grande utilité pour les chercheurs et un candidat parfait pour les mesures crowdsource.

La première contribution de cette thèse est d'évaluer la précision des smartphones pour effectuer des mesures de puissance des ondes radiofréquences. Nous évaluons d'une manière approfondie la précision des mesures de puissance du signal (RSSI) faites par un smartphone. Nous étudions l'impact de l'orientation du smartphone dans l'espace par rapport à la source sur la puissance reçue dans un réseau LTE. On fait des mesures à la fois dans un environnement contrôlé (chambre anéchoïque) ainsi qu'à l'extérieur. Nous montrons que l'orientation peut affecter la précision des mesures du smartphone, et nous proposons une technique de calibration pour améliorer la précision. Nous montrons également qu'à l'extérieur, la réflexion des ondes dans l'environnement et l'utilisation de la diversification de polarisations dans les antennes de transmission peuvent aider à réduire l'impact de l'orientation. Nous étendons l'étude à la technologie Bluetooth. Nous montrons que les mesures de puissance RSSI du Bluetooth sont aussi sensibles à l'orientation du smartphone même dans des environnements réalistes.

Dans la deuxième contribution de cette thèse, nous présentons la plus grande étude basée sur le crowdsourcing de l'exposition de la population aux ondes radiofréquences descendantes produites par les antennes cellulaires, les points d'accès Wi-Fi et les appareils Bluetooth. Notre étude comprend 254410 utilisateurs uniques dans 13 pays, de janvier 2017 jusqu'à décembre 2020. Nous montrons que le niveau d'exposition descendante totale a doublé au cours de la période des quatre années que nous considérons, le Wi-Fi étant de loin le plus gros contributeur. Cependant, les niveaux d'exposition descendante

actuels sont largement inférieurs aux limites définies par les autorités de régulation. La population a tendance à être plus exposée à la maison. Les équipements personnels tels que les points d'accès Wi-Fi et les appareils Bluetooth contribuent autant à l'exposition personnelle que toute autre source. Nous rendons publique l'ensemble des données que nous avons utilisées dans cette étude. Nous prévoyons que nos travaux seront un point de départ pour des études épidémiologiques solides sur l'impact des radiofréquences sur la santé. Nous pensons également que notre ensemble de données unique sera inestimable pour plusieurs autres domaines intéressés par l'usage des technologies de communication sans fil par la population.

Mots clés: ondes, radiation, exposition, technologies sans-fil, grande-échelle, big data, crowdsource, smartphone, RSSI, calibration, mesures.

Abstract

The last two decades have witnessed an extensive usage of radiofrequencies due to the proliferation of wireless technologies, such as cellular, Wi-Fi, and Bluetooth. This caused a lot of concerns regarding the exposure to these radiations. In 2011, the International Agency for Research on Cancer (IARC) categorized the radiofrequency radiations as “possibly” carcinogenic to humans (Group 2B). This classification means that "There is some evidence that it can cause cancer in humans but at present, it is far from conclusive". One way to answer this question is by performing scientifically sound epidemiological studies. However, all studies face the difficulty to accurately assess the population exposure to these radiations. Studying the population exposure to radiofrequency radiations is extremely challenging, requiring extensive measurements data from a large population, over a long period of time.

In tandem with the advancement in wireless technologies, smartphones have evolved to become feature-rich, affordable devices, capable of measuring radio-frequency radiations. They embed various sensors and antennas. This makes them very attractive for researchers and a perfect candidate for crowd-based measurements.

The first contribution of this thesis is to assess the accuracy of smartphones to perform radio-frequency measurements. We make an extensive evaluation of the accuracy of smartphone measurements of the wireless signal strength (RSSI). We evaluate the impact of smartphone orientation in space with respect to the source on the received power in an LTE network. We perform measurements both in controlled and outdoor environments. We show that the orientation can affect the accuracy of the smartphone measurements, and we propose a calibration technique to improve the accuracy. We also show that outdoor, multi-path and polarization diversity can help reduce the effect of orientation. We extend the study to Bluetooth technology. We show that Bluetooth RSSI measurements are sensitive to smartphone orientation even in realistic environments.

In the second contribution of this thesis, we report the largest crowd-based measurement of the population exposure to downlink radio frequencies produced by cellular antennas, Wi-Fi access points, and Bluetooth devices for 254,410 unique users in 13 countries from January 2017 to December 2020. We show that the overall downlink exposure level has doubled in the four years period we consider, Wi-Fi being by far the largest contributor. However, the downlink exposure levels are orders of magnitude lower than the regulation limits. The population tends to be more exposed at home, and their personal Wi-Fi access point and Bluetooth devices contribute as much to their exposure as any other source. We publicly open the dataset we used in this study. We anticipate our work to be a starting point for sound epidemiological studies on the impact of radio frequencies on health. We also believe that our unique dataset will be invaluable for several other fields interested in the usage of wireless communication technologies, and how the population is exposed to either radio frequencies or technologies.

Keywords: radiation, downlink exposure, wireless technologies, large-scale, big data, crowd-source, smartphone, RSSI, calibration, measurement.

Acknowledgment

First of all, I would like to express my gratitude to my thesis supervisors Arnaud Legout and Leonardo Lizzi for their support, help, and guidance throughout this journey. I would like to thank Augustin Chaintreau and Xi Chen for accepting to collaborate with us, and for their contributions to this work.

I would like to thank the jury members: Jean-Yves Dauvignac, Joe Wiart, Navid Nikaein, and Shyam Gollakota. A special thank to Jean-Yves Dauvignac and Shyam Gollakota for being part of my PhD committee not once, but twice.

During my PhD, I was lucky to be part of three amazing teams. I would like to thank the Electrosmart members: Mondi Ravi, David Migliacci, Abdelhakim Akodadi, and all the interns. I would like to thank all DIANA team members, especially: Naoufal Mahfoudi who gave me invaluable support and advice at the start of my PhD; Walid Dabbous who always answered present to discuss and provide feedback; Christine Foggia for her kindness and help in providing administrative support. Also, I would like to thank CMA team members at LEAT, especially Fabien Ferrero, and Laurent Brochier.

I would like to express my gratitude to those who helped me get to where I am today: Dalila Cherifi and Rachid Deriche, thank you for giving me the opportunity to come to study in France. Lyes Khacef for welcoming me to the beautiful *Côte d'Azur* and helping me to settle in. Also, I would like to thank Ali Beikbaghban, Konstanze Beck, Magali Martin for their support in administrative procedures since my arrival to France.

The pandemic was a difficult time for everyone. Being far from loved ones was not easy. I would like to thank everyone who was by my side in those difficult moments. Arnaud Legout in our nearly-daily meetings, and Tareq Si Salem with his periodical phone calls, thank you. This may seem odd, but I would like to thank Chelsea Football Club for those joyful moments after winning the Champions League.

Last but not least, I would like to express my deepest gratitude to my family: my mother Cherifa and my father Mohamed, my sisters and my brothers, my nieces and my nephews. Since my young age, you did your best to provide the necessary conditions for me to focus on my studies to succeed. Here I am today dedicating this achievement to you. Thank you all for your love and your support. *Tanemirt atas atas*! A very special thank to a very special person who gave me courage and support during difficult moments. A person who has always been there through my ups and downs, thank you Sára. Also, I would like to thank my friends from the Ubinet Masters, in addition to Youva Nait Belaid, Messaoud Haddad, and Faycal Aggoune.

Funding

This research work is supported by the French government, through the UCAJEDI Investments in the Future project managed by the National Research Agency (ANR) with the reference number ANR-15-IDEX-01.

...To my Parents

Contents

List of Figures

List of Tables

Introduction 1

1.1 Context

We are constantly exposed to different types of electromagnetic radiations. These radiations can be naturally occurring, such as the visible light, the heat produced by our bodies, and ultraviolet radiations from the sun. Others can be human-made radiations such as the ones used in wireless telecommunication, radio, and television broadcast.

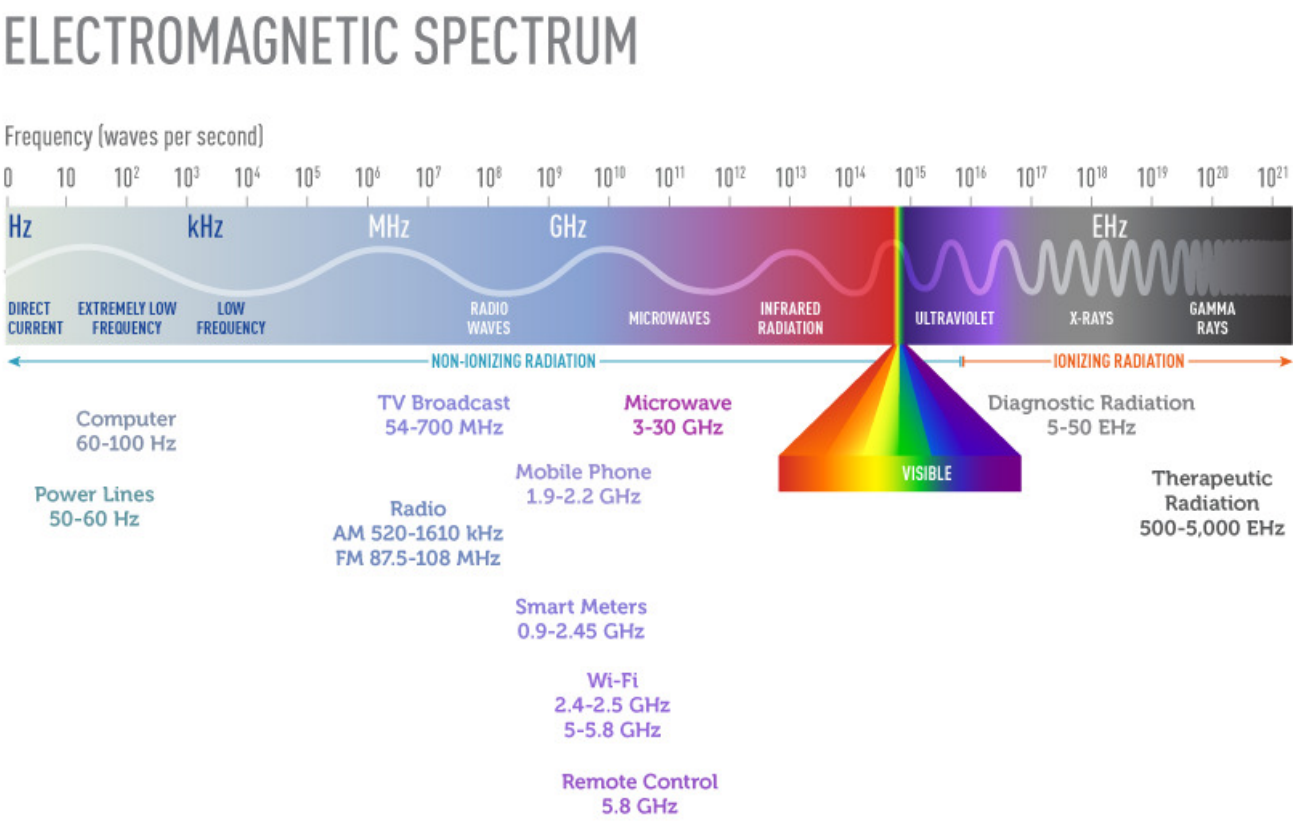

Figure 1.1: The electromagnetic spectrum. Source: NCI [1]

An electromagnetic radiation is a combination of an electric and magnetic fields oscillating through a medium and carrying energy [2]. The number of oscillations per second is called the frequency measured in hertz(Hz), and the energy it carries is defined in Watt (W) [2,

3]. Depending on the amount on energy it carries, the electromagnetic radiation can be considered as ionizing or non-ionizing radiations.

An ionizing radiation is an electromagnetic radiation that carries enough energy to ionize atoms and break chemical bounds. These radiation are proven to cause serious health hazard to humans as they can damage the DNA [4] which can result in cancer. Ionizing radiations can be fatal if a person is exposed to a certain amount. Typical ionizing radiation include nuclear radiations (alpha and gamma particles), and X-rays.

As opposed to ionizing radiations, non-ionizing radiations do not carry enough energy to break chemical bonds [5]. Non-ionizing radiations include radio-frequencies, microwaves, infrared radiation, and ultraviolet radiation.

The last two decades have witnessed a huge technological advancement, and a proliferation of various wireless telecommunication technologies, such as cellular networks, Wi-Fi, and Bluetooth: i) The number of mobile subscribers has increased exponentially, reaching an average of 75% of the world population in 2020, and 125% in developed countries. ii) People have more access to the internet, with 72% households in urban areas have internet, resulting in more than 85% of the population in developed countries use the internet [6]. iii) Different types of electronic devices started to emerge. Smartphones and Internet of Things (IoT) are becoming omnipresent. In 2019, there were more than 5 billion mobile phones worldwide [7]. The global IoT devices is expected to reach 25 billion by 2025, compared to 12 billion in 2019 [8]. All these wireless technologies, and wireless devices use the non-ionizing part of the frequency spectrum.

The amazing proliferation of wireless technologies, the deployment of newer ones (such as the 5G), and the extensive usage of wireless devices is raising public and scientific concerns regarding the effect of the non-ionizing radiations on health. As opposed to the ionizing radiations, there is no conclusive scientific evidence regarding the effect of non-ionizing radiations on health. However, in 2011, the World Health Organization considered these radiations as possibly carcinogenic to humans, and called for more scientific research in monitoring the population exposure levels, and assessing the impact of these radiations on human health at short, medium, and long terms [9]. The International Commission of Non-Ionizing Radiation Protection (ICNIRP) set guidelines to limit the population exposure to radiations in the 100 kHz to 300 GHz frequency range [3].

Radiofrequency Electromagnetic Fields (RF-EMF) is the part of the electromagnetic spectrum comprising the frequency range from 100 kHz to 300 GHz [3]. RF-EMF have shown to cause adverse biological and health effects that we describe in the following. The electric field of the RF-EMF is the main component that affects the body. The energy from the electric field can excite the biological molecules and transforms into kinetic energy, which in-turn results in heating effect. The current exposure guidelines of the ICNIRP are set with respect to the threshold that can cause heating effect. This threshold is then divided by a given factor as a precautionary measure to ensure "safe" exposure limit [3].

Other than heating effect, there are adverse health effect of the RF-EMF exposure. Typical health effects investigated in the literature include: Nerve stimulation, which is described as tingling feeling [10]. Biological cells permeability can be affected, which in turn, can cause other cellular changes [10, 11]. Possible impact on the cognitive performances and central nervous system [12–14], auditory [15] functions, neuroendoctrine system and hormone levels [16–18], neurodegenerative disease [19–25], cardiovascular system [18, 25–28], fertility [29–33] and childhood development [34–36], and cancer [37–39]. However, these studies remain inconclusive, and fail to give substantial scientific evidence [3], Moreover, there is no evidence that continuous and pulsed RF-EMF can affect human health differently [40, 41].

1.2 Motivation and goal of the thesis

The current understanding of the impact of RF-EMF radiations on health is limited. The current regulation guidelines by ICNIRP are *"based on the best science currently available and there may be limitations to this knowledge that could have implications for the exposure restrictions [...] Accordingly, the guidelines will be periodically revised and updated as advances are made in the relevant scientific knowledge."* [3].

Because the impact of the RF-EMF radiations on health is not yet completely understood, continuous monitoring of the population exposure to the RF-EMF radiations remains important to advance the scientific knowledge. Especially with the exponential and invasive usage of wireless devices and telecommunication technologies in the recent years, in addition to the deployment of newer wireless technologies such as the 5G [42].

Epidemiology is a branch of medical sciences that investigates the root causes of diseases and health issues in the population, where the whole population is considered the patient, rather than individuals. It uses data-driven approach to investigate the factors and causes of health risks in the population [43, 44]. Conducting epidemiological studies on the population exposure to RF-EMF radiations will help build better understanding of the health risks of such radiations. However, these studies require more data with better quality about population exposure [45]. To provide such data, multiple scientific projects aimed at evaluating and assessing the population exposure to the RF-EMF radiations, and their impact on health. Major European projects such as EMF-NET [46], Interphone [47], and GERoNiMO [48] studied the population exposure to RF-EMF. To facilitate the exposure assessment, and data collection, the European project COMOS [49] proposed the usage of a mobile application called XMobisense [50], rather than relying on self-reported data, and questionnaires. The usage of such mobile application reduces the subjective bias of the assessment that can be present in the self-reported data, and allows collecting epidemiological data faster, easier, and with better quality.

Studies performed so far to assess the population exposure to RF-EMF radiations are limited in space, population size, and time span [51]. The goal of this thesis is to fill this gap by providing exposure assessment at population scale in 13 countries to RF-EMF radiations used in wireless telecommunication technologies (Cellular, Wi-Fi, and Bluetooth), using crowd-sourced data collected from more than 250000 people for a period of 4 years, from January 2017 to December 2020.

1.3 Outline and Contribution

This manuscript is organized as follows. In Chapter 2 we make an overview of the literature of the RF-EMF exposure, the methods and the tools used to evaluate the radiation levels from wireless sources. In Chapter 3, we present the hardware and software architecture of modern smartphones. We give a short description of the wireless technologies, and provide a low-level explanation on how smartphones can measure the signal power from the wireless sources. In Chapter 4, we evaluate the performance of smartphone to measure wireless signal strength. We make a measurement setup based on open-source software (OpenAirInterface). We evaluate the accuracy

of LTE signal strength measurement both in controlled environment, and outdoor. We show that the smartphone orientation has an impact on the measurement accuracy, especially in reflectionless environment with mono-polarized signal. We propose a calibration technique to compensate for the inaccuracy due to orientation by making use of the smartphone sensors. We obtained similar results for Bluetooth, suggesting the replicability of our approach to other wireless technologies. In Chapter 5, to the best of our knowledge, we propose the largest study to evaluate the population exposure to the RF-EMF radiations used in cellular networks, Wi-Fi access points, and Bluetooth devices. Our study covers 13 countries in the world, spanning through the last 4 years (January 2017 to December 2020). We rely on crowd-sourced measurements collected using Electrosmart mobile application [52] collected from 254,410 unique persons. We show that total exposure has been multiplied by 2.3 in the four-year period considered, with Wi-Fi as the largest contributor. The cellular exposure levels are orders of magnitude lower than the regulation limits and not significantly impacted by national regulation policies. We show that people are more exposed to Wi-Fi at home; personal Wi-Fi routers and Bluetooth devices contributed to more than 50% of their total exposure of the majority of the study subjects. We make our dataset publicly available to provide a starting point for sound epidemiological studies on the health impacts of radio frequencies. We also believe that our unique dataset will be invaluable for several other fields interested in population exposure to radio frequencies or the usage of wireless communication technologies. We conclude this thesis in Chapter 6.

In this thesis, we will only consider the downlink exposure, i.e. radiation power sent towards the smartphone, and not the power transmitted by the smartphone. This includes Wi-Fi access points radiations, mobile cellular towers, and any discoverable Bluetooth device. When presenting our results, we will use the term exposure as a general term to denote the downlink exposure.

State of the art 2

In this chapter, we present the current state of the art in terms of assessing the exposure levels and the tools used for measurements, with a focus on smartphones.

2.1 Population exposure to radio-frequency electromagnetic radiations

The study of the exposure to the RF-EMF radiations can be split into two main categories. Near-field exposure and far-field exposure. Wireless sources that operate very close to the human body, such as mobile phones, are considered near-field exposure sources. Exposure to radiations from sources that operate far from the human body such as Wi-Fi routers and cellular towers is considered far-field exposure.

RF-EMF exposure can be near-field exposure when the source is very close to the human body. Otherwise, it's called far-field exposure

The far-field starts at a distance of $2fD^2/c$ from the source, where D is the largest dimension of the emitting antenna, c is the speed of light, and f is the signal frequency. Typical frequencies used by different wireless technologies are shown in Table 2.1. In contrast to the far-field exposure, for near-field exposure, the electric and magnetic fields are not uniform [53]. Hence, measuring the electric field is not enough to assess the exposure level.

Different metrics for exposure assessments are used for near-field and far-field exposure. For the near-field exposure, the Specific Absorption Rate (SAR) is used. SAR represents the rate of the energy absorbed per unit mass of biological tissue, expressed in W/kg. For the far-field exposure, the electric field intensity (V/m) is usually used, in addition to power density expressed in W/m^2. The power of the radiation (received power), expressed in dBm or Watt, can also be used as an exposure metric. SAR and electric field intensity can

	Frequency band (MHz)
GSM (2G)	800 / 900 / 1800 / 1900
UMTS (3G)	800 / 900 / 1800 / 1900 / 2100
LTE (4G)	800 / 900 / 1800 / 1900 / 2100 / 2600
Wi-Fi	2400 / 5000
Bluetooth	2400

Table 2.1: Main frequency bands used by the different wireless technologies.

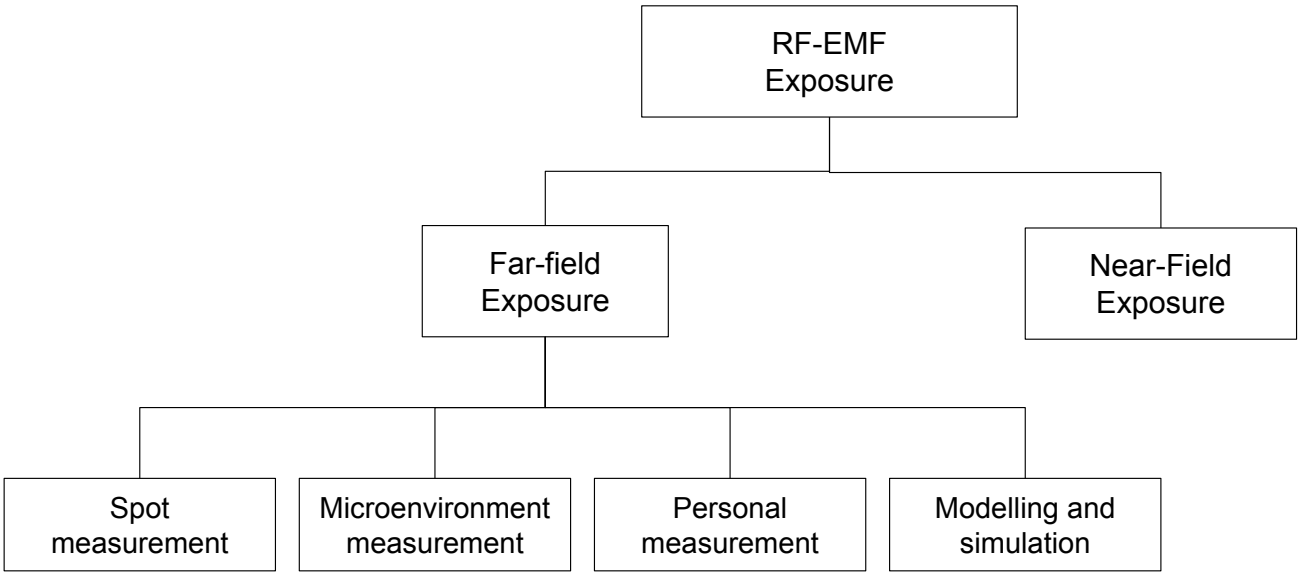

Figure 2.1: RF-EMF exposure assessment. Exposure can be either: 1) near-field exposure which can be assessed through dosimetry techniques and simulations, or 2) far-field exposure which deals with distant sources far from the human body. Assessing far-field exposure can be done using different approaches, such as spot measurements, comparing different microenvironments, personal measurements, or through mathematical models and simulations.

be estimated from the power of the radiations [54, 55]. In Section 5.2, we will show how to estimate the electric field intensity from the radiation power.

In this thesis, we only focus on the far-field exposure, which is usually an involuntary exposure, mostly from sources that are out of the control of the person, such as cellular antennas. As opposed to near-field exposure, which is mainly caused by the person's own devices such as smartphones and wireless earbuds. We keep the power of the radiation (received power) as the main metric for the assessment of exposure levels.

2.1.1 Exposure assessments approaches

To evaluate the exposure levels to the RF-EMF radiations, researchers can rely on different approaches. Here we discuss the main ones.

- **Spot measurements:** In this type of studies [56–58], a given spot (that is a specific location) is monitored for a given duration. It is usually done by placing measurement probes such as spectrum analyzers and collect measurements about the surrounding sources of that spot. This type of measurement is performed usually in specific and sensitive places such as schools, kindergartens, residential areas, or places where the

exposure level is suspected to be close to the regulation limits, typically near cellular base stations. This type of studies is conducted by a qualified technician. The disadvantage of this type of measurement is that it is very limited in space, and it does not offer a good representation of the exposure of individuals as it fails to capture its spatio-temporal characteristics, and setting many probes is expensive and hard to maintain.

- **Microenvironment measurements:** In microenvironmental studies [59–64], researchers compare exposure levels at different types of environments. For instance, compare exposure levels in urban areas compared to rural, offices/homes, indoor/outdoor. The measurements are carried out by the researchers using specialized equipment. The measurement can be taken while standing still, or while walking around in a given environment. The measurement campaign is usually short in time and maybe be performed multiple times to capture more temporal trends (day and night for example). Again, this measurement approach does not capture the exposure level experienced by individuals, as these measurements are limited in space and time, and cannot cover all possible environments of the population.
- **Personal measurements:** This is the approach that gives the closest representation of the exposure to RF-EMF as experienced by the individuals. It is intended to track and monitor the exposure of a person for a continuous period of time in their own environments. In contrast to the two previous approaches, the personal measurement studies [56, 63, 65–69] are directly performed by the individuals. Participants in this type of studies are usually recruited volunteers, and provided with specialized equipment such as personal exposimeters. Once recruited, the participants are given instructions on how to use the equipment along with additional instructions related to the measurement protocol. The participants need to keep wearing the exposimeters on their bodies while they perform their daily tasks. As shown in Table 2.2, the duration of the measurements is usually very short in time, usually 24 hours up to a few days. Even though this approach gives a better representation of the personal exposure, it mostly suffers from a small population size, high costs to equip many peoples with exposimeters, and the relatively short period of measurements makes it hard to assess the effect of exposure on individuals at the long term.
- **Modelling and simulations:** Another approach to study the exposure of the population to RF-EMF radiations is through

Table 2.2: Non-exhaustive comparison of personal measurements studies. Most personal measurement studies are limited in time, population size, and geographical coverage.

Study	Publication year	Time	Population	Place
Zeleke et al. [65]	2018	24 hours	63	Melbourne, Australia
Birks et al. [68]	2018	3 days	529	5 European countries
Gallastegi et al. [56]	2018	3 days	104	Spain
Bhatt et al. [67]	2018	2 months	10	Melbourne, Australia
Ramirez-Vazquez et al. [66]	2019	24 hours	75	Albacete, Spain
Lahham and Ayyad [69]	2019	24 hours	24	West Bank, Palestine
Ramirez-Vazquez et al. [63]	2021	24 hours	63	San Luis Potosi, Mexico

propagation models and simulations [57, 70–72]. This approach estimates the exposure in a geographical area from the position of the fixed radiating sources such as cellular base stations. It uses mathematical models of signal propagation, and the characteristics of the environments, and builds an exposure map using ray-tracing techniques. This approach is suitable for fast estimation of the exposure of large geographical area, at low cost compared to performing real measurements on the field. Simulation-based exposure does not account for the mobile and private sources of exposure such as mobile Wi-Fi access points, Bluetooth devices, and Smart Watches. Other surrogate models have been developed to describe the exposure levels of the population. LEXNET project proposed an exposure metric called Exposure Index (EI) [71]. This metric intends to provide a unique, aggregated value that represents the exposure of a person from both near-field and far-field sources. It represents the average dose per day a person is experiencing in a given geographical area, from a given set of networks, over a period of time. Again, such models are based on assumptions, and cannot capture the heterogeneity and variability of the exposure, and the movement of sources and individuals in space.

Researchers may rely on more than one method, depending on the study context and goals.

2.1.2 Studies on population exposure to RF-EMF radiations

Studies on population exposure to the RF-EMF radiations have covered different aspects. Microenvironment studies showed that the exposure levels differ across different types of environments [59–64]. The exposure is higher in urban areas [59, 68], and exposure

level is directly correlated to population density [60]. Researchers also found that the exposure tends to be higher in downtown areas compared to residential areas [61]. The exposure levels outdoor is mainly caused by cellular radiation from the base stations [59–61, 73]. The exposure to cellular base stations has increased over time [61].

Other studies [60, 61] assessed the effect of legislation on the levels of exposure. Velghe et al. [60] found that stronger legislation in Brussels resulted in lower exposure to base stations. Urbinello et al. [61] studied whether a decrease in the regulation limit could result in a higher cell density, thus a higher exposure. They found that lowering the regulatory limits didn't result in higher exposure levels from base stations. Hence, no counter-intuitive effect of lowering the regulatory limit.

Temporal aspects were also studied. A comparison between day and night [60, 63, 66] or weekdays and weekends [63–65]. The exposure is higher at night [60] and during weekdays [64]. Other studies such as [62] followed the temporal trends of exposure. Urbinello et al. [62] took measurements once each month for one year in 3 European cities. The measurements took place in the daytime during weekdays. Then, linear regression is used to evaluate the trends. They showed that the exposure to base stations has increased with time in the period of 3 years.

Personal exposure studies [56, 63, 65–69] focused on exposure levels of persons. Zeleke et al. [65] studied the exposure levels of 63 Australian adults during 24 hours without constraining them to microenvironments. Some of the participants took measurements during a weekday, others during weekend, but no participant is tracked for the whole week. They found that downlink and Wi-Fi is dominant and exposure levels are lower during weekends. Ramirez-Vazquez et al. [66] studied the exposure levels of 75 volunteers in Albacete, Spain, for 24 hours for each person. The whole study took 4 years from 2010 to 2014. The authors found that people were more exposed during weekdays than weekends, and more during the day than night. However, all participant exposure were below regulatory limits. In this study, no person is tracked for more than 24 hours, which is not enough to capture the spatio-temporal characteristics of the exposure of individuals in the long term. Bhatt et al. [64] studied the environmental and personal exposure of 10 children to RF-EMF in 20 kindergartens in Australia. They found that cellular exposure is dominant and that their personal exposure is lower than the environmental exposure levels. Birks et al. [68] studied the exposure levels of 529 children from Denmark, the Netherlands, Slovenia, Switzerland, and Spain. They found that children are more exposed

to cellular from the base stations than to Wi-Fi. They found that urbanity is the most determinant of the exposure. Similar results were found by Gallastegi et al. [56] when they studied the exposure to RF-EMF of 104 individuals from Spain, during 3 days. Ramirez-Vazquez et al. [63] monitored the exposure levels to Wi-Fi for 63 volunteers in Mexico, during 24 hours. The whole study took place from 2017 to 2018. They showed that people are more exposed to 2GHz Wi-Fi than 5GHz Wi-Fi, and people experience more exposure in workplaces than at home. In 2019, Lahham and Ayyad [69] studied the personal exposure of 24 adult students in Palestine, for 24 hours. They found that the main contributor to the exposure is from the 2GHz Wi-Fi by 45%, and Wi-Fi exposure at home is higher than exposure levels while traveling or at university.

All of the studies, regardless of their approach in assessing the exposure levels of the population to the RF-EMF radiations, all showed that the exposure levels are below the recommended regulatory limits. However, the contribution of the various technologies to the exposure levels differ across studies. Some studies found that cellular downlink is the main source of exposure [56, 64–66, 68]. However, other studies considered Wi-Fi as the main contributor [69, 74], and that 2GHz Wi-Fi is more exposing than 5GHz Wi-Fi[63]. Gajšek et al. [75] suggested that indoor RF exposure is increasing faster than outdoor exposure because of the wide spreading of home wireless devices and short-range communication systems.

All the studies were limited in terms of population coverage, ranging from few individuals [63–67, 69] to a few hundred volunteers [56, 68]. But also limited in time which doesn't allow capturing any temporal trends [51].

2.1.3 Influence of the human body on measurements

The assessment of the RF-EMF exposure can be affected by different sources of biases and uncertainties. This can lead to either an overestimation or an underestimation of the real exposure. This can be caused by measurement artifacts due to hardware or software filters on the measurement tool, or the anisotropy nature of its antennas. In addition to the human body effect [76].

The human body can affect the RF exposure measurement in different ways. It can cause an underestimation if the the human body is between the source and the measurement tool (shadowing effect), or cause an overestimation by reflecting more radiation towards the measurement tool when the latter is in direct line of sight with the

source. This effect can vary depending on the frequency and the polarization of the radiation [76].

Different works have assessed the effect of human body and proposed correcting factors to account for the shadowing effect. This factor can range between 1 to 1.6 [77, 78].

In real life scenarios, it is difficult to compensate the effect of the human body with a single correcting factor as this effect can vary depending on the relative position of the measurement tool with respect to the body. The shadowing effect is stronger in outdoor environment compared to indoor where the measurement tool may not be worn on the body, in addition to the indoor reflections that can compensate for the body shielding effect [76, 79].

In this work, we will not consider the human body effect due to the complexity of accurately compensating for its effect on the measurements.

2.2 Measurement tools for wireless radiations

In this section we discuss the different tools used to measure the signal power (radiation) from wireless sources.

2.2.1 Commodity hardware for wireless power measurements

Previous works explored the possibility to perform measurements of the received power with commodity hardware. Tan et al. proposed *Snoopy* [80], a spectrum analyzer that uses commodity Wi-Fi cards with frequency translators in order to sense a wide range of frequencies. The Wi-Fi card normally scans only at 2.4 GHz and 5 GHz. To extend this range and to scan a wider spectrum, Snoopy uses a radiofrequency translator that senses and translates the signals to adapt them to the frequency supported by the Wi-Fi card. Another work that aimed at using a commodity smartphone as a spectrum analyzer is presented by Ana et al. [81]. They make use of a portable Software Defined Radio (RTL-SDR) dongle that senses a continuous spectrum range from 52 MHz to 2200 MHz, which they connect to a smartphone through USB. The dongle is the spectrum analyzer. The smartphone only processes the data from the dongle. In contrast to the two aforementioned works that rely on external hardware,

CrowdREM [82] relies only on smartphones for spectrum analysis. The authors used an open-source mobile phone (OpenMoko [83]) on which they installed a modified Linux system and replaced the whole baseband system by OsmocomBB [84], an open-source GSM baseband implementation.

2.2.2 Impact of orientation on RSSI measurement

In CrowdREM [82], the authors showed that smartphone accuracy is within 3 dBm while the device is still, however it is very sensitive to the orientation with respect to the source, a difference of up to 10 dB difference. Li et al. [85] showed that RSSI from COTS RFID tags can vary by more than 15 dB across different orientations. Pasku et al. [86] investigated the effect of antenna directivity and receiver orientation on the RSSI in the 2.4 GHz band for RF ranging applications. They showed that the RSSI from a mobile system containing 4 ZigBee nodes has a 5 dB variability at different angles along the azimuth. They proposed an algorithm to obtain a single calibrated RSSI of the mobile system by averaging the individual RSSIs from the 4 nodes. In this way, the authors reduced the RSSI variability to 2 dB.

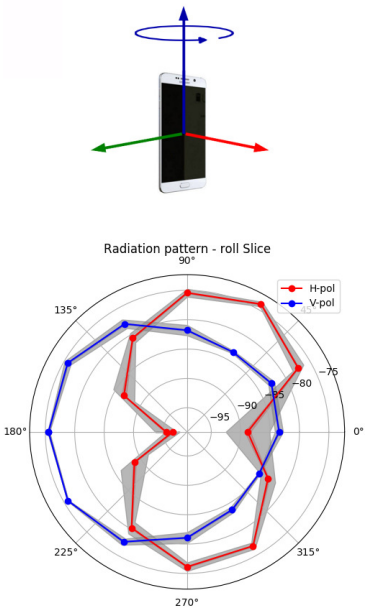

Figure 2.2: The effect of orientation on the signal strength measurements. Rotating an LG 5X in a controlled environment yields different measurements depending on the angle with respect to the source and on the polarization of the signal.

2.2.3 Mobile application on smartphone

Smartphone-based measurements using a mobile application are used in many research contexts.

Smartphones have been used for network measurements and analysis. Vallina-Rodriguez et al. [87] developed a mobile application run on Android devices to monitor the network performance using low-level radio information. They used the Radio Interface Layer (RIL) to access radio message exchange between the Android OS and the baseband chip. Their solution works only on Android devices with Intel Infineon XGold chip and requires root-privileges (software modification on the Android OS). Another tool for network measurements and analysis is called MobileInsight [88]. This tool runs on Commercial Off The Shelf (COTS) smartphones to collect wireless power measurements and low-level network information. Companies such as OpenSignal [89] or Tutela [90] use crowd-based cellular measurements with smartphones to evaluate the coverage of the cellular network.

Smartphones have also been used as an instrument for assessing personal exposure to RF-EMF radiations. XMobiSens [50] is an

Android mobile application used to collect statistics on the usage of mobile phones. It collects information about the phone usage time, how many phone calls, the amount of data exchanged with the network, and the side of the head where the phone is put during calls. These information are then used to investigate the health effects of exposure to radiation depending on phone usage.

XMobiSensPlus [91] is an updated version of the XMobiSens [50] application. XMobiSensPlus collects information about the phone state if there is an ongoing call, Wi-Fi and mobile data status, the received power levels from the wireless sources, GPS coordinates, the device orientation in space to determine the position of the phone with respect to the human body. Electrosmart [52] is another Android application that aims at measuring the exposure from wireless telecommunication technologies. It measures the emitted power from cellular base stations, Wi-Fi routers, and Bluetooth devices, in addition to the GPS coordinates, device orientation in space, smartphone model and brand, and optionally, the contact information of the person and the incentive of using the application (curiosity, electrosensitive, fear of RF-EMF). These information are valuable for epidemiological studies. Electrosmart runs on COTS Android smartphones. It uses standards Android APIs (no software modification), and does not require external hardware. This makes the application easily accessible. The Electrosmart application is used by hundreds of thousands of users worldwide. We will cover more in detail the Electrosmart application in Chapter 5

Figure 2.3: Electrosmart mobile application.

Quanta Monitor [92] and Tawkon [93] are two other Android mobile applications that estimate the near-field exposure levels (SAR) from the emitted radiation from the smartphone. These two applications run only on specific Android devices and require software modification (rooted device) in order to read the transmitted power of the device.

2.2.4 Exposimeters

Exposimeter are specialized mobile, hardware equipments for measuring the RF-EMF radiations. They are designed to facilitate the study of personal exposure to the RF-EMF. They cover a wide range of frequencies from the most popular wireless technologies. Exposimeters use tri-axial prob antennas to account for all possible polarizations of the signal. They may include GPS sensor. Typical exposimeters found in the literature are the EME Spy [94] and ExpoM-RF [95].

Figure 2.4: EME SPY 200 exposimeter.

Table 2.3: Comparing measurement tools. RF-EMF exposure can be due to downlink (DL) radiations, or uplink radiation (UL).

	Smartphone	Rooted smartphone	Exposimeter
Population size	Large	Limited	Limited
Frequency coverage	Limited (DL-only)	Limited UL/DL	Good UL/DL
Accuracy	Acceptable	Acceptable	Good
Price	Cheap	Cheap	Expensive

2.3 Smartphone vs Exposimeters as measurement tools for RF-EMF exposure studies

Smartphones and exposimeters are two different tools to assess the exposure levels to RF-EMF radiations. Both have advantages and limitations. Exposimeters are expensive devices, which make them only suitable for small, limited population studies. However, they provide decent accuracy levels on multiple frequency bands. They cover both the uplink (UL) and downlink (DL) frequencies. Exposimeters suffer from non-detect (values under the lowest detection limit, usually under 0.005V/m) and underestimating the exposure levels from pulsed signals such as Wi-Fi [96] and can give unreliable results [66].

Smartphone as a measurement tool allows covering very large population. It allows reusing the same mobile application on already existing devices owned by people to study their exposure levels. It does not interfere with the daily life of the persons during the measurements, this allows people to keep their usual habits without worrying about carrying another device. The smartphone measurements can be biased by different factors such as body shielding while using the smartphone. These sorts of biases require large populations to provide robust assessments [97]. Smartphones only cover the downlink frequencies. Software-modified smartphones allow measuring the uplink frequencies from the smartphone (Transmitted power) but come to the cost of limiting the potential population size.

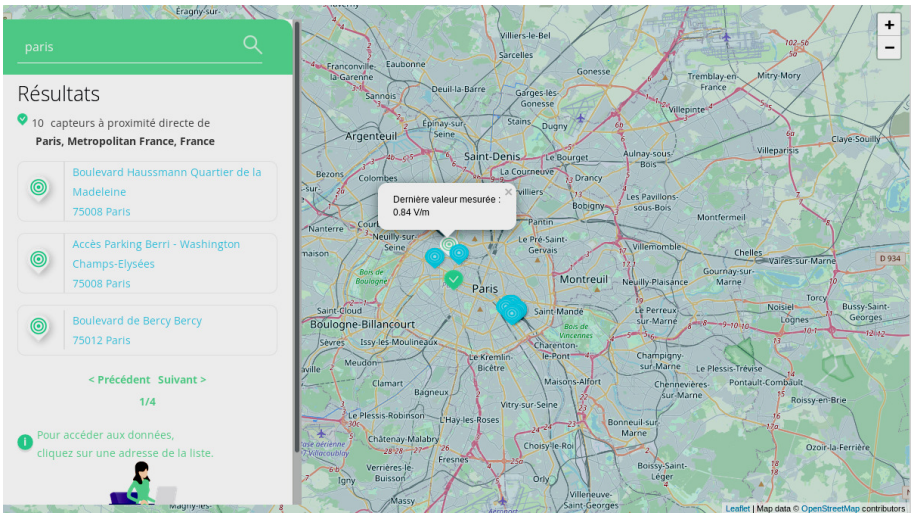

Figure 2.5: Fixed measurements probes in Paris. 10 fixed measurements probes are installed in Paris to monitor the exposure levels in certain areas. When we click on a probe, we can visualize the most recent exposure level measured by that probe (expressed in V/m) [98]

2.4 Regulatory authorities and exposure assessment protocols

In order to make sure the population is not overexposed to the radiofrequencies, regulation authority (agency) within each country continuously monitors the exposure levels. This is mainly done using fixed probes distributed geographically in the country. Figure 2.5 shows a map of the measurement probes installed in Paris city, obtained from the Observatory of Radiations of the French National Frequency Agency (ANFR) [98]. It shows 10 probes that regularly measures and monitors the exposure levels.

In addition to the monitoring provided by the fixed probes, the regulatory agency defines a measurement protocol to make measurements on the field (in-situ), and to be carried out by a qualified engineer. Here we discuss the measurement protocol defined by the French agency ANFR.

2.4.1 The ANFR measurement protocol

The French regulatory agency (ANFR) defines a measurement protocol to evaluate the exposure level of the general public to radiofrequencies. It aims at assessing the exposure levels of radiations between 100 kHz – 300 GHz, and/or the frequency band 9 kHz – 100 kHz [99]. Individuals can make an explicit request to the agency to perform the measurement. It is recommended to switch off any device we can control and which doesn't transmit continuously. For example, WiFi routers and mobile phones should be switched off

during the measurement and only focus on the fixed sources that transmit continuously such as cellular base stations.

The protocol is performed in two main steps.

- **Site inspection:** In this phase, the engineer performing the protocol should detect the location of the emitting sources, and the direction of their radiation. This can be done visually by checking the Cartoradio database [100], or directly by performing measurements with a spectrum analyzer. The measurement points can then be determined either by the explicit request or according to the location of the emitting sources and their radiation patterns.
- **Measurement process:** There are 2 measurement cases: i) Large-band measurement where the radiation levels from all the sources is evaluated. If the resulting exposure level is less than 6V/m, then measurement process ends, and concludes that the exposure levels are under the regulation limit. Otherwise, or if there is an explicit request to evaluate the contribution of individual sources, the process can continue to case 2. ii) Narrow-band measurement. In this case, the exposure from each frequency band is evaluated separately. Either case, the measurements are averaged in time and space. In time: 6 minutes average for frequencies between 100 KHz and 10 GHz; $68/f^{1.05}$ where f is the frequency of the signal in GHz. In space: average of 3 measurements at 3 different heights, at 1.1m, 1.5m, and 1.7m.

This measurement protocol is best used to have a precise assessement of exposure level at a given location. However, it has limitations as it's limited in time and space, and mainly focuses on the fixed radiating sources.It is useful to make sure the exposure does not exceed the regulatory limits, but does not capture the variability of exposure levels experienced by individuals on a daily basis.

2.5 What does this thesis bring?

In this thesis, we present how we can use commodity hardware (smartphones) for wireless power measurements, and conduct large-scale RF-EMF exposure assessment based on crowdsource personal measurements collected with smartphones.

To the best of our knowledge, we are the first study that evaluates smartphone accuracy for measuring wireless signal power. We show how a COTS smartphone without any external hardware or software

modification can give accurate signal strength measurement. We overcome the impact of the orientation on the accuracy of the measurements by exploiting the embedded sensors on the smartphone to calibrate the measurements.

Moreover, in this thesis, we use commodity smartphones in the context of RF-EMF exposure assessment. Previous works relied on specialized exposimeters to perform personal measurements. Here, we show how smartphones can replace exposimeters to allow larger studies on RF-EMF exposure. As opposed to previous works, which used metrics such as electric field strength (V/m) or power density (W/m^2) to express the exposure levels, we use the signal power (dBm or Watt). This is because we are rather interested in assessing the trend in population exposure, and not in exact field strength. However, we show that in an outdoor environment, the impact of orientation on measurement variability is minimized thanks to multipath and polarization diversity used in cellular base stations. This means that smartphone antenna can be considered an isotropic antenna, and electric field intensity (in V/m) can then be estimated from the signal power (in dBm). We will present later in this thesis how to perform such conversion.

By replacing exposimeters with commodity smartphones, we were able to conduct the largest study (to the best of our knowledge) on assessing the world's population to RF-EMF radiations used in cellular, Wi-Fi, and Bluetooth. We analyze the trend of exposure evolution during 4 years, from January 2017 to December 2020. Our study includes more than 250 thousand participants from 13 countries. Each individual has been tracked for 53 days on average, and more than 62 thousand participants (25%) have exposure measurements for more than 45 days. This makes our study the largest in terms of time, population size, and geographical coverage compared to previous works on personal measurement studies, shown in Table 2.2

Smartphone architecture and wireless technologies

3

Modern cell phones, commonly known as smartphones, are arguably the most common mean of wireless telecommunication. Smartphones are feature-rich, multi-purpose devices capable of making phone calls, connecting to the internet, exchanging emails, and more.

In this work, we will only focus on Android smartphones, which represent around 73% of the market share in 2021, compared to only 26% for Apple iOS [101, 102]. Moreover, iOS APIs are very limited compared to Android in terms of accessing network information.

In this chapter, we will present some important concepts about smartphone architecture in terms of hardware and software components. We will mainly focus on the components that get involved in the measurement of wireless radiations. This is important to help us understand the hardware and software capabilities and limitations of smartphones for this type of measurement. Afterward, we will give a brief description of the different wireless technologies (cellular, Wi-Fi, and Bluetooth), their evolution, and the frequencies they use. We will see later in this study how the differences between those technologies can lead to different exposure trends. Finally, we will introduce important mechanisms involved when smartphone performs scanning and measurement of the surrounding RF-EMF sources. We will give low-level details on how scanning works for the different technologies. The knowledge we present is crucial in order to understand the scanning limitations of smartphones (which some of them are dictated by the protocol) and help us better interpret the scan results.

3.1 The building blocs of a smartphone

Early 1990s, cell phones were only capable of making voice calls and exchanging SMS. People used other devices called Personal Digital Assistant (PDA) to exchange emails, make todo-list or calendar management. Modern-day smartphones are feature-rich and have the capabilities of both a cell phone and a PDA. They have high computing power, and lots of sensors embedded in them, all in a small-sized device. This is made possible thanks to a hardware design called System-on-Chip (SoC).

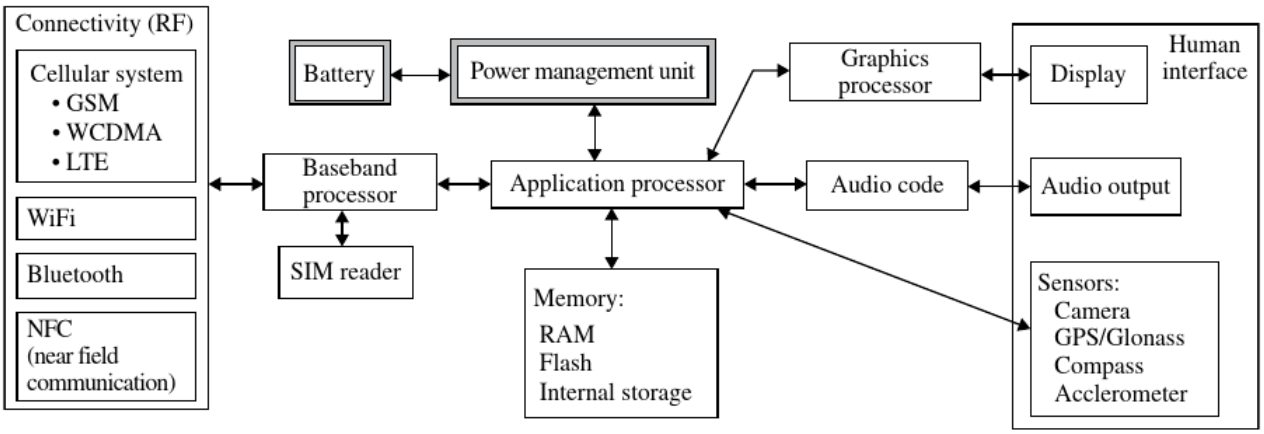

Figure 3.1: Smartphone components. Smartphones use two distinct processors: one for user applications called Application processor, and the other is for the RF connectivity called Baseband processor. Source [103]

In this section, we present the main component of a smartphone and how they coordinate and communicate. We will mainly focus on the hardware and software components that are involved in the wireless telecommunication process.

3.1.1 SoC: System-on-a-Chip

SoC, as its name suggests, it is a complete system built on a single electronic chip. A mobile SoC is a small integrated circuit that integrates the core hardware components of the smartphone. It is considered the brain of the smartphone. It is high performing and power-efficient and very small in size, which makes it perfectly suitable for battery-powered devices such as mobile smartphones.

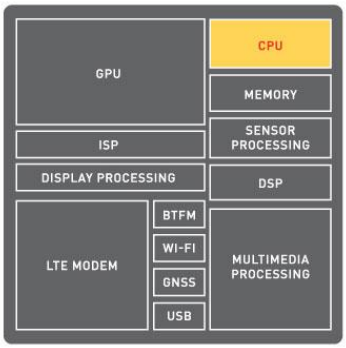

Figure 3.2: SoC is a small integrated circuit that contains all central components of the smartphone. The picture shows typical components inside the SoC. Source: Qualcomm [104]

A typical SoC contains a central processing unit (CPU), a graphics processing unit (GPU), memory, a cellular modem (Baseband), image and signal processing unit, in addition to Near Field Communication (NFC), Global Positioning System (GPS), Wi-Fi, and Bluetooth transceivers. Figure 3.1 shows the interconnections between the SoC and other internal components of a smartphone.

There are different mobile SoC manufacturers such as Qualcomm, Mediatek, HiSilicon, Samsung, and Apple[105]. Qualcomm is the largest provider with 29% of the market share in the second quarter of 2020.

Inside a smartphone SoC, there are two types of operating systems, each running on a separate CPU. The first one is the one we all know and with which we interact directly while using the smartphone. It is called Application OS and is responsible for running user applications. It uses its own CPU called the Application processor.

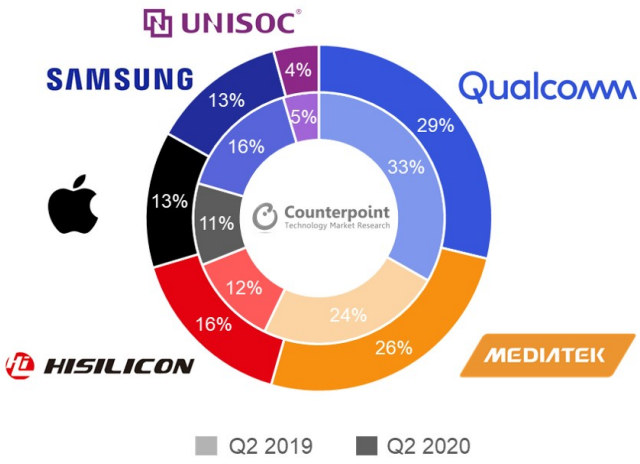

Figure 3.3: Market share of mobile SoC. Qualcomm is the largest provider with its Snapdragon series, followed by MediaTek, Huawei's HiSilicon. Apple and Samsung both have 13% of the market share. Source [106]

Android and Apple iOS are both considered Application OSes. Another type of operating system that runs on the smartphone SoC is called Baseband OS. It runs on the Baseband Processor (BP), independently from the Application Processor (AP)[107].

In the next sections, we present the RF modem and its own operating system. Then, we present the Android application OS, and we describe how these two distinct OSs communicate and exchange information to ensure the functionalities of the smartphone.

Modern smartphones run 2 distinct operating systems at the same time. One for user applications called Application OS. The second is for the RF modem called Baseband OS.

3.1.2 The Baseband

The baseband, or the RF modem is part of the SoC that is responsible for the RF functions such as signal generation, modulation/demodulation, encoding/decoding, frequency shifting. It is the smartphone component that exchanges data with the RF networks such as cellular networks, Wi-Fi, and Bluetooth devices. The modulator unit takes an input baseband signal (hence, the whole RF modem is called a baseband) with low-rate or frequency and modulates it to a high-rate/frequency signal. Analog and digital modulation are used depending on the nature of the baseband signal[103].

The baseband runs its own operating system called baseband OS. It is a proprietary, closed-source, and real-time OS that runs the RF functions of the modem. The benefits of having a separate OS for the baseband with those characteristics are i) performance: since cellular protocols have strict and well-defined time constraints. Hence, having a dedicated CPU for cellular operation will ensure full performance, and avoid load created by user application. ii) Reliability: a separate OS is an isolation from any sort of attacks or instability in the application OS that can be caused by third-party software. iii) Legal: The cellular stack on every smartphone must be

certified by some legal authorities, such as the FCC. This separation of the baseband from the application OS, allows reusing the certified baseband without having to certify the whole equipment.

3.1.3 Android OS

Figure 3.4: Android OS is an open-source application OS for mobile devices.

Android is a Linux-based, open-source operating system for mobile devices such as smartphones and tablets, developed by the Open Headset Alliance led by Google [108]. Android was initially co-founded by Andy Rubin in 2003. Andy was nicknamed 'Android' by his co-workers at Apple because of his love for robots [109]. Hence, the name Android for the OS. In 2005, Google acquired Android [110]. By 2021, Android is considered the most popular mobile operating system with more than 70% market share [111].

Android is an application OS that runs on smartphones. It is built on top of the Linux kernel. The architecture of the Android framework [112] is presented in Figure 3.5.

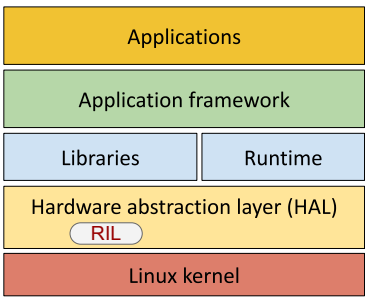

Figure 3.5: The Android software stack.

- **Applications:** is a set of core user applications such as email client, contact, calendar, web browser. Third-party applications can be installed from Google Play Store [113]. The Android applications are usually written in the Java programming language. Kotlin is an alternative programming language that is getting popular for Android development. Developers can use the Android SDK to build their own applications and deploy them on any device running Android.
- **Applications Framework:** is the core, modular system components and services of Android that are accessible for developers through API calls. They are the building blocks of any Android application.
- **Libraries:** are a set of native libraries written in C or C++. Many Android system components and services require these native libraries to interact with the other, lower layers in the software stack.
- **Android runtime:** is the managed runtime used by Android applications and services. It is the successor of the Dalvik runtime. Android runtime (ART) allows applications to run their own processes in a virtual machine. ART is optimized for minimal memory footprint, which allows running multiple virtual machines at the same time on memory-limited devices.
- **Hardware Abstraction Layer (HAL):** as its name suggests, HAL is a layer that abstracts the hardware functionalities for upper layers in the stack. It provides an interface that exposes

the hardware capabilities and loads the corresponding library module for each API call to specific hardware, such as the camera. We will discuss this component later in section 3.1.4, and show the role it plays between the Android OS and the Baseband OS.

- **Linux kernel:** Android is based on Linux and uses its existing functionalities for threads and memory management, in addition to the security layer it offers.

3.1.4 Modems only need ATtention

So far, we have seen that the core components of a smartphone are built on a single SoC. The SoC runs two distinct operating systems on two separate processors, the Application Processor, and the Baseband Processor. We have seen that the Baseband is the one in charge of the RF functionalities, while the Application Processor runs the application OS and the user applications. The two worlds need to communicate between them to provide seamless operations to the users.

AT commands, Attention commands, or Hayes commands are a set of commands for controlling a modem. They were initially developed by Dennis Hayes in 1981 [114–116]. AT commands are short text strings that define specific actions on the modem, such as dialing a number, sending SMS, and accepting or hanging up a phone call. Currently, a set of AT commands has been standardized [116–118]. Some commands are mandatory, and manufacturers can extend AT commands to implement vendor-specific commands in order to control their modem [116, 118].

The Baseband Processor (BP) and the Application Processor (AP) are connected through a serial Universal Asynchronous Receiver-Transmitter (UART) line. This line carries signaling messages (commands) and packets data. The voice data is passed through other interfaces [119]. The communication between the BP and the AP can be intercepted. Fabien Sanglard [120, 121] performed a Man-In-the-Middle technique on the serial line of iOS and Android phones, in order to read the full exchange of messages. He was able to read the AT commands while the smartphone was performing various tasks, such as receiving a phone call or receiving a text message.

Listing 3.1 shows the exchange of messages between the BP and the AP when receiving a phone call [121]. First, the BP tells the AP that there is an incoming call (+CRING). Then, the AP requests the phone number of the caller (AT+CLCC). The BP answers back

```
[Android recv] :+CRING:
    VOICE
[Android send] :AT+CLCC

[Android recv] :+CLIP:"
    +1416839XXXX"
[Android send] :AT+CMUT
    =0
[Android recv] :0
[Android send] :ATA

[Android recv] :0
[Android send] :ATH

[Android recv] :0
```

Listing 3.1: Intercepting the exchange of messages between the BP and AP on Android smartphone.

with +CLIP command followed by the caller number, which is then displayed on the dialer application. After accepting the call on the AP side, a command to unmute the microphone is sent to the BP (AT+CMUT=0). The call can be picked up, then hung up with ATA, and ATH commands, respectively.

The AT commands are powerful and can be used beyond just performing cellular operations.Tian et al. [115] extracted over 3500 AT commands from over 2000 Android smartphones. Each AT command is tested against 8 different smartphones. They managed to perform various actions such as screen unlock, perform touch events, bypass Android security barriers, and even rewriting the whole device firmware.

Radio Interface Layer (RIL) is the bridge that connects the Android phone framework and the hardware (modem) [122]. It is part of Android HAL, as shown in Figure 3.5. It is responsible for parsing and translating the Android API calls and payloads into AT commands and sends them to the baseband, and vice-versa. The RIL handles many aspects of cellular communication such as voice calls, SMS, and network registration. RIL has three main components [122–125].

- **RIL Deamon:** is a simple system daemon that initializes the Vendor RIL at the device startup. It processes all communication from Android telephony services, and dispatches calls to the Vendor RIL as solicited commands.
- **Vendor RIL:** is the core library in the RIL. It is the piece of software that handles the actual communication with the baseband. Vendor RIL is a closed-source, baseband and manufacturer-specific library provided by the manufacturers as a binary file. Manufacturers are often legally bound by non-disclosure agreements to not provide the source code of this library [122].
- **Android RIL (RILJ):** is a Java module that exposes RIL interface to the Android framework.

The RIL commands can be solicited or unsolicited. i) Solicited commands such as DIAL and HUNGUP for dialing and canceling a call, originating from the upper layers of the Android framework. ii) Unsolicited commands are originating from the baseband, such as NEW_SMS [124][126].

Low-level cellular information are processed and stored at the baseband. Only basic information are shared with the Application OS.

The BP does not share all information with the AP. Low-level information about the network are only available and processed at the BP level. The BP shares only some basic information needed by the AP,

the signal strength for example. Other information such as smartphone transmission power is only required at the BP level in order to communicate with the network and is not shared with the AP. These types of information are valuable for RF-EMF exposure assessment. However, they are not easily accessible on smartphones. Proprietary debugging software such as Qualcomm XDM (QXDM) [127] for smartphones with Qualcomm SoC can be used to read the Baseband data. There have been works on accessing and extracting this low-level information directly on the smartphone without the need for debugging software. Vallina-Rodriguez et al. [87] developed RILanalyzer. A tool that aims at extracting low-level cellular information from the baseband. They implemented hooks on the RILJ component of Android to interact with the BP and trigger requests to read cellular information such as control-plane messages. Li et al.[88] developed another tool called MobileInsight that collects and analyzes cellular information from the BP and makes them available at the AP level through an Android mobile application. It provides access to fine-grained cellular information on 3G and 4G protocols. Instead of using the RIL component to access the BP information, the authors of MobileInsight mimic the behavior of the debugging tool (QXDM). They managed to capture the commands sent by QXDM and use these commands afterward on the smartphone-level using the MobileInsight mobile application. The commands are sent through the serial port between the AP and BP. The BP then responds with hex data containing the raw cellular information. The logs are then parsed and presented at the AP level. Unfortunately, these works require the smartphone to be rooted and work only on some particular smartphones equipped with specific SoC, which makes them not suitable for large-scale, crowdsource measurement.

3.1.5 Smartphone antennas

An antenna is a transducer that converts an electromagnetic wave into an electric signal in the reception and converts the electric signal into an electromagnetic wave at the transmission.

Wireless communication consists of sending and receiving information over the air as an electromagnetic wave. This requires the use of antennas. An antenna is a transducer that can convert an electromagnetic wave into an electric signal during the reception, and convert an electric signal to an electromagnetic wave during transmission. The electric field of the electromagnetic wave is a result of voltage changes at the antenna ports, whereas the magnetic field is a result of current change. The opposite process happens at the reception where the electric field causes a change in voltage of the antenna, and the magnetic field causes a change in the electric current [103]. This means that the electric field intensity of the signal

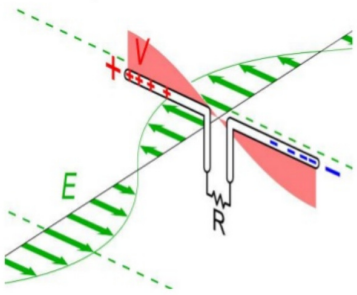

Figure 3.6: Antenna working principle. The electric field of the signal induces an alternating current at the ends of the antenna by pushing electrons from one end to the other, this also induces a potential difference (voltage). That way, the electromagnetic wave is translated into an electric signal. The opposite behavior happens during transmission. Image Source [128]

can be obtained from the voltage change at the antenna. We will use this property later on in this thesis in the study of exposure to wireless radiations.

Physically, an antenna is a metallic conductor, that can be of different shapes and sizes depending on the usage, from dipole antennas, helical, whip, slot, and microstrip patch, each type of antenna has its own characteristics. There are different parameters that determine the performance of the antenna. The main parameters are as follows [103][129][130].

- **Resonant frequency:** is the frequency in which the antenna is the most efficient. It mainly depends on the size and shape of the antenna. The resonant frequency of the antenna is inversely proportional to the size of the antenna. The higher the frequency the smaller the antenna. The size of the antenna is usually expressed in terms of wavelength $\lambda = c/f$, where c and f are the speed of light and the resonant frequency of the antenna, respectively. Most antenna have $\lambda/2$ or $\lambda/4$ in size.
- **Polarization:** The polarization of the antenna is the orientation of the electric field of the electromagnetic wave with respect to the Earth's surface. The polarization is determined by the shape and the orientation of the antenna in space. We can distinguish 4 types of polarization: horizontal, vertical, circular, and elliptical. The wireless communication is optimal when the polarization of the receiving antenna matches the polarization of the transmitting antenna.
- **Radiation pattern:** is a representation of the power or the electric field intensity radiated by the antenna at different angles in space. The radiation pattern can be isotropic, directional, or planar. Isotropic radiates the same power level in all directions, whereas directional directs the power in a given direction.
- **Gain:** The antenna gain represents how much power is radiated in a given direction compared to an isotropic antenna. The gain can be positive (more power), or negative (less power) than an isotropic antenna. The gain is usually expressed in dB.

Modern smartphones support various wireless technologies. Each technology can use a different frequency band. To support all these technologies altogether, multiple antennas are needed. Moreover, to deliver high performance, high data-rate transmission, Multiple-Input, Multiple-output (MIMO) systems are also used, such as the ones used for LTE and Wi-Fi [131]. A standard smartphone includes a primary cellular antenna (Tx/Rx), Additional receive-only antennas called diversity antenna (Rx only), a GPS antenna (Rx only), Wi-Fi antenna (Tx/Rx), and Near Field Communication (NFC).

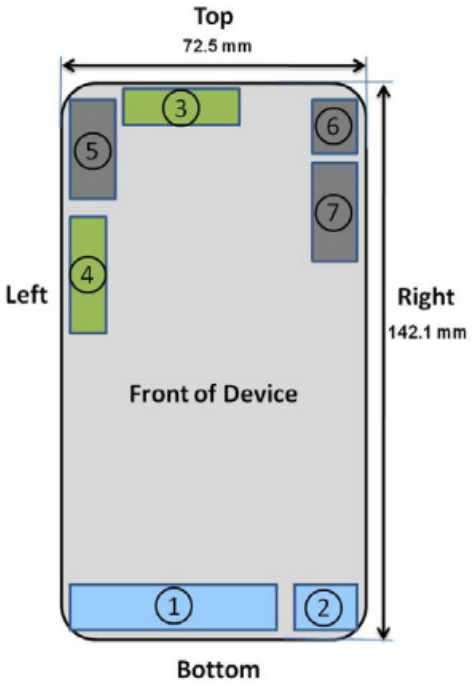

1. **Main Antenna (Tx/Rx)**
   - CDMA/EVDO BC0/1/10
   - 850/1900 MHz GSM/GPRS/EDGE
   - UMTS Band 2/5
   - LTE Band 25/26
2. **LTE B41 Main Antenna (Tx/Rx)**
3. **BT/WLAN Antenna #1 (Tx/Rx)**
   - 2.4 GHz BT/WIFI
   - 5 GHz WIFI
4. **WLAN Antenna #2 (Tx/Rx)**
   - 2.4 GHz WIFI
   - 5 GHz WIFI
5. **MRD Antenna (Rx Only)**
6. **GPS Antenna (Rx Only)**
7. **LTE B41 Sub Antenna (Rx Only)**

Figure 3.7: Typical antennas placement on modern smartphones. The figure shows different antennas placed on the edges of the smartphone casing. Main cellular antennas are placed at the bottom of the smartphone to reduce radiation on the head during phone calls. Mobile Receive Diversity (MRD) antennas are placed on the top since they are receive-only antennas. Source: FCC [132]

Putting multiple antennas in small-sized devices such as smartphones is very challenging, and some design practices and constraints should be respected.

- **Small in size**: Due to space constraints on the smartphone, antennas should not take a lot of space.
- **Multi-band:** Wireless technologies such as cellular, work on multiple frequency bands. Supporting multiple bands allows using the same physical antenna for multiple technologies on different frequency bands.
- **Minimize interference with other components:** It is important to minimize all sorts of interference from surrounding electronic components such as the loudspeaker, the battery, and the display. These components can have an impact on the antenna's performance [131].
- **Minimize the exposure:** Smartphone manufacturer should limit the exposure and the energy absorbed by the human body and head (SAR) while the smartphone is transmitting. Each smartphone undergoes a validation test performed by regulation authorities, such as the FCC to make sure the exposure limits are respected.

Typical placement of the different antennas on the smartphone is shown in Figure 3.7

Planar Inverted-F antenna (PIFA) is the most common antenna type in modern smartphones [131]. They are small in size, can support

multiple bands, and are easy to manufacture at a low cost. Microstrip patch antennas are also being used in mobile smartphones [103].

The radiation pattern of the smartphone antennas can be directive, especially at higher frequencies [131]. This makes the antenna performance sensitive to the orientation with respect to the source. This suggests that smartphone measurement accuracy can be affected by the orientation with respect to the source. In Chapter 4, we will cover more in-depth the impact of orientation on smartphone measurements for wireless signal strength, and propose a calibration technique to compensate for such impact.

3.2 Wireless technologies

The goal of this section is to introduce the various wireless technologies that are omnipresent RF-EMF radiating sources. So, it's important to understand their evolution, deployment, and on which frequency bands they operate.

Since the early 1990s, the wireless telecommunication industry witnessed an impressive revolution. Things we take for granted such as watching movies in high quality, live streams, and video calls, all from a smartphone, is only made possible thanks to the advancement in wireless technologies.

3.2.1 The 2nd generation of cellular: 2G

Introduced in the early 1990s, the second generation of wireless cellular technology. The Global System for Mobile Communications (GSM) was the first version of this technology. GSM was designed to be a circuit-switched system. It allowed for the first time voice and data together, with around 14Kbps datarate. The second improvement in this generation is called GPRS (General Packet Radio Service). It improved the data rate up to 170Kbps. The next improvement is called EDGE (Enhanced Data rate for GSM Evolution), which allowed higher speed at 270 Kbsp [133].

The second generation of cellular uses mainly the 800, 900, 1800, and 1900 MHz frequencies.

3.2.2 The 3rd generation of cellular: 3G

Launched in the early 2000s, the third generation revolutionized cellular networks usage, from only phone calls and short messages to supporting a wider range of applications such as internet connectivity, video calls, and file transfer. It is based on GSM technology and aimed at supporting higher data rates up to 14Mbps. It is known as UMTS (Universal Mobile Telecommunications System) in Europe and CDMA2000 in North America. UMTS uses mainly the Wideband Code Division Multiple Access (WCDMA) standard. More enhancements were used, such as HSPA (High-Speed Packet Access) and HSPA+.

In addition to the frequencies used in GSM, higher frequencies were allocated to the 3G to include the 2100 MHz band [133].

3.2.3 The 4th generation of cellular: LTE

The evolution and enhancements of the UMTS reached some limitations. The Third Generation Partnership Project (3GPP) proposed a complete redesign of the network. The project is entitled LTE for Long Term Evolution. The 4th introduced the usage of the Multiple Input Multiple Output (MIMO) transmissions, which allow the transmission of several data streams over the same carrier simultaneously. This results in a huge increase in the data rates compared to a single-stream transmission. LTE is also the first generation to use an all-internet Protocol (IP) to send all types of data over the internet, except the SMS which is still transmitted over signaling messages.

LTE can be deployed in multiple frequency bands [73][133], depending on the region. Typical LTE bands are Band 1 (2100 MHz), Band 3 (1800 MHz), Band 7 (2600 MHz), Band 8 (900 MHz).

3.2.4 Wi-Fi

The first IEEE 802.11 Wi-Fi standard [134], introduced in 1997, provides 2 Mbps throughput. Since then, the standard has evolved to reach 10 Gbps throughput in its latest generation, the 802.11ax (Wi-Fi 6) [135]. We show in Table 3.1 the evolution of the 802.11 Wi-Fi standard [134–141].

The standard in use is the 802.11ac. According to Cisco, this standard is present in 70% of end devices in 2018 [142]. It is the first standard

Table 3.1: The 802.11 Wi-Fi standards evolution.

Standard	Year	Frequency (GHz)	Throughput
802.11	1997	2.4	2 Mbps
802.11b	1999	2.4	11 Mbps
802.11a	1999	5	54 Mbps
802.11g	2003	2.4	54 Mbps
802.11n	2009	2.4/5	600 Mbps
802.11ac	2013	5	6.8 Gbps
802.11ax	2019	2.4/5	10 Gbps

to break the Gbps barrier, providing a remarkable throughput increase compared to its predecessor. It operates on the 5 GHz band. Wi-Fi routers supporting this standard often offers backward compatibility with clients with older standard support, such as 802.11n and 802.11g.

3.2.4.1 Wi-Fi attenuation by frequency

Table 3.2: Attenuation values (dB) for different materials of the 2.4 GHz and 5 GHz.

Material	2.4 GHz	5 GHz
Wood door	3-4	6-7
Brick/Concrete wall	6-18	10-30
Glass/Window	2-3	6-8
Steel/Fire exit door	13-19	25-32

The 802.11ac standard uses only the 5 GHz band to benefit from more channels with significantly wider bandwidth, which allows higher speed. Also, the 5 GHz band is less crowded and has less interference compared to the 2.4 GHz band, which suffers from interference from neighboring Wi-Fi access points, and other various types of sources such as Bluetooth and Microwave ovens which operate on the same 2.4 GHz band [143]. However, the 5 GHz band suffers from a shorter range and stronger attenuation compared to the 2.4 GHz band. The free space path loss (FSPL) formula we show in Equation 3.1, that can be derived from the Friis transmission formula [144], represents the natural attenuation of the signal with distance. It states that the attenuation of signals in free space is directly proportional to the square of the frequency: the higher the frequency, the higher the attenuation. Moreover, the 5 GHz band has a higher attenuation than the 2.4 GHz band through solid objects. A comparison of the attenuation values between the 5 GHz and 2.4 GHz frequencies for different materials [145] is shown in Table 3.2. The 5 GHz frequencies are attenuated twice as much by a wood door or the glass of a window, compared to the 2.4 GHz. This attenuation is even larger through concrete walls, where we

The natural attenuation of the signal with distance in free space. The higher the frequency, the stronger the attenuation.

$$FSPL = \left(\frac{4\pi df}{c}\right)^2 \quad (3.1)$$

can have up to 30 dB attenuation for the 5 GHz (12 dB more than for the 2.4 GHz).

3.2.4.2 Wi-Fi beamforming:

An important feature of the 802.11ac standard is beamforming. Beamforming means directing the transmission power to the direction of the receiver. So instead of having the antennas of the Wi-Fi router to radiate the power in all directions, it transmits the signal towards the position of the client, aiming to increase the signal-to-noise ratio, which will enhance the speed of transmission. This can be achieved using traditional, omnidirectional antenna arrays to dynamically form a desired transmission pattern. The beamforming results in a 2 to 5 dB power gain at the reception [143] compared to the traditional, omnidirectional transmission on the same band.

3.2.5 Bluetooth

Bluetooth is short-range wireless communication technology. It is widely used for the Internet of Things (IoT) and battery-powered devices such as smartphones, smartwatches, in-car systems, and audio headsets. Bluetooth Low Energy has been introduced to reduce even more the energy consumption in applications that only require intermittent transmission of data, instead of streams of data.

There are 3 different classes of Bluetooth devices according to their transmission power. Class 2 is the most commonly used one, with 4 dBm maximum transmission power, and about 10 meters range [146].

Bluetooth shares the 2.4GHz band with other wireless technologies such as Wi-Fi and uses Frequency-Hopping Spread Spectrum (FHSS) in order to reduce interferences with other sources [133].

3.3 Scans in wireless networks

In this section, we discuss the mechanisms and the process at the protocol level that allows the smartphone to search and detect the available wireless sources. This section describes what happens behind the scenes when a mobile application triggers a scan to measure the RF-EMF radiations. Understanding these mechanisms will help us understand the scanning limitations of smartphones as

imposed by the protocols, the scanning duration, and help us better interpret the scan results.

3.3.1 Wi-Fi scans

In Wi-Fi, there are 2 modes of scanning: active and passive scans [133, 147, 148].

- **Active scan:** the client sends a probe request ("is there someone on the channel?") and listens for a probe response from the access point.
- **Passive scan:** The client listens to each channel for beacons sent periodically by the access point.

Smartphones are able to perform both types of scans in all channels allowed in the country of operation. The passive scan takes a longer time because the client has to wait at each channel to receive the beacon. The access point sends beacons every 100 ms periodically, the client may miss the beacon if it didn't wait enough time on the channel. After sending a probe request, the device starts a timer `MinChannelTimer` which defines the time to remain in the same channel waiting for Probe Responses. If no response is received when the `MinChannelTimer` has expired, the device considers the channel empty. However, if a probe response is received during `MinChannelTimer`, the device sets another timer `MinChannelTimer` to wait for any further probe responses from other APs. The IEEE 802.11 does not specify values for these timers. The values can vary depending on the implementation, but it ranges from a few ms up to 40ms [149][150]. So for example to scan all 13 channels in the 2.4GHz band, it can take from 520ms to 1.04s, and from 960ms to 1.92s to scan all 24 channels in the 5GHz band, depending on the value of `MinChannelTimer`. The number of channels to scan is dependent on the channels allowed at a country level. The active scan starts when the client switches to a new channel, sends a probe request and starts a Probe timer. It remains on the channel listening for probe responses until the timer expires, upon which it switches to the next channel [151]. Probe Timer value is usually a lot shorter than a beacon interval. Ten milliseconds is a common value [152]. The probe request can be targeted towards an AP by specifying SSID field (Directed probe vs. Broadcast probe in which SSID is null) [148].

The Wi-Fi RSSI is obtained by measuring the signal strength of packets sent by AP in response to probe requests in the case of

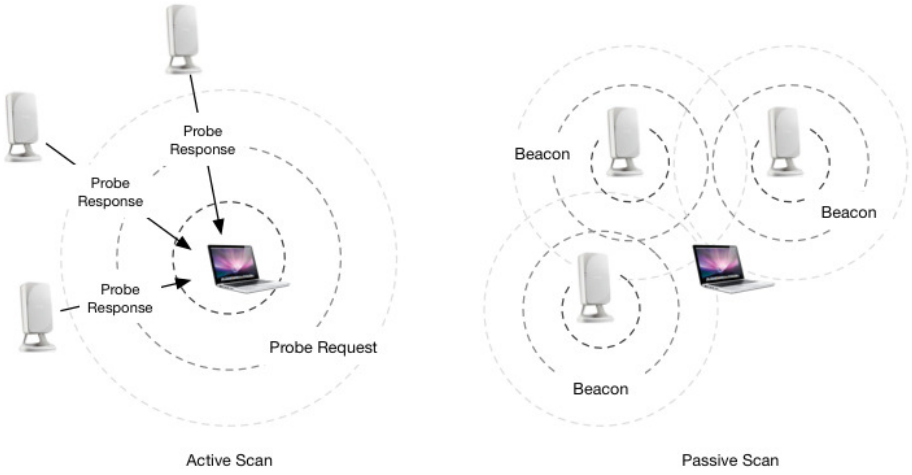

Figure 3.8: Wi-Fi scanning: active vs. passive scan. Source [154]

active scanning or from the beacon frames in the case of passive scanning [153].

The active scan is the preferred one, and when we make an explicit call for scanning, the active scan is performed.

3.3.2 Bluetooth scans

In Bluetooth, there is a master-slave relation between devices. A master device refers to the one scanning (making the inquiry), and slaves are the scanned devices.

To discover other devices, the master device enters the Inquiry State. In this state, the device broadcasts two ID packets per slot on two different frequencies. The listening devices can reply to these inquiry packets. The master sends two ID packets in a 625μs wide slot, then listens for 625μs for responses from other devices. Once the slave received the packet, it enters the Inquiry Response state and transmits a packet containing device information such as its Bluetooth device address to the inquirer[155]. The master device can then measure the RSSI of the signal strength from the response packet.

For a device to be detectable, it has to change to Inquiry Scan State periodically to listen for packet ID on alternating frequencies. The devices change the frequency it listens to every 1.28 seconds. The scan duration is about 11.25 milliseconds per 1.28 seconds interval.

The scanning device is switching faster between frequencies. In 1250μs there are two inquiry messages sent and two "waiting for response" periods [156]. The fast frequency switching by the master device, combined with slow switching of frequency by the slave

device, results in a 90% probability that a device can be detected within a scan period of 10 seconds [133].

There are 79 sub-frequencies, in frequency hopping, the data is not transmitted on 1 single frequency, but the device keeps changing frequency among the 79 frequencies while transmitting the data. This helps reduce the interference with other wireless sources at the same frequency band.

3.3.3 Cellular scans

The procedure to find cells in cellular is pretty much the same in all cellular generations (LTE, UMTS, and GSM). The scanning procedure is called Cell Search followed by Cell Selection. For a smartphone to attach to the network, it has to search for available cells around it. To do so, it has to scan all frequency bands that correspond to the RAT technology (whether LTE, WCDMA, or GSM), and measures the signal strength (SS) of each cell.

The smartphone keeps only cells with SS greater than a certain threshold to ensure a strong enough signal for decoding system information of the cell. Next, the smartphone has to synchronize with the cell. After successful synchronization, it can decode cell information such as cell ID, the PLMN (cellular operator) the cell belongs to. The final step in the Cell Search procedure is to keep only a list of cells that belong to the home PLMN with a strong SS. This list can be used for Cell Selection or Cell Reselection to allow the UE to attach to the network, or to switch to another cell in case of handover.

This procedure is performed periodically to ensure continuity of service. To speed up the Cell Search procedure, the smartphone can use certain RAT technology priority rules and stored information about carrier frequencies and optionally also information on cell parameters, collected during previous scans [103, 133, 157–159].

To summarize the whole process of scanning and measuring wireless signals using smartphones, we present an example of scanning for Wi-Fi sources and measuring the signal strength.

- **1 - Android API call:** To launch the scanning, and obtain the signal strength of neighboring Wi-Fi sources, we need to perform an API call on the Android OS.
- **2 - Solicited command to the badeband:** The RIL translates the Android API call into a solicited command that the baseband can understand.

- **3 - Probe request:** The baseband performs the active scan for Wi-Fi sources by sending probe requests.
- **4 - Probe response:** The Wi-Fi access point responds to the probe request by sending a probe response packet.
- **5 - Unsolicited command:** The baseband receives the probe response through the antenna and measures the power of the signal. The value of the signal strength is passed to the RIL along with other information such as the signal frequency.
- **5 - Android callback:** Upon sending the API call when starting the scan, the Android OS registers a listener to intercept the callback from the hardware containing the results of the scan. Android parses the results and presents them inside Java objects.

3.4 Conclusion

In this chapter, we presented the necessary knowledge about the smartphone's anatomy, its internal hardware and software components that are involved in the measurements of the RF-EMF radiations.

The knowledge presented in this chapter is important in the context of using smartphones as a measurement tool for RF-EMF radiations. We showed that smartphones use two separate operating systems running on two distinct processors. The RF data such as the received power and the transmitted power from the smartphone are processed at the Baseband OS, and only basic information is accessible from the user applications (Application OS). This leads to a limitation in terms of types of information that can be collected using a smartphone.

Moreover, the smartphone antennas design, their small size, placement on the device can affect their performance, and factors such as orientation can lead to imprecision in the measured signal strength.

In addition to that, we gave a brief introduction to the different wireless technologies that produce RF-EMF radiations. We presented their chronological evolution which will help us understand which technology is recent and which is getting deprecated, which in turn can help us interpret the exposure patterns to these technologies. We also presented the frequency bands used. Frequency is an important factor in the propagation of the signal and its penetration range. Frequency can also condition the amount of radiation power that needs to be transmitted by the RF sources. We also presented

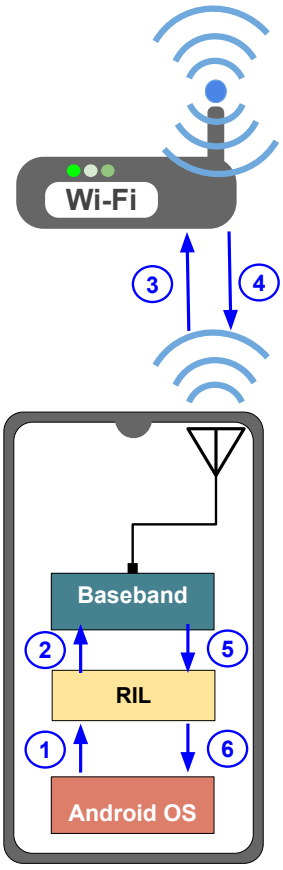

Figure 3.9: Wireless networks scanning with Android smartphone

technical capabilities such as beamforming that intends to direct more radiation towards the persons connected to the Wi-Fi access point, which can impact exposure of the person to Wi-Fi.

Finally, we presented the low-level protocol mechanisms that are triggered when scanning for RF sources. We presented how scans are performed for cellular networks, Wi-Fi, and Bluetooth. Understanding such mechanisms is crucial for the users and the developers of mobile applications for RF-EMF exposure measurement. This knowledge can explain other limitations of smartphones measurements. For instance, the fact that the cellular scans with smartphones can only return results for cellular antennas that belong to the operator of the SIM card is dictated by the protocol.

The information provided in this chapter will be useful to understand the rest of this thesis, and technical choices we make in the analysis, and the methodological limitations we faced.

Evaluating Smartphone Accuracy for RSSI Measurements.

4

Smartphones are today affordable devices, capable of embedding a large variety of sensors such as magnetometers or orientation sensors, but also the hardware needed to connect them to most wireless communication technologies such as Wi-Fi, Bluetooth, or cellular networks. Therefore, they are handy devices able to perform Received Signal Strength Indicator (RSSI) measurements for a wide variety of applications such as cellular coverage maps, indoor localization, or proximity tracking. However, to the best of our knowledge, the accuracy of such measurements has never been rigorously assessed. The goal of this chapter is to assess the accuracy of the RSSI measurements made with a Commercial Off-The-Shelf (COTS) smartphone in a variety of conditions, and how possible inaccuracies can be corrected. We primarily focus on the LTE RSSI, but we also extend our results to the Bluetooth RSSI.

In this chapter, we build a controlled experimental setup based on commodity hardware and on open-source software. We evaluate the granularity and limitations of the Android API that returns the RSSI. We explore how reliable the measurements in a controlled environment with a mono-polarized antenna are. We show that the orientation of the smartphone, the position or orientation of the source, and the transmission power have a significant impact on the accuracy of the measurements. We introduce several correction techniques based on radiation matrix manipulations and on machine learning in order to improve measurement accuracy to less than 5 dBm RMSE, as compared to a professional equipment.

We also explore the reliability of measurements made in an outdoor realistic environment. We show that whereas transmission diversity available in LTE base stations significantly improves the measured RSSI regardless of the smartphone orientation, the Bluetooth RSSI remains largely sensitive to the smartphone orientation.

4.1 Introduction

Smartphones are sophisticated devices with a lot of embedded sensors, but also with the support of several wireless technologies, such as Wi-Fi, Bluetooth, 2G, 3G, 4G, and now 5G. For this reason, they are used to make measurements of the Received Signal Strength

Indicator (RSSI). Such measurements are important in multiple contexts, such as network performance evaluation [89, 90], RF-EMF exposure assessment [50, 52, 91], indoor positioning [160], and most recently, contact tracing [161, 162] in the context COVID-19 pandemic relying on Bluetooth RSSI to infer proximity.

Whereas, the accuracy of the RSSI measurements is a key point in all these contexts, this is still a topic difficult to approach and, to the best of our knowledge, there is no rigorous evaluation of this accuracy for COTS smartphones.

In this work, we evaluate the accuracy of an Android COTS smartphone when performing measurements of the RSSI emitted from a 4G (LTE) source, and we extend our results to a Bluetooth source. Our contributions are the following. i) We evaluate the granularity and limitations of the Android API that provides the RSSI. We show that not all methods to access the RSSI are equivalent. We can expect a 2 dB granularity and an update every second (at the most) for the measurements made. ii) We explore the accuracy of the RSSI measurements in a fully controlled environment with a mono-polarized antenna. We show that the accuracy of the measurements is extremely sensitive to the device orientation, source positioning and orientation, and also to the source Tx power. iii) We propose several correction techniques aimed to the improvement of the accuracy of the RSSI that rely on manipulations of radiation matrices and on machine learning. We show that we can significantly improve the accuracy and obtain a Root Mean Square Error (RMSE) lower than 5 dBm as compared to a calibrated professional equipment. iv) We explore the accuracy of the RSSI measurements in an outdoor realistic environment. We show that transmission diversity available for the LTE base stations dramatically reduces the RSSI sensitivity to the device orientation. However, transmission diversity is not available for all wireless technologies. In particular, we show that the Bluetooth RSSI is still sensitive to the device orientation in a realistic environment v) We make available all the RSSI correction artifacts and measurement data to the industry and to the public in general, in addition to the precomputed calibration matrices for an easier reusability [163].

As opposed to the previous works [80–82, 87, 88] we presented in Chapter 2 that rely on commodity hardware for wireless signal measurements, the solution we propose in this chapter relies solely on an off-the-shelf smartphone without any external hardware, hardware modification, or software modification (no rooting and no custom operating system required) on the smartphone. Moreover, we mitigate the inaccuracy of smartphones due to orientation [82] with

a correction technique that uses the Inertial Measurements Units (IMUs) of the mobile device in order to determine the correction power offset which has to be applied.

The rest of the chapter is organized as follows. In Section 4.2, we present our methodology to experimentally collect RSSI values using commodity hardware and open source software. In Section 4.3, we present the results obtained when the methodology is applied to a commercial smartphone, and we analyze the sensitivity of the smartphone RSSI measurements to various parameters and correction techniques. We conclude this chapter in Section 4.4 with some conclusions.

4.2 Methodology

In the following, we present our methodology to perform wireless experiments for LTE, and we extend some of our experiments to Bluetooth in order to show that our findings expand beyond LTE.

4.2.1 Controlled experimental setup

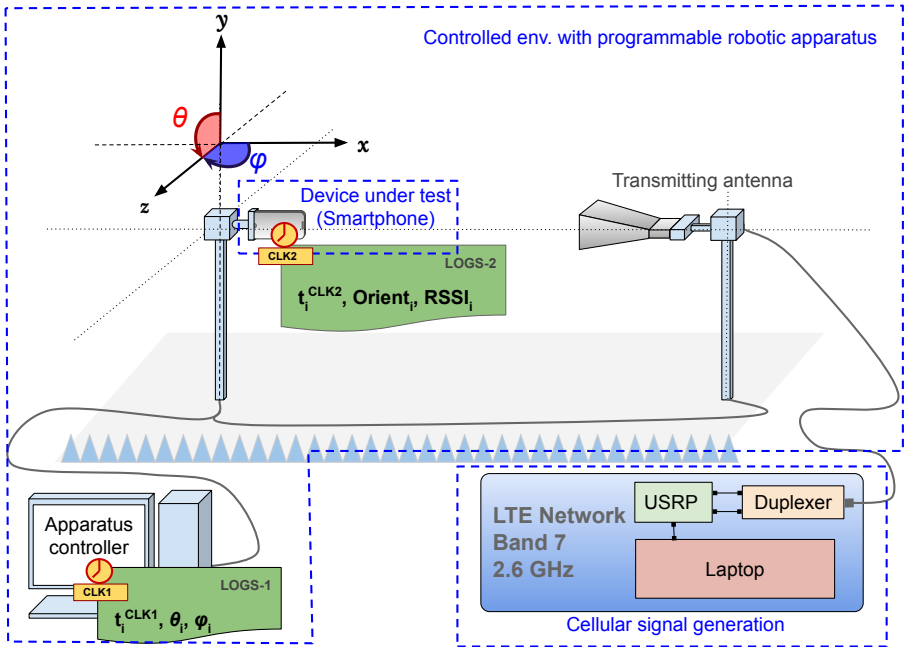

Figure 4.1: The controlled experimental setup. SDR is used for signal generation and a two-axis positioning system is used to rotate the device-under-test in order to study the effect of orientation on the reception performance.

In this section, we present our controlled experimental setup for LTE and Bluetooth experimentation based on commodity hardware and on open-source software [164].

• **LTE signal generation.** Instead of using specialized hardware for the generation of the LTE cellular network signals, we use OpenAirInterface (OAI) [165], a software implementation of an LTE cellular network that can run on general-purpose processors. The Core Network (CN) and the Radio Access Network (RAN) components of OAI usually run on two different machines to ensure real-time performance. As there is no need for Mobile data in our experiments, deactivating it allows us to reduce the computing load on the processor. Hence, both the CN and RAN components can run on the same machine. We use an HP Zbook laptop running Ubuntu 16.04 LTS with Intel i7-6th-gen processor and 32 GB of RAM. We connect the laptop to an Ettus B210 [166] Universal Software Radio Peripheral (USRP). We use a band 7 duplexer to connect both the Rx and Tx channels of the USRP to an ETS-Lindgren's 3115 double-ridged horn Rx/Tx antenna. This is a directional antenna with linear polarization (mono-polarized) having a gain of 10 dB at 2.5 GHz. In our setup, it is called the source or the transmitting antenna, as shown in Figure 4.1.

• **Bluetooth signal generation.** In order to generate the Bluetooth signals, we used two types of devices. We used an Arduino Bluetooth dongle model "Blend Micro" from Red Bear Labs [167]. It uses Bluetooth 4.0 Low Energy. We programmed the dongle to broadcast Bluetooth beacons and connected it through USB for powering. In addition to the Bluetooth dongle, we used a Fossil smartwatch [168] with Bluetooth Low Energy 4.2 and firmware version `HW0.0.2.6r.v1` as a second source. This source is typical of what can be found from a real Bluetooth low energy consumer device. For the Bluetooth experiments inside the anechoic chamber, the Bluetooth dongle is directly mounted to replace the transmitting horn antenna. The dongle generates the Bluetooth signal and transmits it through its own embedded antennas.

• **Device Under Test.** For the device under test, we use a Nexus 5X smartphone running Android 7. To attach the smartphone to the network, we program a SIM card with the authentication parameters that we defined in the OAI database.

• **Controlled environment with programmable robotic apparatus.** We perform our experiment in an anechoic chamber that has programmable robotic equipment both at the transmission and reception sides. As shown in Figure 4.1, the reception platform is a two-axis positioning system that rotates along the two axes x and y: φ (Azimuth, the angle between x and z axes) and θ (Roll, the angle between y and z axes). y can rotate 180° (from -90° to +90°) whereas x can make a 360° rotation. The transmission platform can only rotate along the

x-axis. In Figure 4.1, the transmission system is positioned at φ=0°. By combining the two-axis rotations, we can obtain measurements of the RSSI using the smartphone in different orientations. The reception and transmission are separated by 4 meters and connected to a controller system (Apparatus controller) placed outside of the chamber, which allows us to program the rotation of the platforms by defining the rotation range, the step, and the time duration it remains at each orientation.

4.2.2 Outdoor experimental setup

The controlled experimental setup allows us to perform reproducible experiments with a fine grain control of each experimental parameter. However, in reality, we might have transmission diversity (e.g., for LTE) and multipath transmission due to signal reflections (e.g., for both LTE and Bluetooth).

The goal of the outdoor experimental setup is to assess how the complexity observed outdoor impacts our findings.

• **Cellular outdoor setup.** In order to assess the accuracy of the RSSI measurement from a smartphone with a real LTE base station, we use the same LG Nexus 5x phone described in Section 4.2.1 inside the main transmission lobe of an LTE base station, at a distance of 170 meters. The direction of the main lobe is obtained from the official maps provided by the French National Agency of Radio-frequencies (ANFR) [169]. We lock the smartphone on the same band we had used in the controlled environment, that is on band 7.

We rotate the smartphone on the two axes φ and θ in order to test for different relative orientations between the smartphone and the source. At each orientation, we collect at least 20 RSSI samples and compute the mean value.

• **Bluetooth outdoor setup.** We use a meeting room that contains tables and chairs in order to carry out the Bluetooth experiment in a realistic environment, i.e. in the presence of reflections (by outdoor setup, we mean outside of the anechoic chamber). We place the Bluetooth dongle in the direct line of sight with respect to the smartphone, at a distance of 4 meters, that is the same distance as between the source and the reception in the controlled environment.

We again rotate the smartphone on the two axes φ and θ to test for different relative orientations between the smartphone and the

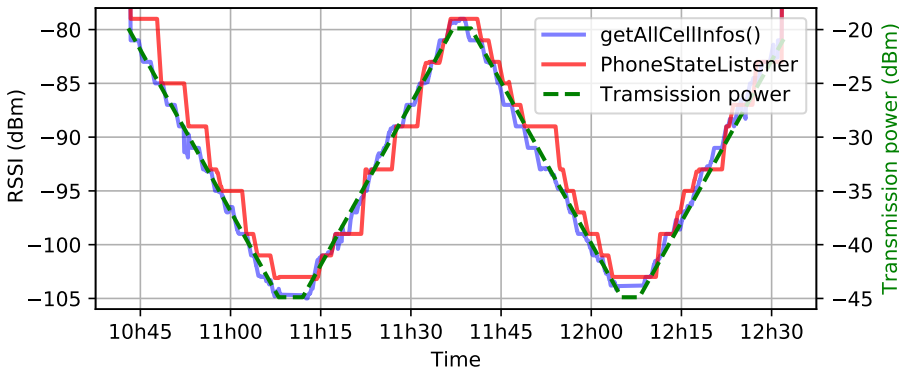

Figure 4.2: Comparing Android API to get the LTE RSSI while varying the Tx power (right y-axis). *The `getAllCellInfos` method (blue line) is more reliable and more sensitive to changes in the signal strength than the `PhoneStateListener` method (red line).*

source. At each orientation, we wait for 1 minute (roughly 5 RSSI samples) and compute the mean value.

4.2.3 Logging the measurements

We log the measurements onto the apparatus controller (*LOGS-1*) and onto the smartphone (*LOGS-2*). The logs are timestamped with the time from the local clock, as shown in Figure 4.1. We synchronize the timestamps in a post-processing phase.

For the smartphone log collections, we use the Electrosmart mobile application [52] in order to collect the Rx power (RSSI) and the device orientation from the IMU sensors.

The apparatus controller creates timestamped logs of the values of its rotation axes each time it reaches a programmed orientation. The values are expressed in terms of φ and θ in degrees. These logs are used as ground true values for device orientation inside the chamber.

4.2.3.1 Getting the LTE RSSI on Android

The Android Application Programming Interfaces (APIs) offer two possibilities to get the LTE RSSI. The two methods are the following.

• **PhoneStateListener** is a callback-based method. It works by registering a listener to monitor the changes in the network signal strength, and get a callback whenever the signal strength changes [170].

• **getAllCellInfo()** is an explicit call to the operating system by invoking the *getAllCellInfo()* method to fetch the most recent signal strength measured by the hardware [171].

The two methods are supposed to report the changes in the signal strength of the network. However, which one is better to monitor the changes in the signal strength? In order to compare between the two methods, we place an LG Nexus 5X smartphone in the anechoic chamber as shown in Figure 4.1. Subsequently, we vary the transmission between -45 dBm and -20 dBm in 1 dB steps, one step per minute. We record the RSSI on the smartphone using the two aforementioned methods. We trigger a call to *getAllCellInfo()* every 1 second. The results are shown in Figure 4.2. The method *getAllCellInfos()* is more sensitive to the changes in the RSSI than the *PhoneStateListener* method. For example, at time 10h45, *PhoneStateListener* keeps giving the same RSSI (-80 dBm) regardless of the fact that the transmission (Tx) power has dropped from -20 dBm to -25 dBm, then it suddenly updates to -85 dBm. In contrast, *getAllCellInfos()* follows exactly every update in the Tx power.

For the rest of this work, we choose the *getAllCellInfos()* method in order to measure the RSSI on the smartphone.

4.2.3.2 Getting the Bluetooth RSSI on Android

The Bluetooth RSSI on Android is obtained by registering a broadcast receiver that listens to events (called *intent* in Android) triggered by the Bluetooth Adapter on the smartphone. Each time a new Bluetooth source is detected, a `BluetoothDevice.ACTION_FOUND` intent is received. We extract the RSSI value from an extra field in this intent called `BluetoothDevice.EXTRA_RSSI`.

4.2.3.3 Getting the smartphone orientation on Android

Android APIs give access to the smartphone orientation using the Rotation Vector Sensor (RVS). RVS is a software sensor that combines many hardware sensors readings (Accelerometer, Magnetometer, and Gyroscope) to estimate the device's orientation in space. The RVS returns a vector that can be transformed into a quaternion of orientation. Quaternions [172] are 4 dimensional complex vectors. They can be averaged by slerping [172] (Spherical Linear intERPolation) and, in contrast to Euler angles, they do not suffer from Gimbal lock, which is a loss of a degree of freedom when representing the orientations in a 3D space [173].

4.2.4 Experimental limitations

For measurement acquisition, we faced some limitations. First, the refresh rate of the smartphone signal strength is in the order of 1 second at the best. This is due to power optimizations restricting the number of messages exchanged between the device's baseband (which has a higher refresh rate) and the Android OS. A higher refresh rate would shorten the time spent collecting the calibration data.

Second, the two-positioner system can only rotate along two axes, which means we cannot test all the relative orientations of the device with respect to the source. This can be solved by rotating the source itself along φ. We limit our study to a subset of relative orientations of the smartphone with respect to the source by considering two polarizations of the source (horizontal and vertical polarizations). All the details about the calibration process we are presenting in this work can be replicated for any different orientations or polarizations without loss of generality.

Last, the LTE RSSI values range from −113 dBm to −51 dBm [174]. Since RSSI values are capped at −51 dBm, we made sure in all our experiments that measurements had never been capped.

4.3 Experimental evaluation of the accuracy of the RSSI measurements from a smartphone

The reception performance of a smartphone can be affected by different parameters such as the device orientation, the source position (the source pointing with its main radiation lobe towards the device), the source orientation (the source no longer pointing with its main radiation lobe towards the device), and the source transmission (Tx) power.

In this section, we start by measuring the reference RSSI that will be a ground true target for the corrected RSSI $\bar{P}$. Subsequently, we explore the sensitivity of the measured RSSI from a smartphone with respect to the device orientation, the source position, the source orientation, and to the source Tx power in a controlled environment. In each scenario, we propose a correction technique to estimate $\bar{P}$. Finally, we evaluate the characteristics of an outdoor environment on the measured RSSI.

Most of our experiments are performed on LTE, but we have also performed some experiments on Bluetooth in order to show how our findings in LTE can be extended to other wireless technologies.

4.3.1 Measuring the reference RSSI

We measure the actual LTE RSSI at the reception point using a spectrum analyzer [175]. We use a horizontal polarization at the source. On the spectrum analyzer we place a horn antenna identical to the transmitting antenna with the same polarization as the source. By removing the antenna gain (10 dB) and compensating for cable loss (1 dB), the RSSI measured at the reception is **-54 dBm**. We call this RSSI *the reference RSSI*.

4.3.2 Evaluating the effect of the device orientation

In this section, we evaluate the accuracy of the smartphone's raw LTE RSSI inside an anechoic chamber for a mono-polarized antenna and quantify the effect of the smartphone orientation with respect to the source on the RSSI.

In order to compare between the smartphone measurements and *the reference RSSI*, we replace the horn antenna at reception with a smartphone. In order to study the effect of the smartphone orientation on the RSSI, we place the device in 684 different orientations along two axis, φ and θ, in front of the transmitting antenna, as illustrated in Figure 4.1. At each position, we collect the RSSI as well as the device orientation.

We keep the device at each orientation for 10 seconds. Then, we average the RSSI and the quaternions measured for each orientation: RSSIs are averaged in Watt and the results are converted into dBm; the orientation is obtained by slerping the quaternions in order to obtain a representative quaternion for each orientation. To verify the stability of the RSSI at each orientation during the measurement period (10 seconds), we compute the standard deviation of the RSSI over time for each orientation. The mean standard deviation of the RSSIs for all the 684 orientations is only 0.06 dBm.

To verify the reproducibility of the measurements, we repeated the same experiment 10 times. For every experiment, we started the experimental process from scratch: we set up the LTE network, we calibrate the orientation sensors of the smartphone [176], we position

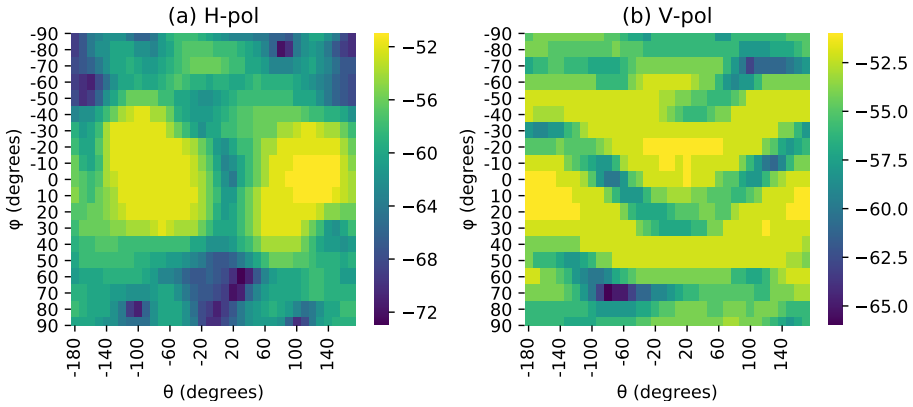

Figure 4.3: Heatmap of the LTE RSSI (in dBm) obtained for the LG Nexus 5X for 684 orientations made for horizontal and vertical polarization of the source. *The reception performance is very sensitive to the device orientation.*

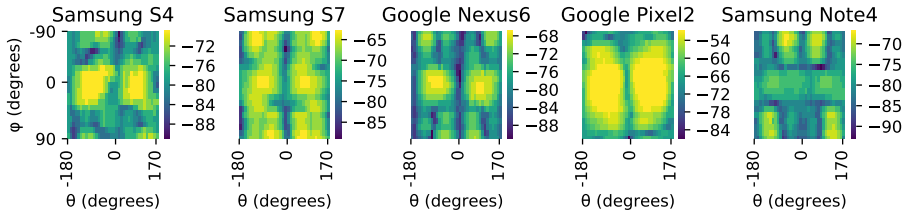

Figure 4.4: Heatmap of the LTE RSSI (in dBm) for 5 different smartphones evaluated using our methodology. *The reception performance is sensitive to the device orientation for all smartphones, but the characteristics of the sensitivity is very different from a smartphone to another.*

it on the two-positioner system, next we launch the controller program to start rotating the device and to collect the measurements. For all 10 experiments, the mean standard deviation of the RSSI for each orientation is 0.51 dBm and 5.5° mean angle error. Finally, we merge all 10 experiments together and, for each orientation, we compute the average RSSI and the mean quaternion. For the rest of our study, we use the resulting averaged RSSIs and orientations. The vertical polarization was also evaluated by repeating the same measurement procedure as described for the horizontal polarization.

By placing the smartphone in 684 different orientations with horizontal polarization, and by measuring the RSSI, we obtain a heatmap of the RSSI shown in Figure 4.3(a). We can see a large variability of the RSSI across the different orientations. The optimal RSSI we measured was −51 dBm at $\theta = +90°$ and $\varphi = 0°$ (same orientation as depicted in Figure 4.1), which is 3 dB more than the reference RSSI (−54 dBm). At some orientations, the reception performance is very poor with a minimum of −73 dBm. The RSSIs for the same 684 orientations, repeated for the vertical polarization are shown in Figure 4.3(b). At this polarization, the RSSI also exhibits a large variability with an offset of 15 dB between the maximum and the minimum RSSI.

In addition to the Nexus 5X, and using the same methodology, we evaluated the reception performance of 5 different smartphones. We tested the Samsung S4, Samsung S7, Samsung Note 4, Google Nexus 6, and Google Pixel 2. We observe in Figure 4.4 that all smartphones

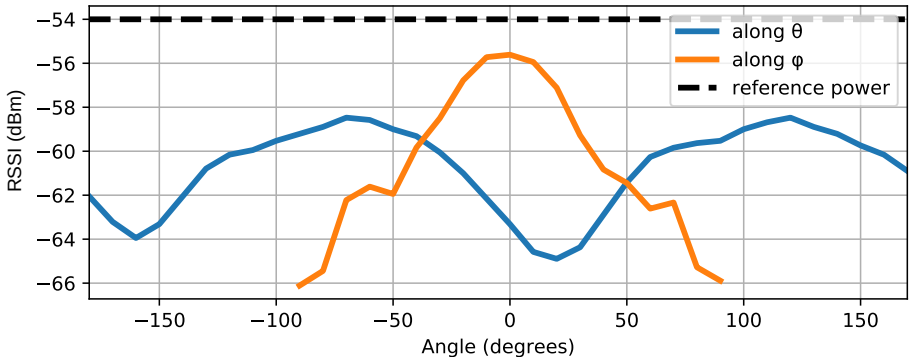

Figure 4.5: Mean LTE RSSI along φ and θ. *The RSSI is optimal when the antenna is in co-polarization with the source (θ = 120° and θ = -60°) and when the smartphone is oriented towards the source (φ = 0°)*

show their measured LTE RSSIs to be largely impacted by the device orientation. However, the reception patterns are very different from one device to another. This difference can be due to many factors, such as the dimensions of the smartphone, the casing, the number of antennas used, and their location within the smartphone.

We also expect to have specific orientations where the RSSI is optimal, this will happen when the smartphone antennas are aligned with the polarization of the source. In antenna theory, *Polarization Matching* [177] (or co-polarization) means that the receiver and the transmitter have the same polarization, thus the power loss being minimal. In contrast, cross-polarization yields minimal power. So by monitoring the RSSI and by knowing the polarization of the source, we can determine at which orientation the co-polarization happens.

In order to determine the polarization scheme of the smartphone, we plot the mean RSSI along the two axes of rotation as shown in Figure 4.5. Along φ axis, the maximum power is received when the smartphone is in the main transmission lobe ($\varphi = 0°$). We also see that the maximum power along θ is produced at angles +120° and -60°, and lowest reception occurs when the smartphone is rotated by 90° along θ. Hence, smartphone antennas are affected by their relative orientation with respect to the source and the optimal performance is observed when their polarization matches the polarization of the source.

For the rest of this work, and for the sake of simplicity, we assume that the source polarization does not change and that it is known beforehand (in practice, we only consider the horizontal polarization). This might not be true in practice, but we can deduce the polarization of the source using the property of polarization matching, that is by placing the device in different polarizations, by monitoring orientations with optimal RSSI, and by knowing the characteristics of the reception pattern of the smartphone. This procedure to find the source polarization can be performed using our mobile application prototype [163].

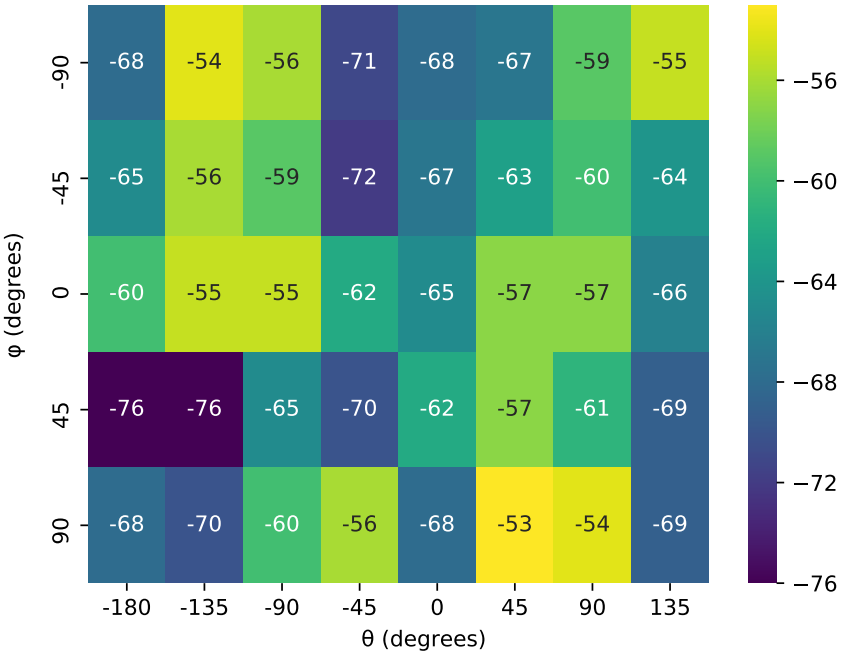

Figure 4.6: Heatmap of the Bluetooth RSSI (in dBm) obtained for the LG Nexus 5X for 40 orientations in a controlled environment. *The reception performance is also sensitive to the device orientation for Bluetooth.*

Finally, in order to validate that our results expand beyond LTE, we explored the effect of the device orientation for Bluetooth RSSI measurements. We used the Arduino dongle as the source in our experimental setup, and we rotated the smartphone using the two-axis positioning system. In Figure 4.6 we show the RSSI measured for the 40 different orientations which have been measured. We can see that the measured Bluetooth RSSI is also very sensitive to the device orientation with up to 23 dB difference between the minimum (-76 dBm) and maximum (-53 dBm) measured RSSI. This proves that orientation does also affect the RSSI accuracy for the Bluetooth power measurements.

In summary, the measured RSSI from COTS smartphones is sensitive to the device orientation. This sensitivity holds for multiple devices and for different wireless technologies.

4.3.3 Correcting the effect of the device orientation

In this section, we show that it is possible to correct the effect of the device orientation on the measured LTE RSSI. We use the orientation sensors of the smartphone to build calibration matrices, which are used to compute a correcting factor which is subsequently applied to the measured RSSI for each orientation

Let Q be a matrix of orientation Quaternions, and let P be a matrix of RSSI having the same dimensions as Q. We call them calibration matrices. In order to build these matrices, we rotate the smartphone

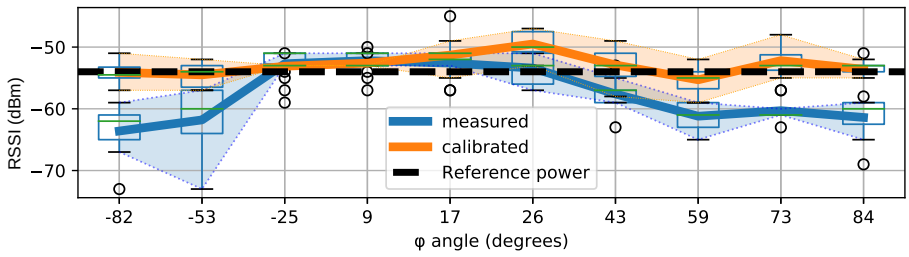

Figure 4.7: RSSI correction results for the 100 random orientations along θ and φ. The colored area represents the variability of the measurements along θ. *The corrected RSSI (orange) is closer to the reference RSSI (black dashed line), and less variable (2.4 dBm RMSE) as compared with the raw measured signal (shown in blue, with 6.4 dBm RMSE).*

as shown in Figure 4.1, and for each orientation, we fill up the matrix Q with the measured quaternion, and the matrix P with the offset between the raw measured RSSI at a given orientation and the reference RSSI we measured in Section 4.3.1. Therefore, in the element with coordinates *(i, j)* in matrix Q we have an orientation, and in the element with the same coordinate in matrix P we have the offset to be applied to the measured RSSI for the specific orientation stored in matrix Q. Once we have these two matrices, whenever we place a device in the orientation defined by a given quaternion q_i, we compare it against all the quaternions in Q and we compute the relative angle. The closest quaternion in Q is the one with minimal angle to q_i. We use its coordinates in Q to obtain the corresponding correction offset from P and apply it to the raw measured RSSI to obtain the corrected RSSI.

To validate this correction technique, we built the calibration matrices by placing the device at θ = -180° and φ = -90°. Subsequently, we varied θ from -180° to +170° in 10° steps. We did that for every φ ranging from -90° to +90° in 10° steps. At each step, we collected the RSSI and the rotation quaternion. Next, we inserted them into the matrices with the corresponding φ and θ coordinates. The dimensions of the matrices P and Q is 36x19*.

As a next step, we selected 100 random orientations for the device under test by computing 100 random couples (φ, θ) selecting 10 random values for φ within the range [-90°, +90°] and 10 random values for θ within the range [-180°, +170°] that were not in Q. Our goal is to obtain random coordinates which do not have an exact match in Q. The source polarization and Tx power are kept unchanged.

In order to correct the measured RSSI at a random orientation, we

* We computed calibration matrices for 5 additional devices: a Samsung S4 and S7, a Nexus 6, a Pixel 2, and a Note 4. We do not discuss the details of these other devices in the rest of this chapter, since they provide us with similar conclusions, however we make all these matrices publicly available [163] so that the interested reader can easily reproduce our results for different devices.

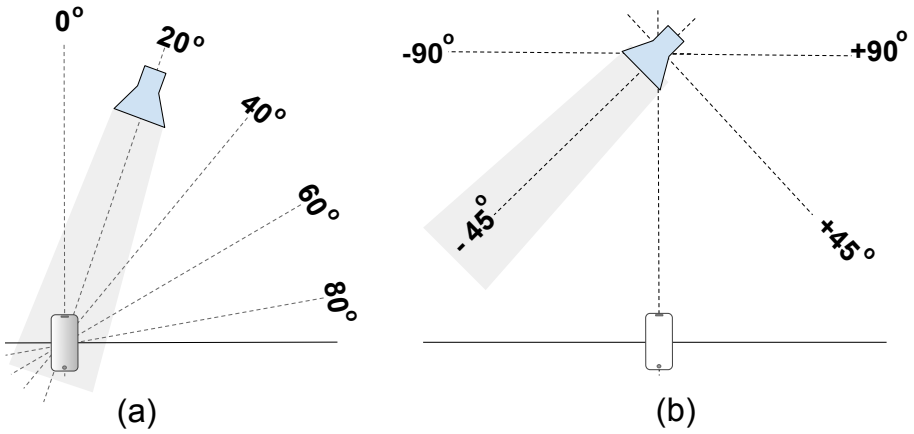

Figure 4.8: (a) Changing the source's position with respect to the smartphone. (b) Pointing the source's main lobe at different angles with respect to the smartphone.

compare a given quaternion against all quaternions in Q to get the closest quaternion and its corresponding coordinates in Q. We use these coordinates to get the RSSI offset in P which allows us to correct the measured RSSI. Figure 4.7 shows that the corrected RSSI (orange line) is closer to the reference RSSI (dashed black line) and has a lower variability than the raw RSSI (blue line). In particular, the raw RSSI RMSE is 6.4 dBm, whereas the corrected received RSSI RMSE drops to 2.4 dBm.

In summary, our proposed technique for correction of the effect of the device orientation on the LTE measured RSSI significantly improves the measurements accuracy. The RMSE error is reduced by 4 dB.

4.3.4 Evaluating and correcting the effect of the source position

In this section, we consider the case where the source's location with respect to the smartphone is unknown, but the distance to the source is kept constant and the smartphone remains in the main transmission lobe of the source, see Figure 4.8(a).

To evaluate the impact of the source position on the measured RSSI, we rotate the source at 20°, 40°, 60°, and 80° from the original orientation along the azimuth (φ). We make sure that the source is shifted by the correct angle and that the smartphone is kept within the main transmission lobe by means of a laser beam. At each new position, we measure the reference RSSI using a spectrum analyzer.

Next, we test whether we can reuse the calibration matrices obtained in Section 4.3.3 to correct the RSSI. Figure 4.9 shows the RSSI patterns for all the tested angles. We see that the patterns seem to be a shifted

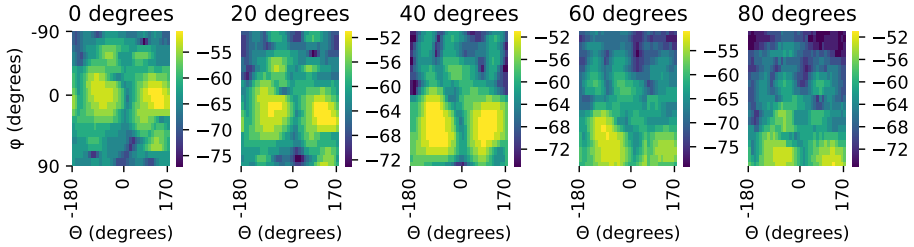

Figure 4.9: Heatmap of the LTE RSSI of the Nexus 5X when the source is placed at different angles. *The reception patterns are a shifted versions of the pattern at 0° with the corresponding angle change in source position.*

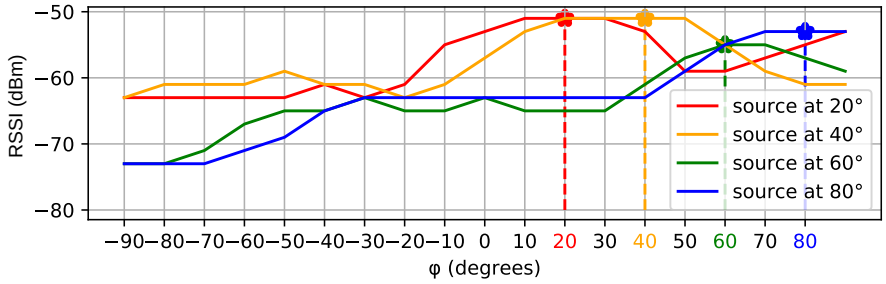

Figure 4.10: Sweeping along the φ axis to locate the source. *The source position is found when maximum RSSI is measured*

version of the reception pattern at 0°. Hence, the reception pattern should be preserved regardless of the source position with respect to the smartphone. To validate this hypothesis, we test the impact of shifting the calibration matrices we had collected when the source was at φ=0° in order to correct the measured RSSI at any angle. In order to compute the matrix shifting we have three steps: i) locating the new position of the source, ii) defining the angle shift from the φ=0 position to the new source position, iii) translating the calibration matrix of orientations Q to adapt it to the new source.

In order to locate the source, we use the property of polarization matching we have described in Section 4.3.2, where the reception is maximum when both the transmitting and the receiving antennas are aligned and co-polarized. Our method is as follows. First, we assume that the source polarization is known, and we place the smartphone in the same polarization. Second, as illustrated in Figure 4.5, and since the smartphone receives more power when θ is +120° or −60°, so we place the smartphone at θ = +120°. Finally, we rotate the phone along the φ axis from −90° to +90° and collect the RSSI for each value of φ. The source's position is determined when we measure the maximum RSSI at an angle $\varphi = \varphi_m$. We can see in Figure 4.10 that the RSSI increases gradually as we point the smartphone closer to the new source location. The maximum RSSI is received when the smartphone is directly aligned with the source along the azimuth (φ), for instance, the red curve corresponding to the scenario with a source rotation of 20° has its maximum when φ is at 20°. This procedure to locate the source can be performed using our prototype mobile application for calibration [163].

Once we have located the source, we need to transform and shift the

matrix of orientation quaternions Q in order to adapt it to the new source position. We apply quaternion rotation using the relative quaternion describing the rotation from $\varphi = 0°$ to $\varphi = \varphi_m$, that is the new source position in the azimuth. Once Q is transformed, we can apply the correction to the measured RSSI using the technique previously presented in Section 4.3.3.

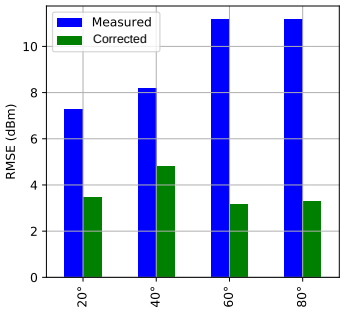

Figure 4.11: RMSE for different source positions between the reference RSSI and the raw RSSI measurements (in blue), and between the reference RSSI and the corrected RSSI measurements (in green). *The impact of the source position on the measured LTE RSSI can be corrected.*

Figure 4.11 shows the RMSE as compared to the reference RSSI for the raw measurements (in blue) and for the corrected ones (in green). We can see that a modification of the source position can significantly increase the RMSE (up to 11.1 dBm at 80°). However, we see a significant improvement of our correction technique when the source position is unknown with an RMSE between 3.3 dBm and 4.8 dBm, so an average reduction in RMSE of 5.7 dB.

In summary, when the smartphone is within the main transmission lobe of the source, but the source position is unknown, the measured LTE RSSI is a shifted version of the measured RSSI when the source is in front of the device. However, we have presented a correction technique that allows us to correct a large fraction of the measured LTE RSSI error, with an average reduction in RMSE of 5.7 dB.

4.3.5 Evaluating and correcting the effect of the source orientation

Now, we consider the case where the source is no longer within the main transmission lobe. In Figure 4.8(b) it can be seen that the main lobe is pointed at different angles with respect to the smartphone. At each angle, we rotate the smartphone along φ and θ in order to collect the RSSI. Figure 4.12 shows the heatmap of the RSSI in all tested cases. Unsurprisingly, we see that the measured RSSI is sensitive to the main lobe orientation.

We try to correct the RSSI when the source's main lobe is not directed towards the smartphone using the calibration matrices P and Q computed in Section 4.3.3, when the smartphone is in the source main lobe, without any modification.

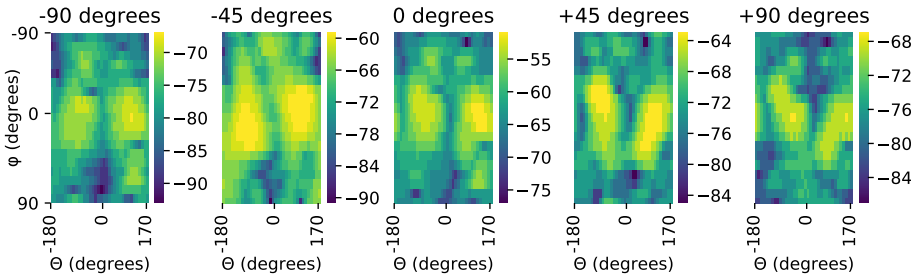

Figure 4.12: Heatmap of the LTE RSSI of the Nexus 5X for different orientations of the main lobe. *The reception patterns are impacted by the orientation of the source main lobe.*

Figure 4.13 shows the RMSE between the raw measurements and the reference RSSI (in blue), and between the corrected measurement and the reference RSSI (in green). The rotation of the source's main lobe significantly increases the RMSE, which ranges between 6.8 dBm and 8.6 dBm. Our correction technique, consisting in applying the calibration matrices without any modification successfully reduces the RMSE, now ranging between 3 dBm and 4.7 dBm, i.e. an average reduction in RMSE of 4.1 dB.

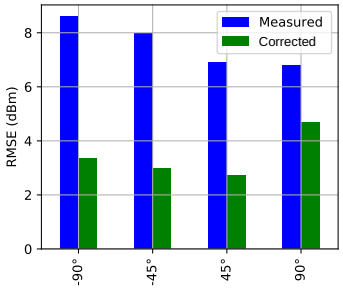

Figure 4.13: RMSE for different source orientation of the main lobe between the reference RSSI and the raw RSSI measurements (in blue), and the reference RSSI and the corrected RSSI measurements (in green). *The impact of the source orientation on the measured LTE RSSI can be accounted for and corrected.*

In summary, the orientation of the source's main lobe has a significant impact of the measured LTE RSSI. The proposed correction technique, consisting in applying the unmodified calibration matrices, can reduce the RMSE on average by 4.1 dB.

4.3.6 Evaluating and correcting the effect of the source Tx power

In this section, we consider a change in the source transmitted (Tx) power[†]. The position of the source and its polarization are the same as in Figure 4.1. We consider three different transmission power levels: Tx1 is the transmission power used in all the previous experiments, Tx2 is Tx1 reduced by 10 dB, Tx3 is Tx1 reduced by 20 dB. In order to achieve this reduction in transmitted power, we change the transmission attenuation parameter `att_tx` found in the configuration file of OAI. For each Tx power, we measure the reference RSSI at the receiver as explained in Section 4.3.1. We measure −54 dBm, −64 dBm, and −74 dBm for Tx1, Tx2, and Tx3, respectively. For each Tx power, we collect the RSSI measurements using the same procedure as described in Section 4.3.3, i.e. by rotating the smartphone along θ and φ. Figure 4.14 shows the received patterns for the three different Tx power levels defined before. Unsurprisingly again, we see that the RSSI measurements are impacted by the Tx power.

[†] Note that we can extend the results of this section to a modification of the distance to the source, as increasing the distance to the source is equivalent to reducing the transmitted power.

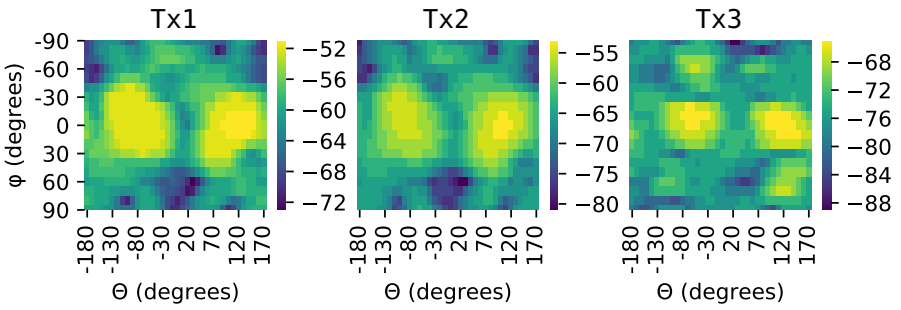

Figure 4.14: The measured RSSI by the Nexus 5X for different Tx power levels. *The reception patterns are impacted by the source Tx power.*

Similarly to what we did in Section 4.3.5, we try to correct the RSSI with the calibration matrices P and Q previously computed in Section 4.3.3, when the source is emitting a Tx power level TX1, without any modification.

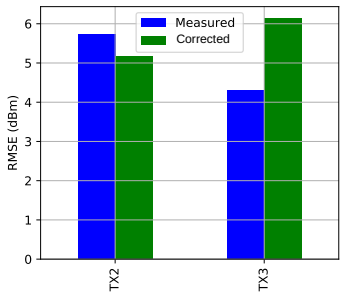

Figure 4.15: Root Mean Squared Error (RMSE) for different source Tx power between the reference RSSI and the raw RSSI measurements (in blue), and the reference RSSI and the corrected RSSI measurements (in green). *The impact of the source Tx on the measured LTE RSSI cannot be corrected with the mere application of the calibration matrices.*

Surprisingly enough, this correction technique fails to improve the mean RMSE. Indeed, Figure 4.15 shows that for the corrected measurements the RMSE corresponding to Tx2 is slightly decreased, but it is increased for Tx3. The average RMSE for the corrected measurements is increased by 0.6 dB.

The reason for this effect is that changing the Tx power affects the reception patterns of the smartphone. Indeed, in LTE, smartphones work with a Multiple Input Multiple Output (MIMO) technology. Depending on the network quality, the smartphone can select a single antenna or it can combine the different antennas to optimize the received signal power [178]. This is called antenna diversity. There exist different techniques for diversity combining [179]. The smartphone may use only one of the antennas for reception (switched diversity) or it can combine the incoming signal from all antennas according to their respective Signal-to-Noise Ratio (SNR), a technique called Maximum Ratio Combining (MRC). This antenna diversity significantly complicates the correction process since there is no previous knowledge about which calibration matrix should be used for the measured RSSI.

In order to deal with this issue, we evaluate the performance of two

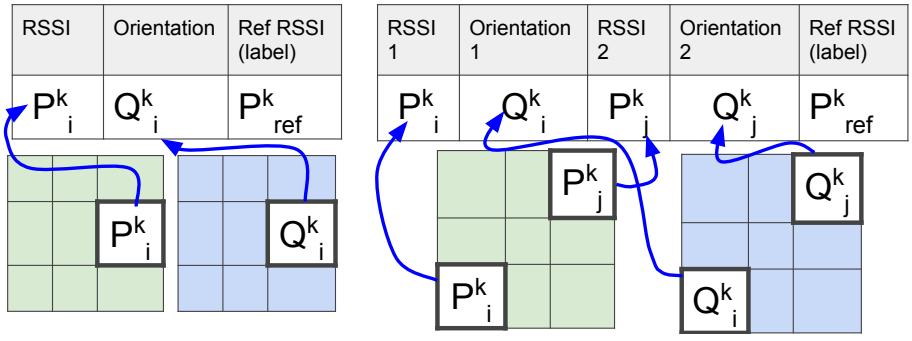

Figure 4.16: ML models for RSSI corrections. One-couple (left) and Two-couple models (right). The model maps the raw RSSI in each orientation to the reference RSSI corresponding k^{th} Tx power.

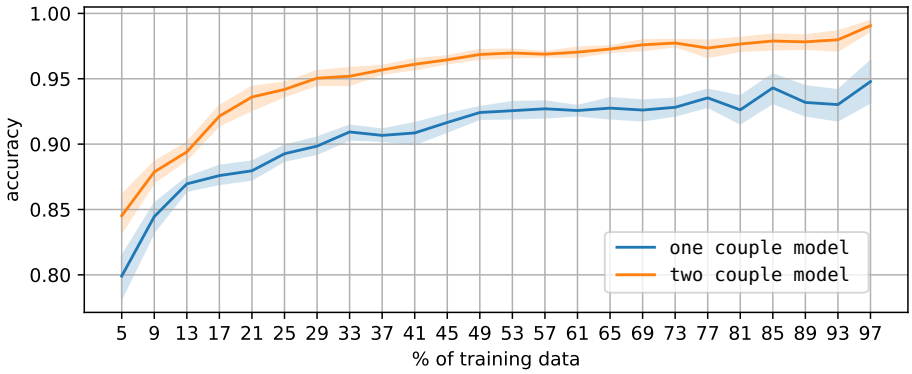

Figure 4.17: Random Forest accuracy for selection of the right RSSI for different amounts of training data. The average (solid line) over 10 independent trainings is computed together with its uncertainty interval for a 95% level of confidence (colored area). *Even a moderate amount of training is enough to have a good accuracy.*

machine learning models based on a Random Forest algorithm to predict the correct RSSI. The first one uses as features one couple *(RSSI, device orientation)* at a time selected from one of the reception pattern matrices presented in Figure 4.14 and labelled with the reference RSSI for this matrix. The second one uses as feature two *(RSSI, device orientation)* couples at a time selected independently from the same calibration matrix labelled with the known reference RSSI for this matrix. The machine learning model building process is illustrated in Figure 4.16. The illustration shows how in the one-couple model, one point at a time is taken from the reception patterns (P) and orientation (Q) matrices, then labelled with the correct reference RSSI (P^{k}_{ref}). Whereas, in the two-couple model, two points at a time are taken from both matrices, and labelled with the reference RSSI corresponding to the given Tx power. The two-couple model captures more features of the smartphone's reception pattern, which allows the model to distinguish with higher accuracy which transmission power the received pattern corresponds to. After training the models, we take one test orientation (in case of the one-couple model) or two test orientations (in case of the two-couple model).

In order to perform the evaluation, we train the model with X% of the couples (or pairs of couples), X ranging from 5% to 97% in 4% steps. The remaining data is used for cross-validation. For each X, we repeat the training 10 times with another uniformly distributed random subset of X% of couples (or pairs of couples).

The accuracy of the model to give the correct RSSI is shown in Figure 4.17. It can be see that with 30% of training data, the model can predict with 90% accuracy the reference RSSI with the one-couple model (blue curve). The accuracy increases to 95% if we use the two-couple model (orange curve). Even with 5% of training data, the accuracy is 80% for the one-couple model. This means that a simple Random Forest model can capture the reference RSSI from a single measurement with high accuracy even with a small amount

of training data.

In Summary, we have shown that the source transmission power has a significant impact on the accuracy of LTE RSSI measurement with a RMSE up to 5.7 dBm due to antenna diversity optimizations on the smartphone. However, we can dramatically improve the accuracy by using machine learning with a simple Random Forest model and with minimal training. We have shown that a 90% accuracy can be achieved with 30% training and using a one-couple model.

4.3.7 Evaluating the effect of an outdoor environment

So far, we have evaluated the RSSI accuracy of a smartphone in a controlled environment with a mono-polarized emitting antenna. In this section, we evaluate the accuracy of the RSSI with a multi-polarized antenna in an outdoor environment with reflections and multipath. Moreover, the LTE base stations nowadays make use of transmission diversity, such as spatial diversity and polarization diversity where the signal is transmitted at two perpendicular polarizations from an antenna array in order to improve cellular reception. Polarization diversity provides a gain of up to 12 dB as compared to single polarization [180]. In Figure 4.18(a), we show a typical sector antenna's interior used at a base station. We can see the arrangement of multiple antennas with vertical and horizontal alignment in order to achieve polarization diversity and thus to minimize the polarization mismatch at reception.

In order to assess the accuracy of the RSSI measurement from a smartphone under these conditions, we follow the methodology already described in Section 4.2.2, and we place the smartphone in 88 different orientations along the two axes φ and θ (which are a subset of the 684 orientations we tested in the controlled environment) inside the main transmission lobe of an LTE base station, see Figure 4.18(b). We compute the variability of the measurements collected outdoors, and we compare it to the variability of the measurements collected in the controlled environment with a mono-polarized source, for the same set of orientations.

In Figure 4.18(b), we can see that the measurements collected outdoors are less variable than those we obtained in the controlled environment. The median variability is about 4 dB outdoors, as compared to the 12 dB variability in the controlled environment. We perform two additional independent experiments with a different subset of orientations using the same experimental arrangement,

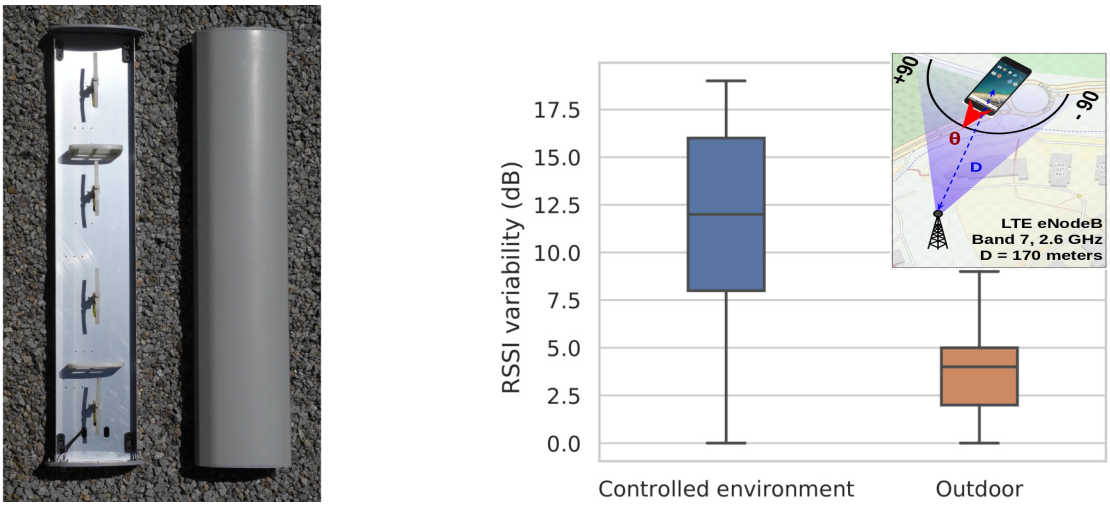

Figure 4.18: (a) Interior of sector antenna (MIT Computer Science & Artificial Intelligence Lab). (b) Outdoor evaluation results.

and both confirm that the LTE RSSI outdoors is less variable and less affected by the orientation of the smartphone than the LTE RSSI in controlled environment.

Since the LTE base station transmits the same signal at two perpendicular polarizations (vertical and horizontal polarizations), the smartphone antennas can compensate for the errors introduced by the radiation patterns by means of a more efficient combination of signals coming from multiple antennas. Therefore, the polarization diversity used at transmission minimizes the chance of polarization mismatch (cross-polarization). Hence, the effect of orientation on the RSSI in an outdoor environment is minimized (low directivity).

In Section 4.3.2 we have seen that the Bluetooth RSSI measurements are also sensitive to the device orientation. However, Bluetooth does not use the technique of transmission diversity. For this reason, we have evaluated the impact of the device orientation in an office environment (described in Section 4.2.2) for two different types of sources: an Arduino dongle and a smartwatch.

Figure 4.19 shows the measured Bluetooth RSSI and its variability with the smartphone orientation. We can see that the orientation has a large impact on the measured Bluetooth RSSI in a realistic environment for both types of sources. Interestingly enough, we observe that the minimum measured RSSI is not obtained for the same orientation. This is due to a different polarization of the two sources.

In summary, in outdoor (uncontrolled) environments, transmission diversity succeeds to compensate most of the effect of the

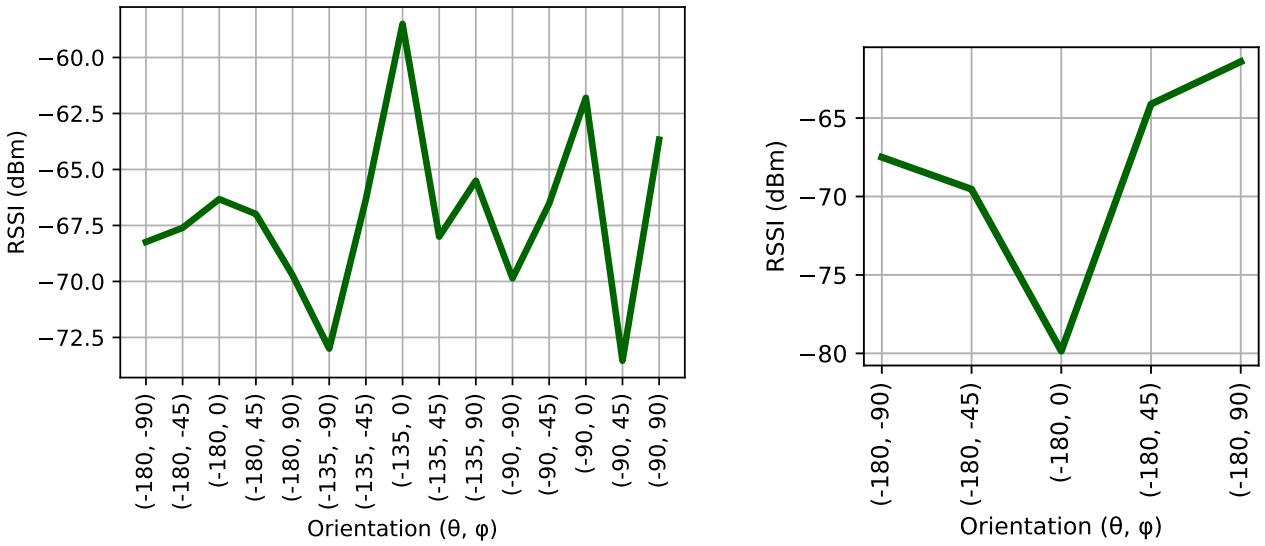

(a) Arduino Bluetooth source

(b) Smartwatch source

Figure 4.19: Sensitivity of the Bluetooth RSSI to the device orientation in an office environment. *We observe a large variability of the RSSI with the device orientation for both sources.*

device orientation on the measured LTE RSSI. However, for Bluetooth, since it does not make use of transmission diversity, even in outdoor environments, the smartphone orientation has a large impact on the measured Bluetooth RSSI.

4.4 Conclusions

In this work, we have evaluated the performance of a Commercial Off-The-Shelf (COTS) smartphone for RSSI measurements. We have three main take-home messages. First, a COTS smartphone cannot be used out of the box to perform accurate RSSI measurements with a mono-polarized source in a controlled environment since these measurements are highly sensitive to the smartphone orientation, source position, source orientation, and to the source transmission power. Second, we propose efficient correction techniques based on the IMU sensors embedded in the smartphone to correct the RSSI measurements for all the conditions which have been evaluated and described here. With these techniques, we can reduce the RSSI RMSE to less than 5 dBm. Third, in an outdoor (uncontrolled) environment, transmission diversity (a technique that can be found, for instance,in 4G base stations), succeeds to mitigate the problem of accuracy due to the smartphone orientation. However, for protocols, such as Bluetooth, that do not support transmission diversity, the RSSI measurements are still highly sensitive to the device orientation.

In this work, we have mainly focused on LTE RSSI measurements, but we also extended our results to Bluetooth. In particular, we showed that Bluetooth RSSI measurements are sensitive to the device orientation even in realistic environments. The correction techniques we developed and described here for LTE should be evaluated for its use with Bluetooth in future investigations.

With the recent development of proximity tracking to help reducing the propagation of the COVID-19 disease, the need to perform accurate Bluetooth RSSI measurements becomes even more important. We do believe that this work provides a ground basis to build more accurate proximity estimations based on RSSI measurements.

Longitudinal Study of Exposure to Radio Frequencies at Population Scale

5

Evaluating population-scale exposure to the radio frequencies used in wireless telecommunication technologies is important for conducting sound epidemiological studies on the health impacts of these radio frequencies [181, 182]. Numerous studies have reported population exposure, but have used very small population samples, ranging from a single volunteer to a few hundred subjects. In this context, the real exposure of the population to radio frequencies remains subject to controversy [34, 183–185]. Here, to the best of our knowledge, we report the largest crowd-based measurement of population exposure to radio frequencies produced by cellular antennas, Wi-Fi access points, and Bluetooth devices for 254,410 unique users in 13 countries from January 2017 to December 2020. All measurements were obtained from the ElectroSmart Android app [52], which instruments a smartphone's baseband, and we applied a thorough methodology to clean and consolidate the measurements. We show that total exposure has been multiplied by 2.3 in the four-year period considered, with Wi-Fi as the largest contributor. The cellular exposure levels are orders of magnitude lower than the regulation limits and not significantly impacted by national regulation policies. Therefore, the mere comparison of exposure levels to regulation limits is a poor way to describe the real evolution of exposure. The population tends to be more exposed at home; for half of the study subjects, personal Wi-Fi routers and Bluetooth devices contributed to more than 50% of their total exposure. We make our dataset publicly available to provide a starting point for sound epidemiological studies on the health impacts of radio frequencies. We also believe that our unique dataset will be invaluable for several other fields interested in population exposure to radio frequencies or the usage of wireless communication technologies.

The long-term impact of radio frequencies on health is a long-standing scientific question that is well illustrated by the classification of radio frequencies as a Group 2B carcinogen by the WHO [186]. This classification means that *there is some evidence that it can cause cancer in humans but at present it is far from conclusive*. [187] Total exposure to various sources of radio frequencies is considered a critical factor for mitigating health hazards, but in the wild, this exposure varies greatly with time and among individuals. Environmental and behavioral factors play a role, as previous assessments have shown[51, 56, 57, 59–69, 79, 188, 189], limiting the generalizability of

results obtained from small study-groups or sparsely instrumented measurements. We present here the first longitudinal analysis of exposure events on a large subject population; results span four years, from approximately a quarter-million unique subjects in 13 countries across Europe, the Americas, Asia, and Australia. The scale of our study allows us to offer the first generalizable findings on critical epidemiological questions regarding the growth of radio exposure worldwide and the respective contributions of different technologies to this growth. We also consider the effectiveness of regulation and some of the factors within an individual's control that affect exposure. Beyond these advances, the release of our data (in a form rendering users unidentifiable) can facilitate large-scale epidemiological studies on the impact of radio frequencies. The data were collected using the crowdsourcing Android app Electrosmart [52] that we developed to instrument a smartphone's baseband and report Received Signal Strength Indicators (RSSI) for radio frequencies received from cellular infrastructures, Wi-Fi access points, and Bluetooth devices. Our dataset includes the exposure of 254,410 unique persons from January 2017 to December 2020.

5.1 Methods

Figure 5.1: Electrosmart mobile application interface.

This study relies heavily on the quality of the data we collected. In this section, we present our data collection methodology, the dataset we collected, and the cleaning we applied to this dataset.

5.1.1 Data collection

The ElectroSmart measurement app

ElectroSmart [52] is an Android consumer app we designed to measure the power that a given smartphone receives from Wi-Fi access points, Bluetooth devices, and cell towers. To reach a large audience, we put a great deal of effort into the user experience, designing ElectroSmart to be an easy-to-use tool that offers users transparent information on their exposure to radio frequencies. ElectroSmart can be installed on any Android smartphone running Android 4.1 or later. The app was first launched in August 2016, and as of May 18th, 2021, it had 900,000 downloads and 190,000 active users.

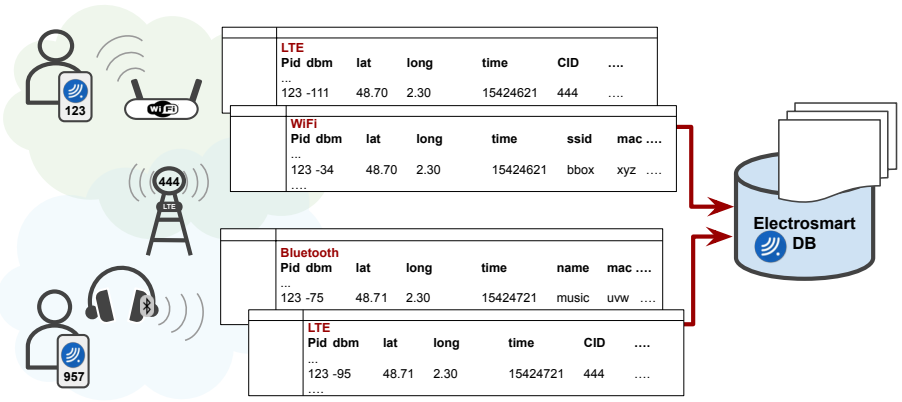

Figure 5.2: Electrosmart data collection

ElectroSmart performs an *exposure scan* every 20 minutes when used in the background. All scans are periodically collected on our servers. Below, we explain how an exposure scan works and describe the information it collects. We discuss user consent and privacy protection in the following section. A scan performs the following actions.

- It creates a timestamp with the local time in UTC. This is a slight approximation as signals might not be measured at exactly the same time in a given measurement scan. However, by considering a window of a few seconds, it is easy to attribute all measured signals to a given measurement scan and timestamp (we specifically discuss the case of Bluetooth in the section *Bluetooth scan synchronization*).
- It collects characteristics of the smartphone (brand and model) and its Android version.
- It measures the smartphone location in terms of latitude and longitude. Android provides this information by combining GPS, Wi-Fi access points, and cell tower information using a proprietary algorithm.
- It measures the *downlink* Received Signal Strength Indicator (RSSI) of all measurable Wi-Fi access points, Bluetooth devices, and cell towers (we discuss limitations below), along with several source-specific data.
    - For Wi-Fi access points, we collect the SSID, the BSSID, the frequency, and whether the user is connected to this access point.
    - For Bluetooth devices, we collect the device name, the device MAC address, and whether the user is bonded to this device.
    - For cell towers, we identify whether the cell is using a 2G, 3G, 4G, or CDMA/EVDO technology. We determine whether the cell is serving (that is, the user is currently

Table 5.1: Valid range of the RSSI (in dBm) for each wireless protocol.

	Wi-Fi	Bluetooth	Cellular (2G, 3G, 4G)
Max	-1	-1	-51
Min	-126	-150	-113

connected to this cell), and we collect cell identification information, such as the Mobile Network Code (MNC), Mobile Country Code (MCC), or Cell ID (CID), to generate a unique identity for each cell tower.

Ethical and legal considerations

We submitted the study protocol to our institutional ethical committee (Inria COERLE [190]). They provided guidelines for respecting user privacy, consent, and data protection.

ElectroSmart requires explicit user consent for all information collection. In particular, we are fully compliant with the European General Data Protection Regulation (GDPR) [191].

In addition, ElectroSmart is used anonymously by default, unless a user decides to provide an email address. The email address field is clearly identified as optional.

All scans are associated with a unique user ID. This user ID is randomly generated on our server at the app installation time. It is not linked to any unique smartphone or user information.

Limitations

We perform all scans with a vanilla version of Android using the regular Android API. That is, we do not have access to low-level data available from rooted smartphones or customized drivers. This approach is beneficial for targeting a large-scale audience, but it limits what we can measure, as elaborated below.

First, we only measure the downlink received by the measuring smartphone. Therefore, the contribution of the uplink to the exposure, that is, the emission of the measuring smartphone, is not considered in this study. Also, we do not measure the uplink of surrounding devices.

Second, the minimum and maximum measurable power for each wireless technology is capped by the Android API and the technology standards. We show in Table 5.1 the valid ranges of measurements for each technology. For example, if a smartphone is exposed

to a higher power than the maximum measurable power, it will always report the maximum value presented in Table 5.1. We explain in *Dataset Cleaning* how we filter out-of-range scans.

Third, for 2G, 3G, and 4G, the RSSI is provided by the Android API as an *Arbitrary Strength Unit* (ASU), an integer value between 0 and 31. It is converted to dBm according to the formula: $\text{dBm} = \text{ASU} * 2 - 113$. For this reason, the granularity of the cellular RSSI is 2 dB.

Fourth, each wireless technology comes with some additional limitations. Bluetooth sources can only be measured when they are *discoverable*. Wi-Fi sources can only be measured when they are configured as access points, that is, the emitting power of the connected devices is not measured. Measurements of cellular sources suffer from several limitations. i) A smartphone with an active SIM card can only measure the RSSI from the operators declared in the SIM card. In practice, it is either the cellular operator that owns the SIM card (MNO), the cellular operator that is operating the cellular infrastructure for the virtual operator (MVNO), or the operators that partner with the MNO of the SIM card in foreign countries (Roaming). We explain in the Dataset Processing section how we mitigate this issue. ii) The measurement coverage is largely dependent on the version of Android and the cell phone maker. Indeed, the Android API can return the RSSI of the serving cell for all smartphones, but only the most recent versions of Android can also return the neighboring cells' RSSI. In addition, this API tends to be quite buggy due to the Android RIL (Radio Interface Layer, which is closed-source and vendor-specific. In particular, some smartphones return invalid RSSI measurements (outside of the range given in Table 5.1). We discuss in *Dataset Cleaning* how we identify and remove invalid measurements. iii) Smartphones periodically scan for cellular networks to ensure continuity of service. To speed up network scanning, smartphones follow priority rules that are defined by the network and stored in the SIM card. This means that a given smartphone may not scan for all the cellular Radio Access Technology (RAT), but instead, scan only high priority RATs. For example it may scan only 4G and 3G networks, excluding 2G. As a result, we expect the cellular scans not to include all the cellular generations in a single scan.

Last, the received power is measured using the Received Signal Strength Indicator (RSSI). Therefore, our measurements do not take into account the effective load of the wireless channel.

5.1.2 Dataset characteristics

In this study, we use all the exposure scans collected from January 2017 to December 2020 (4 years) representing 506,100 user profiles and 6,438 million measured RSSI.

We first clean this raw dataset as follows: i) we remove all measurements with invalid GPS coordinates, ii) we remove all measurements with invalid RSSI values, iii) we keep only measurements from the 13 countries with the largest number of measurements, iv) we remove all CDMA/EVDO measurements.

Then, we process the remaining measurements: v) we convert all timestamps to the local time of the country of origin, vi) we identify the Wi-Fi physical sources, vii) we attribute each Bluetooth measurement to an atomic scan. The following sections detail each of these seven steps.

Dataset cleaning

Invalid GPS coordinates removal Background measurements are quite fast (typically a few seconds). There is usually not enough time to get a valid GPS coordinate from scratch, that is, when the GPS was not activated before the scan or when no prior information is cached to help the GPS converge faster to a location. However, location is a system-wide property, so if another app or the system has recently accessed the device location, we will benefit from this when we make the scan. Also, when the device is not power-constrained, we can allow more time to get a valid GPS location.

When a GPS coordinate cannot be retrieved in the ElectroSmart app, we set both the latitude and the longitude associated with a scan to either 0 or -1 depending on the root cause (in this chapter, we do not exploit this root cause). As one of our goals is to explore the evolution of the exposure per country, we removed all scans with a GPS coordinate set to either 0 or -1. We removed 7.9% of the Wi-Fi measurements, 9% of the Bluetooth measurements, 18.2% of the 2G measurements, 19.8% of the 3G measurements, and 12.8% of the 4G measurements. Overall, we removed 11.2% of all the raw measurements by filtering out invalid GPS coordinates.

Invalid RSSI removal The Android OS is an open-source software program that is common to all Android devices, but each smartphone manufacturer adapts it to their hardware by performing

customization and developing drivers, all of which are proprietary. Therefore, each smartphone model can come with specific bugs [91]. This step focuses on the RSSI, which is produced by the proprietary Radio Interface Layer (RIL).

Fortunately, each wireless standard comes with a valid range for the RSSI value, as shown in Table 5.1. We can therefore easily filter out each measurement with an out-of-range RSSI value. We removed 0.07% of the Wi-Fi measurements, 0.04% of the Bluetooth measurements, 0.8% of the 2G measurements, 2.4% of the 3G measurements, and 14.1% of the 4G measurements. After this removal step, 85.9% of all the raw measurements remained.

In addition to the out-of-range values, we also observed in-range abnormal values for cellular measurements (2G, 3G, 4G). Abnormal values are in the valid range but tend to appear with higher frequency in the same *exposure scan*. The root cause of these abnormal values is hard to pinpoint as it most likely comes from bugs in the proprietary RIL. In particular, we observed that all smartphones with an Exynos [192] System on Chip (SoC)* have an abnormally high number of -51 dBm measurements: for all cellular measurements performed from smartphones with an Exynos SoC, the -51 dBm values represent 71% of all cellular measurements, whereas, they represent 1.91% for all smartphones running any SoC other than Exynos.

We found that the cells reporting abnormal values correspond to fake cells, that is, when the RIL reports a cell, but it does not correspond to a real measured cell. Indeed, when a smartphone connects to a cellular operator, it measures various performance indicators (including the RSSI), and connects to the cell with the best performance indicator; we call this cell the *serving cell*. All the other cells are called *neighboring cells*. We found that for 3G, the percentage of neighboring cells measured by smartphones with an Exynos SoC is 21.8% of all measured cells, whereas it is 2.7% for smartphones running any SoC other than Exynos. This is a clear indication that smartphones with an Exynos SoC report fake neighboring cells, at least for 3G.

Due to the bogus behavior of smartphones running an Exynos SoC, we decided to adopt a conservative strategy by removing all measurements (Wi-Fi, Bluetooth, 2G, 3G, 4G) performed by a smartphone with an Exynos SoC. Even if the issue does not concern Wi-Fi and Bluetooth, removing only cellular measurements (while

* Most likely, the issue comes from the modem associated with the Exynos SoC, but we only have access to the SoC name from the Android API.

keeping Wi-Fi and Bluetooth measurements) would have affected our discussion of personal exposure by changing the proportion of the sources of exposure. We removed 24.4% of the Wi-Fi measurements, 33.5% of the Bluetooth measurements, 7.9% of the 2G measurements, 40.6% of the 3G measurements, and 10.8% of the 4G measurements. After this removal step, 62.6% of all raw measurements remained.

For the sake of completeness, we note that we also observed an abnormally large number of measurements with a -113 dBm RSSI for 2G and, to a lesser extent, for 3G. We did not, however, find any correlation between these -113 dBm measurements and a specific SoC, device brand, or Android version. As dBm are in a logarithmic scale, and since we perform all our computations in Watt, which is in a linear scale, the impact of these measurements on the rest of this chapter is negligible.

Included countries ElectroSmart was released in August 2016 in two languages, English and French. We added Italian and German in March 2019, and Spanish and Portuguese in January 2020. France is the country with the largest number of measurements (36% of all measurements after removing invalid GPS and RSSI), followed by the USA (27.5%), Italy (7.9%), and Germany (4.6%).

We restricted this study to the 13 countries with the largest number of measurements. In addition to France, the USA, Italy, and Germany, we included (in order from the highest to the lowest number of measurements) Canada, the United Kingdom, Switzerland, Belgium, Spain, the Netherlands, India, Australia, and Brazil. Although Brazil accounts for only 0.5% of all measurements, this still represents 21.6 million measurements and 2668 unique users.

Altogether, the excluded countries represent 9.3% of all measurements. So, after this step, 56.8% of all raw measurements and 50.3% of all user profiles remained.

CDMA removal The term CDMA refers to a large family of cellular protocols (cdmaOne, CDMA2000, EVDO) deployed mainly in North America. ElectroSmart can measure CDMA cells, but, apart from in the USA, we did not find CDMA measurements in any of the selected countries. In the USA, all CDMA measurements represent 0.95% of all cellular measurements (4G measurements represent 64% of all cellular measurements). As CDMA measurements are only used in the USA in our filtered dataset and represent a negligible fraction of all cellular measurements, we decided to remove all CDMA measurements from our dataset.

Cleaned dataset characteristics In the rest of this chapter, we will only refer to the cleaned dataset that resulted from the previous removal steps. This dataset contains 254,410 user profiles and 3,656 million measured RSSI. This represents 56.8% of all the measurements and 50.3% of all the profiles available in the raw dataset.

In this cleaned dataset, Wi-Fi represents 58.3% of all measured RSSI, Bluetooth 6.6%, 2G 10.5%, 3G 7.6%, and 4G 17%.

Dataset processing

Adapting to local time All the raw measurements in the dataset are associated with a timestamp in UTC that corresponds to the instant the corresponding signal was detected. In order to identify day and night periods, we need to convert all timestamps into local time. To do so, we reverse-geocode the GPS coordinate of each measurement using OpenStreetMap's Nominatim[193] to determine the corresponding country. Then we convert the timestamp in UTC to a timestamp in the local timezone of the GPS coordinate using `timezonefinder` python library[194].

Identifying physical and logical Wi-Fi sources Identifying the physical sources of radio frequencies is particularly important for assessing exposure. This notion of physical source can be tricky. In this chapter, a physical source is the source of a carrier signal, that is, the source of a signal at a specific frequency. For Bluetooth, 2G, 3G, and 4G, one detected signal corresponds to one physical source, but this is not the case for Wi-Fi.

A Wi-Fi access point usually has one or two physical sources of emission, but the signals we measure correspond to logical sources, and it is common to have multiple logical sources for one physical source. We can obtain the carrier signal frequency for each measured source, and one might argue that this information is enough to identify the physical sources. However, it is not the case, as different physical sources can use the same frequency. This is a common issue in Wi-Fi as the number of available frequencies (called channels) is limited, and the density of sources is high.

Wi-Fi networks are based on the notion of a service set, that is, the idea that logical networks can be layered on top of a physical network. Such logical networks are identified by a Service Set ID (SSID) (usually a human-readable string) associated with a Basic Service Set ID (BSSID), which is a 6-byte, internationally unique

identifier usually derived from the MAC address of the access point. The strategy used to derive a BSSID from a MAC address depends on the equipment and administrator. We observed three strategies: the BSSID differs from the MAC address by the first byte, the last byte, or both the first and last bytes.

Therefore, the rule we apply to identify a physical source in a user scan is the following: if several Wi-Fi measurements report the same frequency and have the same BSSID (excluding the first and last bytes in the comparison), we associate them to the same physical source. In addition, as logical sources for the same physical source might report different RSSI (because the measurements might not be performed at the exact same time), we consider that the RSSI of the physical source is the maximum RSSI of all the associated logical sources for a given scan.

In the rest of this chapter, all results we report for Wi-Fi are for physical sources.

Bluetooth scan synchronization When counting the number of sources, it is important to use the concept of an atomic scan, that is, a scan that reflects the instantaneous exposure as measured by the smartphone. Cellular and Wi-Fi scans are atomic because the Android API returns all current sources in a single call or callback. However, this is not the case for Bluetooth. When we start a Bluetooth scan, the smartphone will perform a Bluetooth inquiry request and wait for an answer from devices in the vicinity [195]. Therefore, devices will reply one by one, usually within 15 seconds of the start of the scan.

The heuristic we use to attribute replying devices to an atomic scan is to group together all Bluetooth devices whose inter-arrival is less than 15 seconds.

In the rest of this chapter, each time we count the number of Bluetooth devices, we count the number of devices in an atomic scan as defined in this section.

Mitigation of the cellular scans limited to the SIM operator We have explained in the *Limitations* section that the cellular measurements only take into account the RSSI from the operator declared in the SIM card. This limitation results in a significant underestimation of the cellular exposure. To mitigate this issue, in each scan, we multiple the RSSI corresponding to a cellular measurement with

the number of operators in the country in which the scan was performed.

5.1.3 Personal exposure definition and calculation

We define personal exposure as the received power from all the electromagnetic field sources on the radio frequency bands exposing humans. The received power is a function of the emitting power that is expressed in Equation (5.1) where P_r is the received power, P_e is the emitting power, K is a constant dependant on the emitting and receiving antennas' characteristics, d is the distance to the source, and f is the signal frequency [144]. We see in Equation (5.1) that distance plays an important role in personal exposure, as does signal frequency: higher frequency signals fade faster than lower ones.

$$P_r = K\left(\frac{1}{4\pi df}\right)^2 P_e \tag{5.1}$$

The analysis we perform in this chapter is based on three main calculation steps that we describe and justify in the following. i) First, for all computations based on an exposure scan (as defined in Methods), we consider the sum of the received power in Watt of all signals in this scan. Computing the sum is relevant because an exposure scan is atomic in terms of time, so it represents all the signals simultaneously exposing an individual. ii) Second, we average the exposure scans of each user per month. This gives a per-user monthly average exposure. The rationale of computing per-user monthly averages is to prevent users with a large number of measurements from biasing the monthly average. iii) Third, for each country, we group the per-user monthly average exposures. When a user has been in different countries for a given month, we compute one monthly average exposure per country. Then, we compute the mean of these per-user monthly average exposures to obtain a monthly average exposure per country. Finally, we obtain the yearly average exposure by computing the mean of the monthly average exposure per country. Computing the yearly average exposure this way avoids bias that could be introduced by months with a larger than average number of users.

Similar calculation can be performed to compute the average number of sources, where we take the total number of wireless sources of

each exposure scan, instead of taking the sum of the received power for computing the exposure level.

5.2 Results

5.2.1 World-wide sustained growth of ratio exposure is primarily driven by Wi-Fi

Table 5.2 shows the evolution of the total personal exposure in the 13 countries with the largest number of measurements (as discussed in Methods). We observe an overall trend of increased exposure across all countries from 2017 to 2020. To confirm this trend, we computed the Spearman correlation on the monthly average exposure to evaluate the relationship between time (months) and the monthly average exposure for each country. Table 5.3 shows a significant positive correlation between time and exposure for most countries.

It is interesting to understand how each wireless technology contributes to this exposure trend. Figure 5.3 shows that the total exposure (brown curve) has been multiplied by 2.3 (from -34.6 dBm in 2017 to -31 dBm in 2020) over the four-year period. The trend we observe for each wireless technology corresponds to the adoption or decline of the corresponding technology. We observe a clear increase in the exposure due to Wi-Fi and Bluetooth technologies, but a decrease in the exposure due to 2G and 3G technologies. Interestingly, Wi-Fi is by far the largest contributor to exposure.

In summary, we observe an overall increase in total personal exposure with time (a 2.3-fold increase from 2017 to 2020), with Wi-Fi being the largest contributor to personal exposure.

5.2.2 Exposure growth is not explained by the multiplication of sources

We focus now on how each source contributes to total exposure. This is a central question because an improved understanding of the most exposing sources could inform strategies for reducing personal exposure.

Since the measurement of the number of sources is not reliable for cellular technologies (see Methods), we focus on Wi-Fi and Bluetooth technologies. We consider this limitation reasonable because, as

Table 5.2: The yearly average exposure increased from 2017 to 2020 worldwide. This table represents the evolution of the yearly average exposure per country. We use an ISO 3166 [196] alpha-2 country code to represent each country using a two-letter code. We compute the mean and the 95% confidence interval for the mean using empirical bootstrap resampling with replacement (N=1,000) [197] on the monthly average exposure for each country. The change column shows the increased (in blue) or decreased (in red) exposure as a percentage compared to the previous year. This percentage change is computed in Watt instead of dBm to have a linear interpretation of the change in exposure.

	2017		2018			2019			2020		
Country	Mean	95%CI	Mean	95%CI	Change	Mean	95%CI	Change	Mean	95%CI	Change
BR	-39.4	[-41.1, -38.1]	-36.3	[-39.1, -34.1]	+105%	-34.4	[-37.3, -32.4]	+56%	-32.0	[-33.1, -31.0]	+71%
AU	-34.2	[-37.4, -31.5]	-34.1	[-36.5, -32.1]	+2%	-31.0	[-34.0, -28.4]	+104%	-31.1	[-31.9, -30.4]	-3%
NL	-39.1	[-41.9, -36.9]	-37.1	[-39.6, -34.9]	+57%	-36.3	[-38.7, -34.3]	+19%	-33.6	[-35.3, -32.1]	+87%
IN	-29.8	[-35.1, -26.3]	-27.6	[-37.0, -23.6]	+64%	-32.2	[-33.8, -30.9]	-65%	-30.6	[-32.2, -29.4]	+46%
ES	-37.4	[-40.2, -35.1]	-35.4	[-37.6, -33.6]	+60%	-32.9	[-34.6, -31.7]	+77%	-31.6	[-32.9, -30.5]	+35%
BE	-40.7	[-42.0, -39.7]	-35.9	[-37.7, -34.3]	+204%	-35.4	[-36.5, -34.4]	+13%	-32.5	[-33.8, -31.5]	+91%
CH	-31.6	[-33.4, -30.2]	-32.9	[-34.4, -31.7]	-25%	-33.1	[-34.9, -31.6]	-6%	-32.6	[-34.3, -31.2]	+13%
GB	-39.2	[-41.0, -37.7]	-34.7	[-36.8, -32.9]	+182%	-32.7	[-35.1, -30.6]	+60%	-30.9	[-32.3, -29.8]	+49%
CA	-35.6	[-37.8, -33.8]	-32.3	[-33.5, -31.0]	+112%	-31.9	[-33.3, -30.6]	+9%	-29.2	[-30.1, -28.3]	+89%
DE	-36.6	[-37.5, -35.9]	-36.9	[-38.4, -35.8]	-7%	-32.8	[-34.8, -31.3]	+158%	-32.1	[-33.0, -31.0]	+19%
IT	-33.8	[-38.4, -30.7]	-33.9	[-35.3, -32.7]	-2%	-33.3	[-34.1, -32.4]	+16%	-32.1	[-33.1, -31.4]	+30%
US	-33.5	[-34.9, -32.0]	-30.5	[-31.2, -29.9]	+98%	-29.8	[-31.0, -28.5]	+18%	-27.3	[-28.3, -26.4]	+76%
FR	-33.5	[-34.1, -33.0]	-33.0	[-33.8, -32.2]	+14%	-33.3	[-33.9, -32.7]	-7%	-31.8	[-32.2, -31.4]	+42%

Table 5.3: The Spearman correlation shows a significant positive correlation between time and exposure for most countries. The Spearman correlation is computed on the monthly averages for each country from 01/2017 to 12/2019. We exclude 2020 from this correlation as the COVID-19 period would have significantly impacted the interpretation of this correlation. In blue, we show the positive correlations, and in red, the negative ones. The grey two-sided p-values are above the threshold of 0.05. When including 2020, we observe an increase in the Spearman coefficients between 0.1 and 0.2 for most countries and lower p-values for all countries (except CH), showing the impact of lockdowns on exposure. The most significant difference is France, with a Spearman coefficient of 0.42 ($p<0.01$).

Country	BR	AU	NL	IN	ES	BE	CH	GB	CA	DE	IT	US	FR
Score	0.44	0.45	0.37	0.14	0.42	0.63	-0.21	0.7	0.57	0.47	0.36	0.62	0.00
p-value	0.0066	0.0058	0.026	0.4	0.011	3.4E-05	0.23	2.2E-06	0.0003	0.0039	0.03	5.8E-05	0.99

shown in Figure 5.3, these two are the most significant contributors to total exposure.

Figure 5.5 shows the relationship between individual exposure and the number of sources in a vicinity. We observe that beyond four to five sources, additional sources do not significantly increase individual exposure. Although this finding might seem counter-intuitive, it is mainly explained by the important fading with the distance of the electromagnetic fields (see Equation 5.1). In addition, we see in Figure 5.4 that in 50% of the exposure scans, the most exposing Wi-Fi source (resp. Bluetooth) represents at least 83% (resp. 91%) of the total exposure due to Wi-Fi (resp. Bluetooth). Thus, the number of sources in the vicinity is not a good predictor of personal exposure; rather, the most exposing source is the primary contributor to exposure.

The question now is how actionable this information is with respect

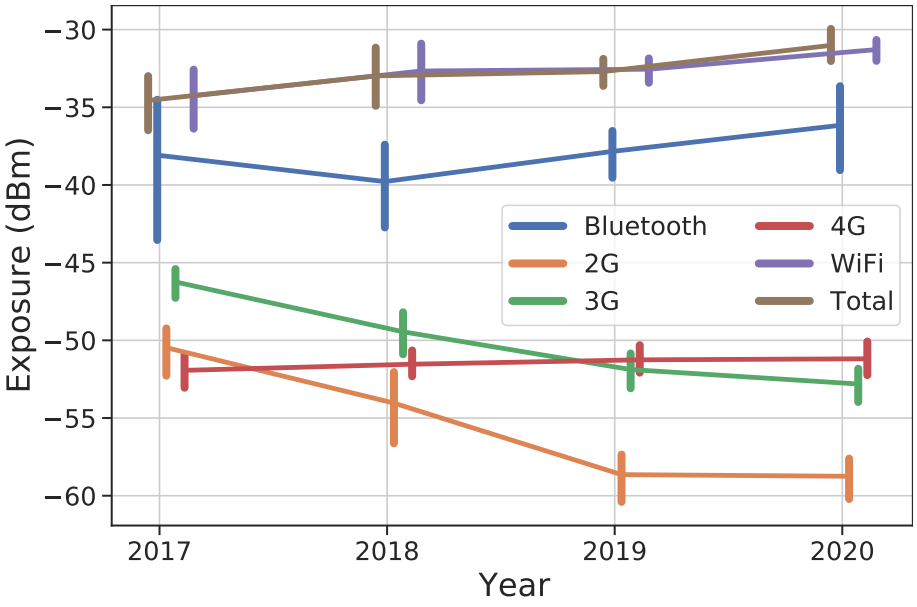

Figure 5.3: The total exposure of the population has been multiplied by 2.3 in 4 years. For each year, we take the yearly average exposure as given in Table 5.2, convert it to Watt, compute the mean for all 13 countries, and convert it back to dBm. The bars represent a 95% confidence interval for the mean using empirical bootstrap resampling with replacement (N=1,000) on the yearly average exposure per country. Plots are shifted horizontally to avoid confidence interval overlap. An increase of 3 dB results in the doubling of the exposure.

to exposure reduction. To answer, we focus on the Wi-Fi-connected sources and Bluetooth-bounded devices to which a user has already connected. Connected sources or bounded devices are usually owned or controlled by the user and can therefore be switched off or moved to reduce exposure. Taking all scans into account, we computed that 41% of the time, the most exposing of all the Wi-Fi sources is a connected one. For Bluetooth, the most exposing source is a bounded device 10% of the time. Then, we computed what the individual personal exposure would have been if all connected sources and bounded devices had been switched off. While this is an overly optimistic situation, the goal is to assess the degree to which an individual could control exposure. Figure 5.6 shows that, by switching off the connected sources and bounded devices, half of the users could have reduced their total exposure by 50% (a reduction by 3.1 dB), and 25% could have reduced their total exposure by 90% (a reduction by 10 dB).

In summary, the growth of total exposure is not explained by a multiplication of sources. On the contrary, a handful of sources generate most of the personal exposure at any given time, and it is not uncommon that an individual's exposure is almost entirely the result of sources they either own or associate with (for a quarter of our subjects, such sources account for 90% of exposure).

5.2.3 Impact of regulation on personal exposure

Electromagnetic field emissions are regulated, which means that both the spectrum used and the emitting power per frequency band

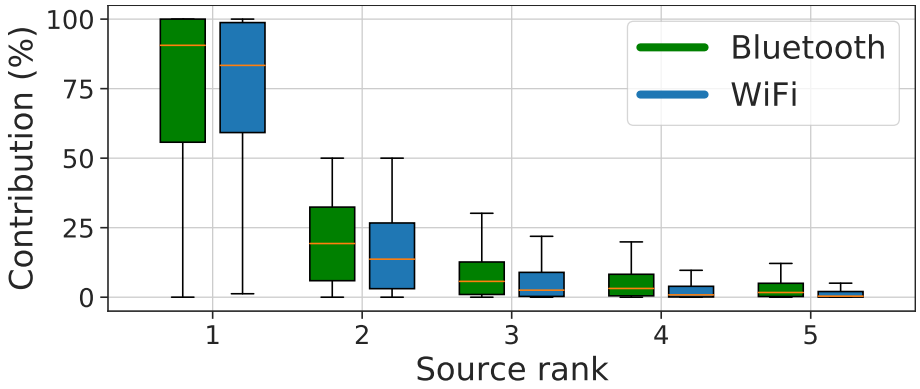

Figure 5.4: The most exposing source is the primary driver of individual exposure. This figure represents the distribution of the percentage contribution of the top five exposure sources in all exposure scans, with Bluetooth in green and Wi-Fi in blue (the boxplot convention is the following: the middle line shows the median, the lower and higher hinges show the first and third quartiles, respectively, and the lower and higher whiskers show a limit of 1.5x the interquartile range from the lower and higher hinges, respectively). For instance, the first green box shows the distribution of the contribution of the most exposing Bluetooth source to the sum of the exposure of all Bluetooth sources for each exposure scan. We observe that for 75% of the exposure scans (containing at least one Bluetooth measurement), the most exposing Bluetooth source represents at least 56% of the entire Bluetooth exposure.

are fixed by a regulatory authority. The types of cellular and Wi-Fi sources we explore in this chapter are regulated on a country-specific basis. Therefore, the maximum emitting power per frequency band is not uniform in the top 13 countries we consider. By contrast, Bluetooth uses the same emitting power in all the countries we consider. We explore next how cellular and Wi-Fi regulation impacts the received power.

Cellular regulation

The maximum allowed exposure of the population is fixed by the ICNIRP international body [3]. However, each country is free to lower the maximum exposure depending on local policies. In addition, some countries have policies specific to some areas (e.g., Belgium has different limits for Flanders, Wallonia, and Brussels) or specific to some contexts (e.g., Italy enforces lower exposure near schools). Finally, the limits are specific to the frequencies used by cellular technologies. Here, we specifically focus on the frequencies 900 MHz, 1800 MHz, and 2100 MHz. For each country, we build a regulation limit triplet, one limit per frequency.

To the best of our knowledge, there is no central repository of exposure limits for all countries. To obtain a regulation limit triplet for each of the 13 countries we consider, we consolidated several sources [61, 198, 199], and when multiple limits were provided (due to local policies or context), we keep the limit covering the largest population.

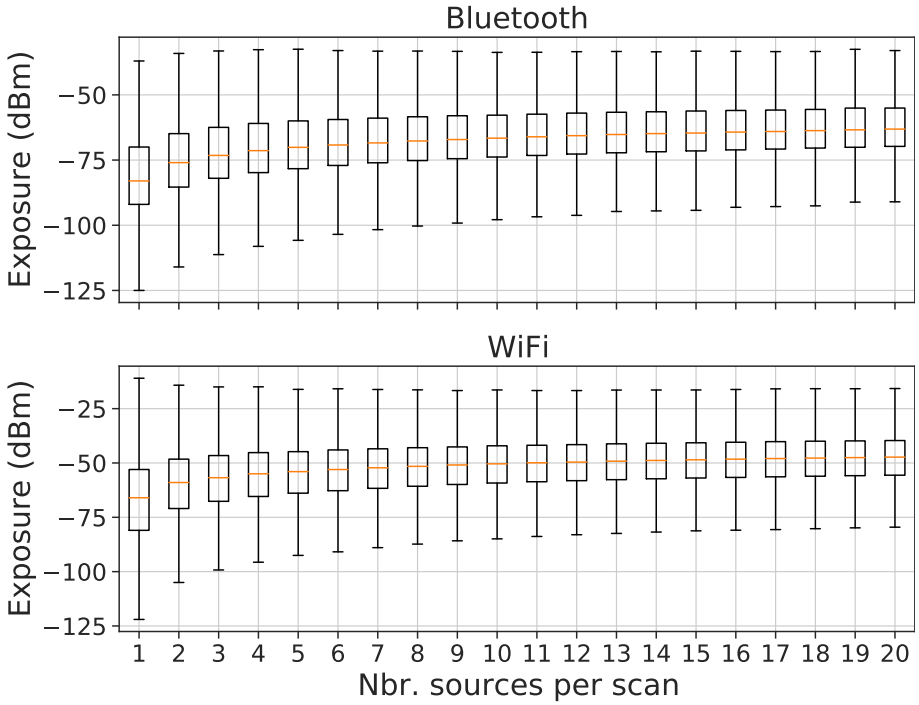

Figure 5.5: A large number of sources in the vicinity marginally increases individual exposure. The figure represents the distribution of all the exposure scans in Bluetooth (top) and Wi-Fi (bottom) when there is a given number of (Bluetooth or Wi-Fi) sources in the scan (the boxplot convention is the following: the middle orange line shows the median, the lower and higher hinges show the first and third quartiles, respectively, and the lower and higher whiskers show a limit of 1.5x the interquartile range from the lower and higher hinges, respectively). For instance, the last box in the top figure represents the sum of the received power in Bluetooth for exposure scans with exactly 20 detected Bluetooth sources. We observe that beyond 4 to 5 sources in the vicinity, any additional sources marginally change the individual exposure.

Figure 5.7 does not show any clear correlation between regulation limits and exposure. We must be careful interpreting this result as there are several external factors that we do not control, such as the deployment strategy of the cellular operators. For example, operators might decide, in a densely populated area, to have a higher density of base stations (to increase the supported load) emitting at a lower power (to reduce interference). In such cases, base stations expose the population at a level that is significantly lower than what the regulation permits [61, 62]. Therefore, in practice, the regulation is an upper bound to the population exposure in some extreme cases, but in most cases, the population is exposed at levels much lower than the regulation limits.

To confirm this hypothesis, we computed the distribution of the cellular measurements in V/m. We obtain the electric field E in V/m from the measured received power in dBm with the formula:

$$E = \frac{9.73 f \sqrt{50 \times 10^{\frac{P-30}{10}}}}{c\sqrt{G}} \tag{5.2}$$

where G is the antenna gain, f is the frequency in Hz, P is the power in dBm, and c is the speed of light [200]. The antenna gain of the smartphone is unknown, so we assume an isotropic antenna (i.e.,

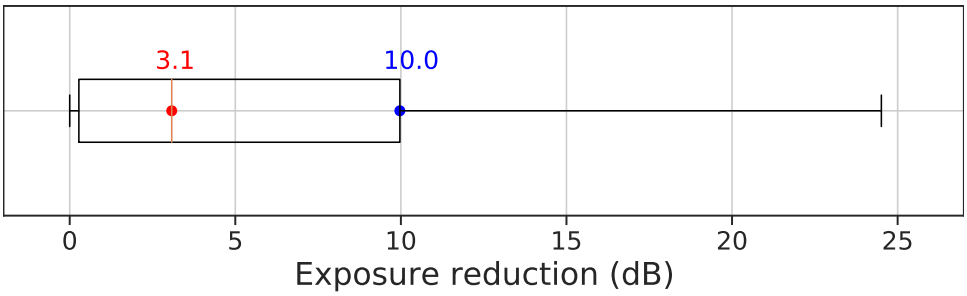

Figure 5.6: By switching off connected Wi-Fi sources and bounded Bluetooth devices, 50% of the users can reduce their exposure by 3.1 dB, and 25% of the users can reduce it by at least 10 dB. This figure shows the distribution of the individual exposure reduction for each user when we remove connected Wi-Fi sources and bounded Bluetooth devices. In red, we show the median and in blue, the 75th percentile. For each user and month, we first compute the per-user monthly average exposure. Then, for each user and month, we collect all connected Wi-Fi sources and bounded Bluetooth devices, and we re-compute the per-user monthly average exposure by removing all collected connected sources and bounded devices from the exposure scans. Finally, we compute the difference between the per-user monthly average exposure in each case. The result is the distribution shown in this figure for each user. Note that in some rare cases, the difference can be negative. This can occur when an exposure scan contains only one connected source. By removing connected sources, we change the number of samples on which we average. As a result, a user with only a few samples could end up with a higher average without connected sources. In this figure, we drop users with a negative gain; they represent 0.92% of all users.

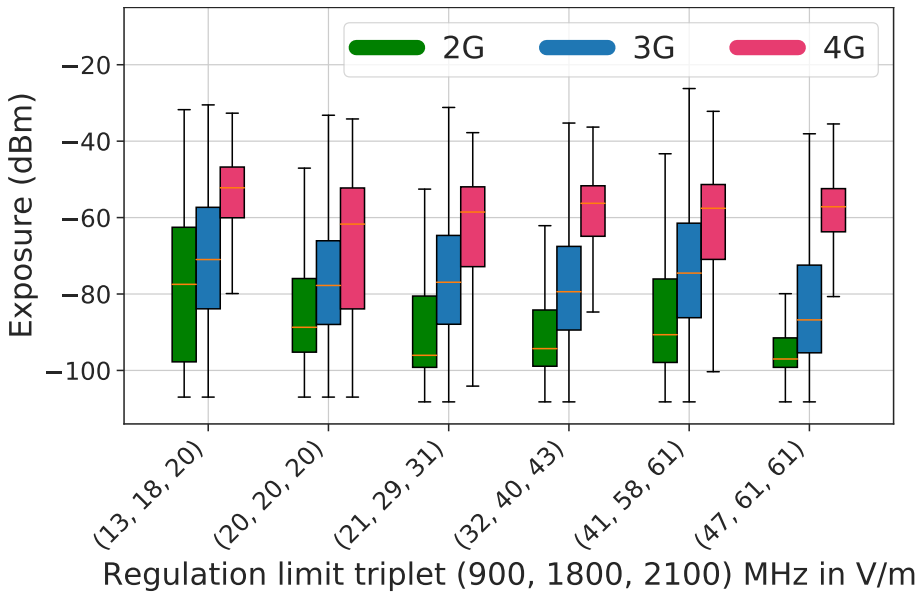

Figure 5.7: We observe no correlation between regulation limits and exposure. This figure shows the correlation between the exposure and a regulation limit triplet for the three cellular technologies we measure, 2G, 3G, and 4G (the boxplot convention is the following: the middle orange line shows the median, the lower and higher hinges show the first and third quartiles, respectively, and the lower and higher whiskers show a limit of 1.5x the interquartile range from the lower and higher hinges, respectively). Here is the association between regulation limit triplets and countries: (13, 18, 20) is for IN; (20, 20, 20) is for IT; (21, 29, 31) is for BE; (32, 40, 43) is for CA; (41, 58, 61) is for FR, DE, GB, CH, ES, NL, AU, BR; (47, 61, 61) is for US.

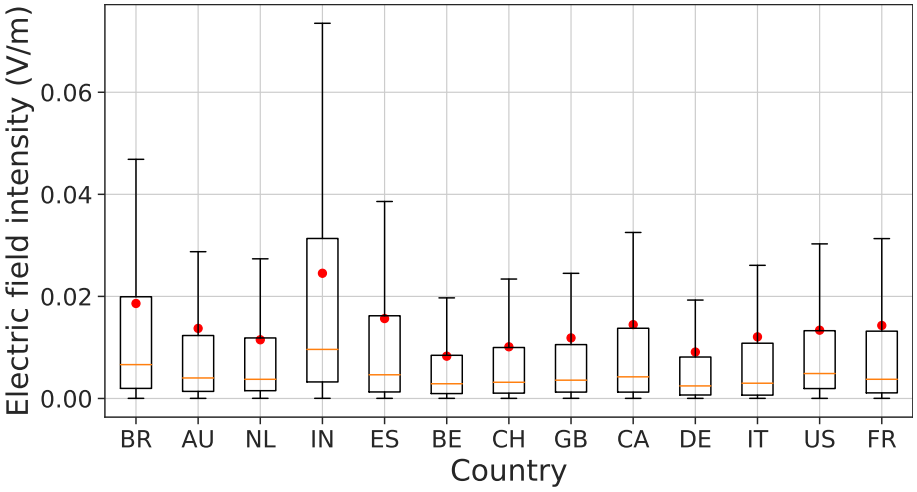

Figure 5.8: The population exposure is orders of magnitude lower than any existing regulation limits for the considered countries. This figure shows the distribution of the estimated electric field produced by cellular antennas at the receiver per country using boxplots, where the middle orange line shows the median, the lower and higher hinges show the first and third quartiles, respectively, and the lower and higher whiskers show a limit of 1.5x the interquartile range from the lower and higher hinges, respectively. The red dot shows the mean. Considering all signals together, we have a median at 0.005 V/m, and a 99th percentile at 0.18 V/m.

$G = 1$). In our dataset, we have access to the cellular frequency f for serving cells only. Therefore, we only keep exposure scans with a serving cell containing a valid frequency (they represent 74.5% of all exposure scans). We sum all the cellular RSSI[†] in each exposure scan and convert the summed RSSI into V/m using the frequency of the serving cell.

Figure 5.8 shows the distribution of the measured electric field for each exposure scan per country. We see that the current population exposure is orders of magnitude lower than any current regulation limit. We found that by considering all countries together, only 1% of the scans are above 0.18 V/m.

Admittedly, this estimation is a coarse description of reality. We now explore how the different limitations and approximations of our estimation will impact our conclusion. First, as described in Methods, the maximum cellular RSSI that we can measure is −51 dBm, so measurements above −51 dBm are capped. However, measurements at −51 dBm represent only 1.8% of all measurements, a very small fraction that cannot fundamentally change our conclusions. Second, we apply the same frequency (that of the serving cell) to all cellular measurements in the same exposure scan. Considering that 98% of the frequencies are within [782, 2660] MHz and Equation 5.2 is linear with f, we have at most a factor of 3.4. Note that this is a very conservative estimate, as the median frequency is 1,745 MHz. Last,

[†] As explained in Methods, we perform the sum in Watt, and because we only measure the RSSI for the operator declared in the SIM card, we multiply each RSSI by the number of operators in the country in a pre-processing phase.

in Boussad et al.[201], we show, using calibrated measurements in an anechoic chamber, that the average deviation between the real received power at a calibrated isotropic antenna and a smartphone is 2.5 dB. If we translate this offset in Equation 5.2, we find that it results in a multiplying factor of $\sqrt{10^{\frac{2.5}{10}}} \approx 1.3$.

By combining the two main sources of error, the actual exposure in V/m could be 4.7 times higher than what we report in Extended Data Figure 5.8, which is still orders of magnitude lower than the most restrictive regulation limits in the countries we consider.

In summary, 99% of our exposure scans report a cellular exposure lower than 0.18 V/m (corrected to 0.85 V/m if we take into account the multiplying factor of 4.7, corresponding to a worst-case estimate scenario), which is orders of magnitude lower than any regulation limits in the considered countries.

Wi-Fi regulation

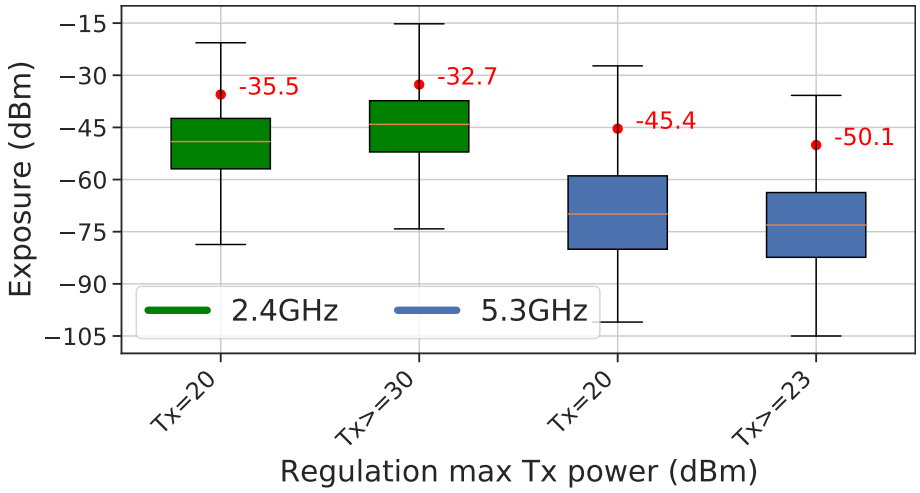

Figure 5.9: The mean exposure is significantly higher when the Tx power is higher in the 2.4 GHz band, but significantly lower in the 5.3 GHz band. The figure shows the distribution of the per-user monthly average exposure using boxplots. The middle orange line shows the median, the lower and higher hinges show the first and third quartiles, respectively, and the lower and higher whiskers show a limit of 1.5x the interquartile range from the lower and higher hinges, respectively. The red dot shows the mean. To compute the significance of the mean, we perform a permutation test (N=1,000,000). The test statistic is the difference of the means for the same frequency band. The two-sided p-value is lower than 0.001 for both bands.

Wi-Fi is a generic term that gathers together a large number of standards covering a wide spectrum of frequencies in the 2.4 GHz and 5 GHz bands. For Wi-Fi, the goal of regulation is to reduce interference by limiting the maximum transmission power. This limit might be different for each country and each frequency. Getting a consolidated view of the various international regulations on Wi-Fi is tricky. For this purpose, we rely on the efforts of J. W. Linville

and S. Forshee, who maintain a consolidated file containing the Wi-Fi emitting power per country and frequency for the Linux kernel [202].

To understand the impact of regulation on exposure, we focus on two frequency bands that include a large enough number of countries using different regulations: 2.4 GHz ([2400, 2483] MHz) and 5.3 GHz ([5250, 5350] MHz). The 2.4 GHz (resp. 5.3 GHz) band represents 76% (resp. 2%, still 37 million measurements) of all Wi-Fi measurements. In the 2.4 GHz band, the maximum transmission power is 36 dBm for Australia, 30 dBm for the USA and Canada, and 20 dBm for all the other considered countries. In the 5.3 GHz band, the maximum transmission power is 24 dBm for Brazil, India, and Canada, 23 dBm for the USA, and 20 dBm for all the other considered countries.

Figure 5.9 shows that in the 2.4 GHz band, a Tx power of 20 dBm leads to significantly lower exposure than a Tx power higher than 30 dBm. Therefore, this regulation clearly impacts population exposure. Surprisingly, when we observe the exposure for the 5.3 GHz band, we have the opposite result: a Tx power of 20 dBm leads to significantly higher exposure than a Tx power over 23 dBm.

We can explain this seemingly contradictory result. Unlike regulations for cellular, regulations for Wi-Fi limit the Tx power; therefore, it is not surprising to see that Tx power impacts population exposure. When the difference in Tx power is large (a minimum of 10 dB between the two groups in the 2.4 GHz band), the Tx power dominates the other factors that affect population exposure. However, when the difference in the Tx power is small (a maximum of 4 dB for the 5.3 GHz band), other factors dominate the population's exposure. Indeed, as the attenuation increases with the frequency (see Equation 5.1), a small 4 dB difference in the Tx power will have a marginal impact on the total exposure compared to, for instance, the deployment and density of Wi-Fi access points per country.

In summary, the impact of Wi-Fi regulation on population exposure depends not only on the Tx power, but also on the frequency bands. It is worth noting that the goal of this regulation is to limit interference rather than population exposure.

5.2.4 The population is most exposed at home

User location is also a factor that may affect personal exposure. In the following, we focus on two location categories: at-home and

out-of-home. The rationale is that, according to the results reported in the previous sections, Wi-Fi is the greatest contributor to total exposure. We hypothesize that users are more exposed at home because most users have Wi-Fi at home[‡] and are closer to their router than would be the case in other environments. The goal of this section is to explore the difference between at-home and out-of-home exposure.

To cluster measurements according to the user location, we need users with a large enough number of measurements to identify the home location; we call them *dense users*. More precisely, when we compute the per-user monthly average exposure, we only keep users with at least 14 days of data in that month and at least 80% hourly sampling density. To calculate sampling density, we count the number of hours between the first and last day we see a user in a given month. An 80% hourly sampling density means that the user has at least one exposure scan for 80% of the counted hours.

In our entire dataset, we have 22,907 dense users, which is 9% of all users.

Finally, we use the DBSCAN algorithm [205] (ϵ = 100 meters, minPts = 24, distance = haversine) on the GPS coordinates of the dense users for each month, independently. We label the cluster that most frequently appears between 10PM and 8AM as the home cluster. All the other clusters are labeled "out-of-home". Therefore, out-of-home gathers together all other indoor and outdoor locations, including those frequented for work, transportation, etc.

Figure 5.10 shows that users at home are significantly less exposed to cellular radiation. The main reason is that cellular antennas are outside, so walls attenuate the radiation. Conversely, exposure to Wi-Fi is more important at home than out-of-home. Here, the increased adoption of Wi-Fi technology at home is a reasonable explanation. We computed how many hours (per month) each dense user is connected to a Wi-Fi source at home and out-of-home. We found that half of the users (median) are connected 91% of the time at home, and 29% of the time out-of-home. Finally, we found that the difference of exposure to Bluetooth between at-home and out-of-home is not significant.

In summary, user location has a significant impact on exposure. In particular, users are more exposed to Wi-Fi at home. As they are largely connected

[‡] According to the US Census Bureau, 81% of USA households had internet access in 2016 [203]. In 2019, more than 80% of the households in the European countries included in our study had internet access, with 83% coverage in France and 98% in the Netherlands) [204].

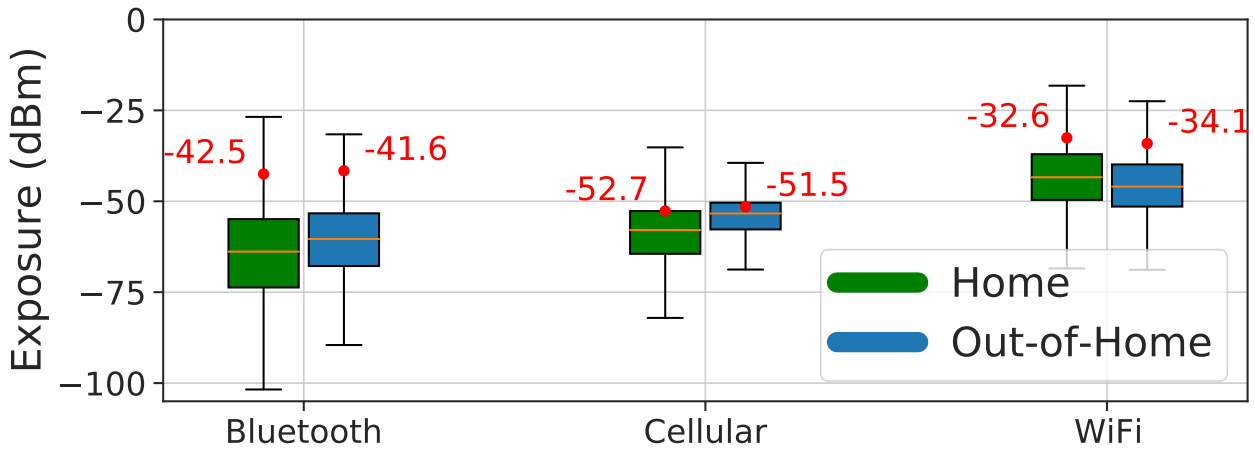

Figure 5.10: The mean exposure is significantly lower at home for cellular (-1.19 dB) and higher at home for Wi-Fi (+1.55 dB). This figure shows the distribution of the per-user monthly average exposure for dense users when they are at home (in green) and out-of-home (in blue) for Bluetooth, Cellular, and Wi-Fi sources. In the boxplots, the middle orange line shows the median, the lower and higher hinges show the first and third quartiles, respectively, and the lower and higher whiskers show a limit of 1.5x the interquartile range from the lower and higher hinges, respectively. The red dots and labels show the mean exposure. We performed a permutation test (N=1,000,000) between at-home and out-of-home for each of the three types of sources. We obtained a two-sided $p < 0.001$ for Wi-Fi and Cellular, and a two-sided $p = 0.09$ for Bluetooth.

to Wi-Fi at home, we further conclude that personal Wi-Fi routers are the most significant factor in at-home exposure.

5.3 Discussion and conclusion

Understanding the potential human health impacts of exposure to radio frequencies is a long journey. An important challenge in performing sound epidemiological studies is the complexity of characterizing the real exposure of the population. The methods and dataset we present here offer the first analysis of the evolution of radio frequency exposure at population-scale for 13 countries over four years. This change of paradigm from previous small-scale studies has direct consequences for the current debate on population exposure and the impact of this exposure on health.

The Council of Europe, following the principle of precaution, has called for an *As Low As Reasonably Achievable* (ALARA) rule [206]. In line with this principle, one proposal is to reduce exposure levels as low as 0.6 V/m and even 0.2 V/m in the medium term. The debate currently includes proponents, who see ALARA as a necessary drastic reduction to curb the current level of exposure, and cellular operators, who oppose ALARA by arguing that it would impede the deployment of communication infrastructure,

and thus, eventually, access. We reveal that for the vast majority of the population, exposure is already below the lowest ALARA level. However, reducing the current regulation levels would still benefit the small fraction of the population that is currently more exposed than recommended by the ALARA rule.

Our work also fundamentally changes the debate on frequency exposure, currently heavily centered on the regulation of cellular operators. Not only do we show that Wi-Fi is by far the largest contributor to population exposure, but also that a few sets of sources, namely those used by individuals and those present at home, are the key contributors. Offering tools for individuals to prevent unnecessary exposure at home, or working on technology that automatically reduces exposure are just some examples of short and medium term ways to expand the precautionary principle. Such approaches have not yet received the attention that they deserve.

Beyond these direct implications, we envision our work and dataset providing a foundation for future epidemiological studies.

Conclusion and perspectives 6

Conclusion

In this thesis, we performed an interdisciplinary study of the RF-EMF radiations used in wireless telecommunication technologies. We covered theoretical properties of electromagnetic waves, technical and hardware aspects of modern smartphones, and the low-level mechanisms at protocol-level that allow the measurements of the radiations. We analyzed the performances of smartphones for wireless power measurements. Then, we performed the largest longitudinal study (to the best of our knowledge) on the population exposure levels to the RF-EMF radiations during 4 years, from 2017 to 2020, in 13 different countries in the world.

In chapter 1, we started this manuscript by motivating the study by showing the increasing concerns about the potential impact of electromagnetic radiations, especially with the proliferation of multiple wireless technologies that became omnipresent in modern daily life. Since 2011, when the World Health Organization considered the non-ionizing radiations as possibly carcinogenic to humans, a lot of research works have been done to assess the adverse health effects of these radiations. Unfortunately, most of these studies are inconclusive, and the current regulation about exposure is solely based on the heating effect of the biological tissues.

We presented the current state-of-the-art in terms of assessing and monitoring the population exposure to the RF-EMF radiations. We presented the different approaches that can be used such as spot measurements, microenvironmental measurements, simulations and model-based, and personal measurements. Each approach has its own advantages and disadvantages, researchers can pick one approach or use a hybrid approach depending on the aim of the study. We showed that the personal measurement approach is the one that gives a better representation of the exposure levels as perceived by individuals in their daily life. However, most of the studies using this approach can face limitations in space, time, and most importantly, population size. The personal exposimeters are specialized equipment for measuring personal exposure to the RF-EMF radiations. Researchers explored the possibility of using commodity hardware such as smartphones for measuring

wireless power. However, the performances and the accuracy of the measurements can be impacted by the device orientation. Some researchers rely on a mobile application running on mobile devices to collect measurements on the population exposure to the RF-EMF radiations and used it as a replacement for personal exposimeters.

To better understand how modern smartphones can be used to measure the wireless power from the exposing RF-EMF sources, especially the ones used in cellular networks, Wi-Fi, and Bluetooth, we presented in Chapter 3 the hardware and software component of Android smartphones. We showed how two processors running two distinct operating systems run on a single piece of hardware, the System-On-Chip. We showed how the Application Processor is handling all the user applications, whereas the Baseband Processor handles the low-level, telecommunication protocols aspects. We showed how these two separate words communicate and exchange messages through an abstraction layer, governed by old-school commands called AT commands. Then, we gave a short introduction of the different cellular generations (2G, 3G, and 4G), Wi-Fi, and Bluetooth. We presented a low-level protocol description of the mechanisms that occur when the smartphone performs scans of the wireless sources. We finished Chapter 3 by summarizing the scanning operation of the Wi-Fi network, from initiating the scan at the software level from the Application processor to the network exchange between the Baseband processor and the physical network, until the reception of the scan results by the Application processor.

In Chapter 4, we performed a thorough analysis of the performances of modern smartphones for performing wireless power measurements. We built an experimental setup based on open-source software (OpenAirInterface) to set up an LTE network, and perform power measurements using an Android smartphone inside a controlled environment. We evaluated the impact of smartphone orientation in space with respect to the source on the accuracy of the measurements. We showed that the accuracy of the measurements can vary according to the orientation and polarization configuration of the transmitting and the receiving antenna. We proposed a calibration technique that uses the orientation sensors already embedded in the smartphone to compensate for the error in the measurements induced by the orientation. We extended the study to outdoor measurements, and we showed how the environment characteristics such as multi-path, in addition to the polarization diversity used at the cellular base stations, can help reduce the impact of the smartphone orientation on the measurements. However, in situations where there is no polarization diversity, such as for

Bluetooth, the orientation can still impact the measurement accuracy, even in a realistic environment. This is a great deal as many modern applications rely on Bluetooth RSSI measurements, especially the Covid-19 tracing applications.

Last but not least, we presented in Chapter 4 a longitudinal study to characterize the population exposure to the RF-EMF radiations during 4 years, from January 2017 to December 2020. We used crowd-based measurements collected using the Electrosmart mobile application, running on Android smartphones. The study included measurements from 254,410 unique persons, from 13 different countries. We showed that the population exposure level has doubled within 4 years. The population is exposed more to Wi-Fi, especially in their home location, where they are exposed to their own Wi-Fi routers. We showed how much exposure is under the control of the person; by switching off their Wi-Fi routers and Bluetooth devices, people can reduce their exposure levels by 50%. The dataset we present in this work is valuable for multiple purposes, especially to conduct epidemiological studies on the effect of the RF-EMF radiations on a large population. We make this dataset publicly available for the scientific community for further scientific exploitation.

Perspectives

We showed in this work that population exposure to the RF-EMF radiation from wireless telecommunication technologies has increased in the last 4 years. The concerns from the general public and scientists regarding the impact of RF-EMF radiations are still of actuality. These concerns are intensified with the arrival of the latest cellular generation 5G, which is expected to fundamentally change the cellular networks, and wireless telecommunication in general. Some countries already started deploying this technology [207]. The 5G is advertised to bring a much higher throughput reaching 20 Gbps with very low latency, which is considered 500% faster than the 4G [208, 209]. It allows more devices to be connected to the same network simultaneously, which makes it ideal for the proliferation of IoT devices [209, 210].

Figure 6.1: 5G: the latest cellular generation.

We believe that monitoring the exposure of the population to the 5G networks at very early stages as it gets deployed is crucial to help detect and understand any possible impact on population health. We also believe that collecting the measurements of the exposure to 5G must be done at a large scale. The work presented in this thesis sets the ground for future studies to make use of 5G-capable

smartphones to assess the population exposure to 5G network and IoT devices through crowdsourcing.

One of the limitations of this work is that the uplink power from the smartphone is not considered, which gives a partial image of the exposure of the population. This is due to the software limitation on the smartphones that do not give access to this low level information. As we explained in Chapter 3, accessing low-level information on the smartphone requires software modification, but this can limit the population size that can be covered. To address this issue, we can rely on machine learning to infer the transmitted power by the smartphone from a set of reception indicators. Such technique is used by Falkenberg et al.[211] to predict the transmitted power by a smartphone in an LTE network using machine learning model. They used passive downlink indicators as features, and trained the model to predict the transmitted power. Building such model and deploying it at large scale will enrich even more our data and give us more information about the exposure level of the population from their own smartphones.

Another important information that we believe will help us better assess the exposure absorbed by individuals is to determine the human body posture at the time of the measurement. In Electrosmart [52], we collect the smartphone orientation in space. This orientation is represented in form of quaternions (as discussed in Chapter 4). This information can help us know whether the smartphone was held near the human head during a phone call, if the smartphone is put flat on a table, or is carried inside a pocket.

Chapter 5 Appendix A

In this section, we present the results of exposure evolution per technology in the 13 countries included in our study. We present the evolution of the exposure levels and the number of exposing sources (for Wi-Fi and Bluetooth only) during the 4 years, from January 2017 to December 2020.

A.5 Exposure evolution by technology

A.5.1 Wi-Fi

Table A.1: Evolution of the Wi-Fi personal exposure. FCC countries highlighted in gray.

Country	2017 Mean	95%CI	2018 Mean	95%CI	Change	2019 Mean	95%CI	Change	2020 Mean	95%CI	Change
BR	-40.0	[-41.7, -38.5]	-36.0	[-38.4, -34.0]	+151%	-34.1	[-36.8, -32.3]	+53%	-31.9	[-32.9, -31.0]	+66%
AU	-33.9	[-37.1, -31.2]	-33.2	[-36.0, -31.1]	+15%	-30.9	[-34.3, -28.4]	+71%	-30.7	[-31.6, -29.8]	+6%
NL	-39.5	[-42.7, -37.4]	-36.4	[-38.7, -34.4]	+106%	-36.4	[-39.0, -34.1]	+0%	-33.4	[-35.0, -31.9]	+97%
IN	-29.3	[-34.5, -26.1]	-27.3	[-36.6, -23.2]	+60%	-31.4	[-32.8, -30.3]	-61%	-29.9	[-31.6, -28.7]	+40%
ES	-37.1	[-40.2, -34.6]	-35.2	[-37.7, -33.3]	+53%	-33.7	[-35.5, -32.2]	+43%	-31.2	[-32.5, -30.1]	+78%
BE	-40.2	[-41.5, -39.1]	-36.0	[-38.2, -34.5]	+162%	-34.6	[-35.9, -33.5]	+39%	-33.1	[-34.4, -32.0]	+39%
CH	-30.9	[-32.8, -29.5]	-32.5	[-33.9, -31.3]	-30%	-32.6	[-34.4, -31.2]	-2%	-32.6	[-34.2, -31.2]	-1%
GB	-39.6	[-41.5, -38.1]	-34.2	[-36.9, -32.1]	+250%	-32.9	[-35.2, -30.9]	+34%	-31.5	[-32.8, -30.4]	+39%
CA	-35.0	[-38.0, -32.6]	-31.9	[-33.2, -30.6]	+102%	-31.7	[-33.0, -30.6]	+4%	-29.1	[-30.0, -28.3]	+86%
DE	-36.8	[-38.0, -35.8]	-36.7	[-38.2, -35.5]	+4%	-32.4	[-34.0, -30.9]	+169%	-32.5	[-33.1, -31.9]	-3%
IT	-33.8	[-38.8, -30.7]	-33.9	[-35.2, -32.7]	-2%	-32.6	[-33.5, -32.0]	+33%	-31.8	[-32.6, -31.1]	+21%
US	-33.3	[-34.8, -31.8]	-30.2	[-30.9, -29.6]	+102%	-30.2	[-30.8, -29.6]	+0%	-29.9	[-30.2, -29.4]	+8%
FR	-33.4	[-34.0, -32.9]	-33.0	[-33.8, -32.2]	+11%	-33.2	[-33.8, -32.6]	-3%	-31.5	[-32.0, -31.1]	+45%

Table A.1 shows the evolution of the mean exposure to Wi-Fi on the top 13 countries. The personal exposure to Wi-Fi has increased from 2017 to 2020 in most of the countries. The increase in exposure varies across different countries ranging from +4% to 250%. Switzerland had less exposure in 2018 compared to 2017, to remain stable around 32.5 dBm in 2019 and 2020. India had a decrease in exposure in 2019 by -61% compared to 2018, but gained +40% in 2020 to reach -29.9 dBm. The FCC countries (highlighted in gray) are among the most exposed countries to Wi-Fi.

The Spearman correlations between the monthly personal exposure to Wi-Fi and time (excluding 2020) shows a significant increasing trends in 8 countries (min=0.41, max=0.69, with $p<0.05$). The increase is not significant for France, Spain, India, and the Netherlands. Switzerland shows an insignificant decrease with Spearman score

country	score	p_val
BR	0.53	7.80e-04
AU	0.41	1.20e-02
NL	0.32	5.70e-02
IN	0.15	3.90e-01
ES	0.30	7.70e-02
BE	0.66	1.20e-05
CH	-0.19	2.60e-01
GB	0.69	3.70e-06
CA	0.56	3.50e-04
DE	0.59	1.60e-04
IT	0.43	8.50e-03
US	0.58	2.10e-04
FR	0.10	5.80e-01

Table A.2: Spearman correlation between Wi-Fi exposure and time (excluding 2020)

of -0.19 (p>0.05). Including 2020 data, the Spearman scores increase by 0.13, and the p-values decrease by 8%, on average. The effect of adding 2020 data is mainly noticeable for France and India, with an increase in Spearman score by 0.38 and 0.16, respectively, with a decrease in the p-values by 36% and 58%, respectively.

The increase in Wi-Fi exposure does not correspond to an important increase in the number of Wi-Fi sources. As described in Section 5.1.3, we compute the evolution of the number of Wi-Fi sources from 2017 to 2020. The results are shown in Table A.3. The slight change in the number of Wi-Fi sources ranges from -12% to +11%. People see different number of Wi-Fi sources in the different countries, ranging from around 5 to 12 sources. Countries with higher Wi-Fi household penetration such as the Netherlands [203, 204], have higher number of Wi-Fi sources.

Table A.3: Evolution of the number of Wi-Fi sources. FCC countries highlighted in gray.

Country	2017 Mean	95%CI	2018 Mean	95%CI	Change	2019 Mean	95%CI	Change	2020 Mean	95%CI	Change
BR	7.71	[6.9, 8.5]	7.27	[6.8, 7.8]	-6%	8.05	[7.4, 8.7]	+11%	7.58	[7.3, 7.8]	-6%
AU	7.15	[6.1, 8.3]	6.38	[5.8, 7.0]	-11%	6.30	[5.8, 6.8]	-1%	6.42	[6.1, 6.7]	+2%
NL	10.67	[9.4, 12.1]	11.72	[10.7, 12.8]	+10%	11.03	[9.9, 12.1]	-6%	11.36	[10.8, 11.8]	+3%
IN	5.12	[4.2, 6.0]	4.64	[4.0, 5.4]	-9%	5.02	[4.7, 5.3]	+8%	4.42	[4.2, 4.6]	-12%
ES	9.24	[8.3, 10.2]	9.28	[8.6, 9.9]	+0%	9.57	[9.0, 10.3]	+3%	9.87	[9.6, 10.2]	+3%
BE	7.97	[7.2, 8.8]	7.95	[7.4, 8.5]	+0%	7.62	[7.2, 8.1]	-4%	7.56	[7.3, 7.8]	-1%
CH	8.09	[7.2, 8.9]	8.24	[7.8, 8.7]	+2%	8.22	[7.8, 8.6]	+0%	7.67	[7.4, 8.0]	-7%
GB	9.03	[7.7, 10.3]	9.22	[8.5, 9.9]	+2%	8.05	[7.6, 8.5]	-13%	8.23	[8.0, 8.4]	+2%
CA	9.88	[9.0, 10.8]	10.39	[9.9, 10.8]	+5%	10.88	[10.6, 11.2]	+5%	12.00	[11.7, 12.3]	+10%
DE	8.20	[7.6, 8.9]	7.45	[7.2, 7.7]	-9%	7.53	[7.3, 7.7]	+1%	7.55	[7.3, 7.8]	+0%
IT	5.28	[5.0, 5.6]	5.62	[5.3, 5.9]	+6%	5.88	[5.7, 6.1]	+5%	5.72	[5.5, 5.9]	-3%
US	10.53	[10.0, 11.1]	10.79	[10.5, 11.0]	+2%	10.38	[10.1, 10.6]	-4%	11.33	[11.0, 11.6]	+9%
FR	7.28	[7.0, 7.6]	6.51	[6.3, 6.7]	-10%	6.24	[6.0, 6.4]	-4%	6.04	[5.9, 6.2]	-3%

A.5.2 Bluetooth

The exposure to Bluetooth had an increasing rate in most of the countries from 2017 to 2020. As shown in Table A.4, in 2018, the increase ranged from +39% to +522% in most countries, except in Brazil, the Netherlands, India, Germany, and USA, with a decrease in exposure by -37% to -95% compared to 2017. The exposure levels increased in 2019 by +18% to +1124% in 10 countries, except Belgium, Switzerland, and France. The exposure to Bluetooth didn't increase by much, except in 4 countries (Belgium, Switzerland, Germany, and USA).

The increase in the Bluetooth exposure level corresponds to an increase in the number of Bluetooth devices. The population of the

13 countries had more Bluetooth sources around them year after year, except in 2020, where people had no almost no increase, and rather a decrease in the number of Bluetooth sources in some countries such as Brazil. The results are shown in Table A.5. Again, the increasing trend in the Bluetooth devices has been impacted by the pandemic in 2020, with the application of the lockdown.

Table A.4: Evolution of Bluetooth exposure.

Country	2017 Mean	95%CI	2018 Mean	95%CI	Change	2019 Mean	95%CI	Change	2020 Mean	95%CI	Change
BR	-38.5	[-44.8, -35.5]	-49.9	[-52.9, -47.9]	-93%	-42.2	[-50.7, -38.0]	+484%	-43.5	[-48.3, -41.1]	-26%
AU	-51.8	[-55.5, -49.2]	-44.1	[-47.4, -41.6]	+484%	-38.9	[-44.5, -35.8]	+236%	-40.0	[-42.1, -38.2]	-23%
NL	-40.5	[-53.7, -36.8]	-45.4	[-50.8, -42.2]	-68%	-36.1	[-44.9, -32.2]	+767%	-40.4	[-44.3, -38.1]	-63%
IN	-40.9	[-50.7, -36.5]	-45.9	[-50.3, -43.5]	-68%	-41.5	[-44.2, -39.2]	+170%	-41.2	[-42.4, -40.0]	+8%
ES	-45.2	[-48.7, -43.0]	-37.2	[-41.8, -34.1]	+522%	-35.1	[-43.6, -31.5]	+62%	-40.0	[-41.7, -38.7]	-68%
BE	-46.0	[-50.9, -43.5]	-39.5	[-41.8, -37.9]	+349%	-44.1	[-47.3, -42.0]	-65%	-35.0	[-40.9, -32.0]	+710%
CH	-45.4	[-49.3, -43.0]	-39.1	[-42.2, -36.8]	+323%	-41.8	[-43.3, -40.8]	-47%	-36.4	[-40.4, -33.4]	+252%
GB	-45.2	[-53.3, -41.7]	-41.1	[-44.3, -38.8]	+155%	-36.4	[-40.1, -33.7]	+195%	-35.3	[-38.6, -32.6]	+31%
CA	-48.5	[-52.0, -46.3]	-45.2	[-48.9, -42.9]	+115%	-43.2	[-46.4, -40.3]	+56%	-41.6	[-42.8, -40.6]	+45%
DE	-29.0	[-43.2, -25.5]	-41.8	[-45.2, -39.3]	-95%	-41.1	[-43.3, -39.2]	+18%	-36.6	[-40.0, -33.6]	+180%
IT	-39.3	[-43.7, -36.7]	-37.9	[-42.1, -35.5]	+39%	-34.4	[-41.3, -30.4]	+122%	-38.5	[-39.5, -37.6]	-61%
US	-44.4	[-48.2, -42.1]	-46.4	[-47.3, -45.6]	-37%	-35.5	[-42.4, -31.5]	+1124%	-29.1	[-31.0, -27.7]	+337%
FR	-37.9	[-39.3, -36.9]	-33.2	[-36.1, -31.2]	+195%	-36.6	[-37.6, -35.7]	-54%	-36.3	[-38.2, -34.8]	+7%

Table A.5: Evolution of Bluetooth number of sources.

Country	2017 Mean	95%CI	2018 Mean	95%CI	Change	2019 Mean	95%CI	Change	2020 Mean	95%CI	Change
BR	1.61	[1.3, 1.9]	2.10	[1.6, 2.7]	+31%	3.00	[2.3, 3.7]	+43%	2.20	[2.0, 2.4]	-27%
AU	2.23	[1.9, 2.7]	3.26	[2.6, 4.0]	+46%	3.41	[2.9, 3.9]	+5%	3.74	[3.5, 4.0]	+9%
NL	2.39	[1.8, 3.1]	3.54	[2.7, 4.4]	+48%	4.02	[3.2, 4.9]	+14%	3.66	[3.4, 4.0]	-9%
IN	1.87	[1.6, 2.2]	2.07	[1.5, 2.7]	+11%	2.27	[1.9, 2.6]	+10%	2.48	[2.0, 3.2]	+10%
ES	3.01	[1.6, 5.4]	3.09	[2.6, 3.7]	+3%	4.31	[3.6, 5.0]	+39%	3.74	[3.4, 4.0]	-13%
BE	1.71	[1.5, 1.9]	2.42	[2.1, 2.7]	+41%	3.22	[2.8, 3.6]	+33%	3.02	[2.7, 3.5]	-6%
CH	1.91	[1.6, 2.2]	3.23	[2.8, 3.6]	+69%	4.49	[4.0, 4.9]	+39%	4.55	[4.1, 5.0]	+1%
GB	2.94	[2.3, 3.7]	3.51	[2.9, 4.1]	+20%	4.16	[3.5, 4.7]	+18%	3.52	[3.2, 3.8]	-15%
CA	2.67	[2.3, 3.0]	2.79	[2.5, 3.1]	+4%	4.39	[4.1, 4.7]	+57%	4.54	[4.3, 4.8]	+3%
DE	1.66	[1.4, 1.9]	2.53	[2.2, 2.9]	+53%	3.34	[3.0, 3.6]	+32%	3.34	[3.1, 3.5]	+0%
IT	1.61	[1.5, 1.7]	2.10	[1.9, 2.3]	+31%	2.78	[2.5, 3.0]	+32%	2.80	[2.6, 3.0]	+1%
US	2.22	[2.0, 2.5]	2.86	[2.6, 3.1]	+28%	4.28	[4.1, 4.5]	+50%	4.14	[4.0, 4.3]	-3%
FR	1.76	[1.6, 1.9]	2.08	[1.9, 2.3]	+18%	2.95	[2.7, 3.2]	+41%	3.16	[3.0, 3.3]	+7%

A.5.3 Cellular networks

During the 4 years, the exposure levels to 2G and 3G has decreased in almost all 13 countries. The exposure to 2G has decreased by about 10 dB, and by about 6 dB for 3G. As opposed to the two previous cellular generations, the exposure to 4G has slightly increased in most countries during the 4 years, to reach around -52 dBm by 2020. This trends across the different cellular generations can be linked

with the deprecation of the older generations (2G and 3G), and the adoption and deployment of the newer generation, the 4G LTE.

Table A.6: Evolution of 2G exposure.

Country	2017 Mean	95%CI	2018 Mean	95%CI	Change	2019 Mean	95%CI	Change	2020 Mean	95%CI	Change
BR	-60.9	[-66.0, -58.4]	-57.7	[-60.5, -55.4]	+109%	-58.2	[-60.2, -56.7]	-12%	-55.8	[-60.0, -52.5]	+75%
AU	-53.0	[-78.8, -48.4]	-69.7	[-80.3, -66.4]	-98%	-61.7	[-66.4, -59.2]	+530%	-61.9	[-79.9, -58.1]	-4%
NL	-58.0	[-60.5, -56.4]	-55.0	[-61.1, -52.0]	+96%	-61.8	[-63.7, -60.2]	-79%	-59.0	[-63.8, -55.4]	+91%
IN	-48.1	[-50.1, -46.6]	-48.2	[-50.2, -46.6]	-2%	-55.4	[-56.4, -54.5]	-81%	-55.5	[-56.7, -54.1]	-1%
ES	-54.3	[-59.7, -51.5]	-56.9	[-59.9, -54.8]	-45%	-56.6	[-60.7, -54.1]	+8%	-58.4	[-61.9, -55.5]	-35%
BE	-53.1	[-56.2, -51.3]	-60.3	[-61.8, -58.7]	-81%	-63.0	[-63.6, -62.4]	-46%	-58.9	[-64.2, -55.2]	+157%
CH	-48.0	[-51.9, -45.6]	-56.6	[-59.6, -54.5]	-86%	-60.7	[-65.9, -58.1]	-61%	-62.6	[-67.8, -59.5]	-35%
GB	-47.5	[-51.7, -45.2]	-56.9	[-63.0, -53.9]	-88%	-63.2	[-64.3, -62.3]	-77%	-61.5	[-64.5, -58.7]	+48%
CA	-48.7	[-54.5, -46.2]	-52.3	[-60.5, -48.6]	-56%	-55.3	[-66.8, -51.5]	-49%	-60.9	[-65.4, -57.7]	-73%
DE	-49.2	[-50.7, -48.2]	-53.2	[-54.7, -51.8]	-60%	-58.0	[-59.1, -56.9]	-67%	-57.2	[-61.2, -53.9]	+19%
IT	-49.2	[-52.0, -47.4]	-51.9	[-54.0, -50.3]	-46%	-58.9	[-60.1, -57.8]	-80%	-58.8	[-62.5, -55.5]	+3%
US	-57.8	[-62.7, -54.8]	-62.6	[-66.3, -60.0]	-67%	-68.2	[-69.4, -67.3]	-72%	-65.8	[-69.2, -63.0]	+75%
FR	-49.1	[-50.7, -48.1]	-52.0	[-54.1, -50.2]	-49%	-56.9	[-57.6, -56.2]	-67%	-57.7	[-60.6, -54.9]	-16%

Table A.7: Evolution of 3G exposure.

Country	2017 Mean	95%CI	2018 Mean	95%CI	Change	2019 Mean	95%CI	Change	2020 Mean	95%CI	Change
BR	-49.8	[-53.5, -47.1]	-53.1	[-54.0, -52.4]	-54%	-51.7	[-53.3, -50.6]	+39%	-51.3	[-53.7, -48.8]	+10%
AU	-43.9	[-47.8, -41.6]	-49.5	[-52.4, -47.6]	-73%	-51.4	[-53.5, -49.8]	-36%	-53.1	[-56.6, -50.0]	-32%
NL	-47.7	[-53.7, -44.8]	-48.8	[-51.1, -47.0]	-21%	-51.8	[-53.4, -50.6]	-50%	-54.7	[-57.6, -51.9]	-48%
IN	-45.5	[-48.2, -44.0]	-45.5	[-47.0, -44.5]	+1%	-48.3	[-49.7, -47.1]	-47%	-49.4	[-51.2, -47.8]	-22%
ES	-47.3	[-49.1, -45.9]	-49.9	[-51.9, -48.3]	-45%	-50.3	[-51.7, -49.1]	-8%	-50.7	[-53.3, -48.3]	-10%
BE	-49.0	[-52.3, -47.1]	-54.9	[-56.3, -53.7]	-74%	-57.0	[-57.7, -56.4]	-38%	-53.9	[-56.6, -51.3]	+103%
CH	-44.6	[-46.6, -43.3]	-52.0	[-53.1, -51.2]	-82%	-52.7	[-53.8, -51.7]	-14%	-53.5	[-55.5, -51.6]	-18%
GB	-45.2	[-48.4, -43.3]	-51.7	[-54.7, -49.5]	-78%	-53.7	[-54.5, -53.0]	-36%	-53.3	[-56.0, -50.6]	+9%
CA	-47.2	[-51.0, -45.1]	-49.9	[-50.6, -49.2]	-46%	-55.8	[-58.4, -53.8]	-74%	-57.5	[-59.4, -55.3]	-33%
DE	-48.8	[-51.1, -47.0]	-49.2	[-49.9, -48.7]	-9%	-51.5	[-52.0, -51.1]	-41%	-52.9	[-53.5, -52.0]	-27%
IT	-45.8	[-47.7, -44.6]	-48.7	[-49.7, -47.9]	-49%	-53.2	[-54.2, -52.2]	-64%	-53.6	[-55.6, -51.2]	-9%
US	-47.2	[-49.5, -45.4]	-51.6	[-52.5, -50.8]	-64%	-53.4	[-54.0, -52.8]	-33%	-56.7	[-57.8, -55.8]	-54%
FR	-44.1	[-45.7, -43.1]	-46.8	[-48.5, -45.4]	-47%	-50.5	[-51.1, -49.9]	-56%	-52.4	[-54.7, -50.0]	-36%

Table A.8: Evolution of 4G exposure.

Country	2017 Mean	95%CI	2018 Mean	95%CI	Change	2019 Mean	95%CI	Change	2020 Mean	95%CI	Change
BR	-55.8	[-57.5, -54.5]	-52.2	[-53.1, -51.3]	+132%	-50.5	[-51.4, -49.7]	+47%	-49.5	[-49.8, -49.3]	+25%
AU	-52.1	[-53.0, -51.3]	-51.1	[-51.8, -50.4]	+25%	-51.1	[-51.7, -50.6]	-1%	-51.0	[-51.4, -50.5]	+4%
NL	-50.4	[-51.7, -49.3]	-50.4	[-50.9, -49.9]	+1%	-50.8	[-51.3, -50.3]	-9%	-51.1	[-51.3, -50.9]	-7%
IN	-48.3	[-48.8, -47.7]	-48.3	[-48.7, -47.8]	-1%	-47.8	[-48.2, -47.5]	+12%	-47.4	[-47.8, -47.1]	+9%
ES	-50.9	[-51.7, -50.2]	-51.3	[-51.5, -51.0]	-7%	-50.7	[-51.0, -50.3]	+15%	-50.9	[-51.1, -50.7]	-6%
BE	-52.5	[-53.1, -51.9]	-52.6	[-52.9, -52.1]	-1%	-52.2	[-52.5, -51.9]	+8%	-53.2	[-53.4, -53.0]	-19%
CH	-53.3	[-53.8, -52.8]	-53.2	[-53.4, -53.0]	+2%	-52.9	[-53.1, -52.7]	+6%	-53.3	[-53.6, -53.0]	-7%
GB	-51.5	[-52.8, -50.6]	-51.5	[-51.9, -51.2]	+1%	-51.5	[-51.8, -51.2]	+0%	-52.0	[-52.2, -51.7]	-10%
CA	-53.8	[-55.0, -52.4]	-52.1	[-52.4, -51.9]	+48%	-51.7	[-52.0, -51.4]	+9%	-51.9	[-52.0, -51.7]	-4%
DE	-53.3	[-53.6, -52.9]	-52.7	[-53.1, -52.3]	+14%	-53.4	[-53.5, -53.3]	-14%	-53.5	[-53.7, -53.3]	-3%
IT	-51.7	[-52.2, -51.2]	-52.2	[-52.5, -52.0]	-12%	-52.5	[-52.8, -52.3]	-7%	-52.0	[-52.1, -51.8]	+14%
US	-54.1	[-54.8, -53.5]	-53.2	[-53.3, -53.0]	+23%	-52.6	[-52.7, -52.4]	+14%	-52.3	[-52.5, -52.1]	+7%
FR	-52.5	[-52.8, -52.3]	-51.9	[-52.0, -51.8]	+16%	-51.8	[-51.9, -51.7]	+3%	-51.7	[-51.8, -51.6]	+2%

Bibliography

[1] *National Cancer Institute*. [Online; accessed 22. Apr. 2021]. URL: https://www.cancer.gov/ (cited on page 1).

[2] *Anatomy of an Electromagnetic Wave | Science Mission Directorate*. [Online; accessed 16. Jun. 2021]. June 2021. URL: https://science.nasa.gov/ems/02_anatomy (cited on page 1).

[3] ICNIRP. *The ICNIRP Guidelines for Limiting Exposure to Electromagnetic Fields (100 kHz - 300 GHz)*. [Online; accessed 19. Jun. 2021]. June 2021. URL: https://www.icnirp.org/en/publications/article/rf-guidelines-2020.html (cited on pages 1–3, 77).

[4] Jean-Luc Ravanat and Thierry Douki. 'UV and ionizing radiations induced DNA damage, differences and similarities'. In: *Radiat. Phys. Chem.* 128 (Nov. 2016), pp. 92–102. DOI: 10.1016/j.radphyschem.2016.07.007 (cited on page 2).

[5] *Radiofrequency (RF) Radiation*. [Online; accessed 16. Jun. 2021]. June 2021. URL: https://www.cancer.org/cancer/cancer-causes/radiation-exposure/radiofrequency-radiation.html (cited on page 2).

[6] *Measuring digital development: Facts and figures 2020*. [Online; accessed 17. Jun. 2021]. June 2021. URL: https://www.itu.int/en/ITU-D/Statistics/Pages/facts/default.aspx (cited on page 2).

[7] *Digital 2019: Global Internet Use Accelerates - We Are Social*. [Online; accessed 18. Jun. 2021]. Jan. 2019. URL: https://wearesocial.com/blog/2019/01/digital-2019-global-internet-use-accelerates (cited on page 2).

[8] *The Mobile Economy - The Mobile Economy 2020*. [Online; accessed 18. Jun. 2021]. Feb. 2021. URL: https://www.gsma.com/mobileeconomy (cited on page 2).

[9] *IARC classifies Radiofrequency Electromagnetic Fields as possibly carcinogenic to humans – IARC*. [Online; accessed 18. Jun. 2021]. June 2021. URL: https://www.iarc.who.int/pressrelease/iarc-classifies-radiofrequency-electromagnetic-fields-as-possibly-carcinogenic-to-humans (cited on page 2).

[10] Richard D Saunders and John GR Jefferys. 'A neurobiological basis for ELF guidelines'. In: *Health Physics* 92.6 (2007), pp. 596–603 (cited on page 3).

[11] The Hong Phong Nguyen et al. '18 GHz electromagnetic field induces permeability of Gram-positive cocci'. In: *Scientific reports* 5.1 (2015), pp. 1–12 (cited on page 3).

[12] Zsuzsanna Vecsei et al. 'Short-term radiofrequency exposure from new generation mobile phones reduces EEG alpha power with no effects on cognitive performance'. In: *Scientific reports* 8.1 (2018), pp. 1–12 (cited on page 3).

[13] Sabine J. Regel and Peter Achermann. 'Cognitive Performance Measures in Bioelectromagnetic Research - Critical Evaluation and Recommendations'. In: *Environ. Health* 10.1 (Dec. 2011), pp. 1–19. DOI: 10.1186/1476-069X-10-10 (cited on page 3).

[14] Ju Hwan Kim et al. 'Possible Effects of Radiofrequency Electromagnetic Field Exposure on Central Nerve System'. In: *Biomol. Ther. (Seoul).* 27.3 (May 2019), p. 265. DOI: 10.4062/biomolther.2018.152 (cited on page 3).

[15] Ju Hwan Kim et al. 'Early exposure to radiofrequency electromagnetic fields at 1850 MHz affects auditory circuits in early postnatal mice'. In: *Sci. Rep.* 9.377 (Jan. 2019), pp. 1–10. DOI: 10.1038/s41598-018-36868-1 (cited on page 3).

[16] Özlem Sangün et al. 'The Effects of Electromagnetic Field on the Endocrine System in Children and Adolescents.' In: *Pediatric endocrinology reviews: PER* 13.2 (2015), pp. 531–545 (cited on page 3).

[17] Michal Karasek and Woldanska-Okonska Marta. 'Electromagnetic Fields and Human Endocrine System'. In: *ScientificWorldJournal* 4 Suppl 2.Suppl 2 (Nov. 2004), pp. 23–8. DOI: 10.1100/tsw.2004.175 (cited on page 3).

[18] David R Black and Louis N Heynick. 'Radiofrequency (RF) effects on blood cells, cardiac, endocrine, and immunological functions'. In: *Bioelectromagnetics* 24.S6 (2003), S187–S195 (cited on page 3).

[19] Jesus Gonzalez-Rubio. 'Radiofrequency Electromagnetic Fields (RF-EMF) and Neurodegenerative Diseases: Is there any Connection?' In: *Journal of Dementia* 1.2 (Sept. 2017), pp. 1–2 (cited on page 3).

[20] Claudia Consales et al. 'Electromagnetic Fields, Oxidative Stress, and Neurodegeneration'. In: *Int. J. Cell Biol.* 2012 (2012). DOI: 10.1155/2012/683897 (cited on page 3).

[21] Giovanna Del Vecchio et al. 'Effect of radiofrequency electromagnetic field exposure on in vitro models of neurodegenerative disease'. In: *Bioelectromagnetics* 30.7 (Oct. 2009), pp. 564–572. DOI: 10.1002/bem.20507 (cited on page 3).

[22] Ju Hwan Kim et al. 'Long-term exposure to 835 MHz RF-EMF induces hyperactivity, autophagy and demyelination in the cortical neurons of mice'. In: *Sci. Rep.* 7.41129 (Jan. 2017), pp. 1–12. DOI: 10.1038/srep41129 (cited on page 3).

[23] Joanna Wyszkowska, Milena Jankowska, and Piotr Gas. 'Electromagnetic Fields and Neurodegenerative Diseases'. In: *Przeglad Elektrotechniczny* 95.1 (Jan. 2019), pp. 129–133. DOI: 10.15199/48.2019.01.33 (cited on page 3).

[24] Omer Dasdag, Nur Adalier, and Suleyman Dasdag. 'Electromagnetic radiation and Alzheimer's disease'. In: *Biotechnol. Biotechnol. Equip.* 34.1 (Jan. 2020), pp. 1087–1094. DOI: 10.1080/13102818.2020.1820378 (cited on page 3).

[25] Stefan Braune et al. 'Influence of a Radiofrequency Electromagnetic Field on Cardiovascular and Hormonal Parameters of the Autonomic Nervous System in Healthy Individuals'. In: *Radiat. Res.* 158.3 (Oct. 2002), pp. 352–6. DOI: 10.1667/0033-7587(2002)158[0352:IOAREF]2.0.CO;2 (cited on page 3).

[26] Fatma Mohamed et al. 'Study of the Cardiovascular Effects of Exposure to Electromagnetic Field'. In: *Life Science Journal* 8.1 (Jan. 2011), 260–U209 (cited on page 3).

[27] Jakub Misek et al. 'Heart rate variability affected by radiofrequency electromagnetic field in adolescent students'. In: *Bioelectromagnetics* 39.4 (May 2018), pp. 277–288. DOI: 10.1002/bem.22115 (cited on page 3).

[28] Onur Elmas. 'Effects of electromagnetic field exposure on the heart: a systematic review'. In: *Toxicol. Ind. Health* 32.1 (Sept. 2013), pp. 76–82. DOI: 10.1177/0748233713498444 (cited on page 3).

[29] Chidiebere Emmanuel Okechukwu. 'Does the use of mobile phone affect male fertility? A mini-review'. In: *Journal of Human Reproductive Sciences* 13.3 (Jan. 2020), p. 174. DOI: 10.4103/jhrs.JHRS_126_19 (cited on page 3).

[30] Kavindra Kumar Kesari, Ashok Agarwal, and Ralf Henkel. 'Radiations and male fertility'. In: *Reprod. Biol. Endocrinol.* 16 (2018). DOI: 10.1186/s12958-018-0431-1 (cited on page 3).

[31] Valborg Baste, Trond Riise, and Bente Moen. 'Radiofrequency electromagnetic fields; male infertility and sex ratio of offspring'. In: *Eur. J. Epidemiol.* 23.5 (May 2008), pp. 369–77. DOI: 10.1007/s10654-008-9236-4 (cited on page 3).

[32] Nasibeh Roozbeh et al. 'Influence of Radiofrequency Electromagnetic Fields on the Fertility System: Protocol for a Systematic Review and Meta-Analysis'. In: *JMIR Research Protocols* 7.2 (Feb. 2018), e9102. DOI: 10.2196/resprot.9102 (cited on page 3).

[33] B. J. Houston et al. 'The effects of radiofrequency electromagnetic radiation on sperm function'. In: *Reproduction* 152.6 (Dec. 2016), R263–R276. DOI: 10.1530/REP-16-0126 (cited on page 3).

[34] Jin-Hwa Moon. 'Health effects of electromagnetic fields on children'. In: *Clin. Exp. Pediatr.* 63.11 (Nov. 2020), p. 422. DOI: 10.3345/cep.2019.01494 (cited on pages 3, 63).

[35] Leeka Kheifets et al. 'The sensitivity of children to electromagnetic fields'. In: *Pediatrics* 116.2 (Aug. 2005), pp. 303–313. DOI: 10.1542/peds.2004-2541 (cited on page 3).

[36] Aaron Skaist. 'The Effects of RF-EMF on the Child Brain'. In: *The Science Journal of the Lander College of Arts and Sciences* 12.2 (2019), p. 7 (cited on page 3).

[37] R. Mehdizadeh A and J. Mortazavi S. M. '5G Technology: Why Should We Expect a shift from RF-Induced Brain Cancers to Skin Cancers?' In: *J. Biomed. Phys. Eng.* 9.5 (Oct. 2019), p. 505. DOI: 10.31661/jbpe.v0i0.1225 (cited on page 3).

[38] Michael Carlberg et al. 'Increasing incidence of thyroid cancer in the Nordic countries with main focus on Swedish data'. In: *BMC Cancer* 16.1 (Dec. 2016), pp. 1–15. DOI: 10.1186/s12885-016-2429-4 (cited on page 3).

[39] Fernando Pareja-Peña et al. 'Evidences of the (400 MHz – 3 GHz) radiofrequency electromagnetic field influence on brain tumor induction'. In: *International Journal of Environmental Health Research* (Mar. 2020), pp. 1–10. DOI: 10.1080/09603123.2020.1738352 (cited on page 3).

[40] Christine Kowalczuk et al. 'Absence of nonlinear responses in cells and tissues exposed to RF energy at mobile phone frequencies using a doubly resonant cavity'. In: *Bioelectromagnetics* 31.7 (2010), pp. 556–565 (cited on page 3).

[41] Jukka Juutilainen et al. 'Review of possible modulation-dependent biological effects of radiofrequency fields'. In: *Bioelectromagnetics* 32.7 (2011), pp. 511–534 (cited on page 3).

[42] *5G Appeal*. [Online; accessed 21. Jun. 2021]. June 2021. URL: https://www.5gappeal.eu (cited on page 3).

[43] *What is Epidemiology? | Teacher Roadmap | Career Paths to Public Health | CDC*. [Online; accessed 1. Jul. 2021]. May 2019. URL: https://www.cdc.gov/careerpaths/k12teacherroadmap/epidemiology.html (cited on page 4).

[44] *Principles of Epidemiology | Lesson 1 - Section 1*. [Online; accessed 1. Jul. 2021]. May 2020. URL: https://www.cdc.gov/csels/dsepd/ss1978/lesson1/section1.html (cited on page 4).

[45] Maria Feychting, Anders Ahlbom, and Leeka Kheifets. 'EMF AND HEALTH'. In: *Annu. Rev. Public Health* 26.1 (Oct. 2004), pp. 165–189. DOI: 10.1146/annurev.publhealth.26.021304.144445 (cited on page 4).

[46] CORDIS project. *Final Report Summary - EMF-NET (Effects of the exposure to electromagnetic fields: from science to public health) | Report Summary | FP6 | CORDIS | European Commission*. [Online; accessed 31. Jan. 2020]. Jan. 2020. URL: https://cordis.europa.eu/project/id/502173/reporting/fr (cited on page 4).

[47] International Agency for Research on Cancer. *The Interphone Study*. [Online; accessed 31. Jan. 2020]. Jan. 2020. URL: http://interphone.iarc.fr (cited on page 4).

[48] GERONIMO Project. *Generalised EMF Research using Novel Methods – an integrated approach: from research to risk assessment and support to risk management | GERONIMO Project | FP7 | CORDIS | European Commission*. [Online; accessed 31. Jan. 2020]. Jan. 2020. URL: https://cordis.europa.eu/project/id/603794 (cited on page 4).

[49] The COSMOS project. [Online; accessed 31. Jan. 2020]. URL: http://www.thecosmosproject.org (cited on page 4).

[50] Institute for Risk Assessment Sciences || Utrecht University. *XMobiSense app*. [Online; accessed 9. Jun. 2021]. June 2021. URL: http://www.thecosmosproject.org/xmobisense-app (visited on 06/09/2021) (cited on pages 4, 14, 15, 40).

[51] Sanjay Sagar et al. 'Radiofrequency electromagnetic field exposure in everyday microenvironments in Europe: A systematic literature review'. In: *Journal of exposure science & environmental epidemiology* 28.2 (2018), pp. 147–160 (cited on pages 4, 12, 63).

[52] ElectroSmart. [Online; accessed 31. Jan. 2020]. Jan. 2020. URL: https://electrosmart.app (cited on pages 5, 15, 40, 44, 63, 64, 90).

[53] James C. Lin. 'DOSIMETRIC COMPARISON BETWEEN DIFFERENT QUANTITIES FOR LIMITING EXPOSURE IN THE RF BAND: RATIONALE AND IMPLICATIONS FOR GUIDELINES'. In: *Health Phys.* 92.6 (June 2007), pp. 547–553. DOI: 10.1097/01.HP.0000236788.33488.65. (Visited on 06/10/2021) (cited on page 7).

[54] Azeddine Gati et al. 'Duality Between Uplink Local and Downlink Whole-Body Exposures in Operating Networks'. In: *IEEE Trans. Electromagn. Compat.* 52.4 (Sept. 2010), pp. 829–836. DOI: 10.1109/TEMC.2010.2066978. (Visited on 06/10/2021) (cited on page 8).

[55] Samuel Y. Liao. 'Measurements and Computations of Electric Field Intensity and Power Density'. In: *IEEE Trans. Instrum. Meas.* 26.1 (Mar. 1977), pp. 53–57. DOI: 10.1109/TIM.1977.4314484. (Visited on 06/10/2021) (cited on page 8).

[56] Mara Gallastegi et al. 'Children's exposure assessment of radiofrequency fields: Comparison between spot and personal measurements'. In: *Environment international* 118 (2018), pp. 60–69 (cited on pages 8–12, 63).

[57] Sam Aerts et al. 'Assessment of long-term spatio-temporal radiofrequency electromagnetic field exposure'. In: *Environmental research* 161 (2018), pp. 136–143 (cited on pages 8, 10, 63).

[58] Marta Fernandez et al. 'Measurements and analysis of temporal and spatial variability of WiFi exposure levels in the 2.4 GHz frequency band'. In: *Measurement* 149 (2020), p. 106970 (cited on page 8).

[59] Sanjay Sagar et al. 'Comparison of radiofrequency electromagnetic field exposure levels in different everyday microenvironments in an international context'. In: *Environment international* 114 (2018), pp. 297–306 (cited on pages 9–11, 63).

[60] Maarten Velghe et al. 'Characterisation of spatial and temporal variability of RF-EMF exposure levels in urban environments in Flanders, Belgium'. In: *Environmental research* 175 (2019), pp. 351–366 (cited on pages 9–11, 63).

[61] Damiano Urbinello et al. 'Radio-frequency electromagnetic field (RF-EMF) exposure levels in different European outdoor urban environments in comparison with regulatory limits'. In: *Environment international* 68 (2014), pp. 49–54 (cited on pages 9–11, 63, 77, 78).

[62] Damiano Urbinello et al. 'Temporal trends of radio-frequency electromagnetic field (RF-EMF) exposure in everyday environments across European cities'. In: *Environmental research* 134 (2014), pp. 134–142 (cited on pages 9–11, 63, 78).

[63] Raquel Ramirez-Vazquez et al. 'Personal Exposure Assessment to Wi-Fi Radiofrequency Electromagnetic Fields in Mexican Microenvironments'. In: *International Journal of Environmental Research and Public Health* 18.4 (2021), p. 1857 (cited on pages 9–12, 63).

[64] Chhavi Raj Bhatt et al. 'Radiofrequency-electromagnetic field exposures in kindergarten children'. In: *Journal of exposure science & environmental epidemiology* 27.5 (2017), pp. 497–504 (cited on pages 9–12, 63).

[65] Berihun M Zeleke et al. 'Personal exposure to radio frequency electromagnetic fields among Australian adults'. In: *International journal of environmental research and public health* 15.10 (2018), p. 2234 (cited on pages 9–12, 63).

[66] Raquel Ramirez-Vazquez et al. 'Characterisation of personal exposure to environmental radiofrequency electromagnetic fields in Albacete (Spain) and assessment of risk perception'. In: *Environmental research* 172 (2019), pp. 109–116 (cited on pages 9–12, 16, 63).

[67] Chhavi Raj Bhatt et al. 'Estimating transmitted power density from mobile phone: an epidemiological pilot study with a software modified phone'. In: *Australasian physical & engineering sciences in medicine* 41.4 (2018), pp. 985–991 (cited on pages 9–12, 63).

[68] Laura Ellen Birks et al. 'Spatial and temporal variability of personal environmental exposure to radio frequency electromagnetic fields in children in Europe'. In: *Environment international* 117 (2018), pp. 204–214 (cited on pages 9–12, 63).

[69] Adnan Lahham and Haitham Ayyad. 'Personal exposure to radiofrequency electromagnetic fields among palestinian adults'. In: *Health physics* 117.4 (2019), pp. 396–402 (cited on pages 9–12, 63).

[70] Shanshan Wang and Joe Wiart. 'Sensor-Aided EMF Exposure Assessments in an Urban Environment Using Artificial Neural Networks'. In: *International journal of environmental research and public health* 17.9 (2020), p. 3052 (cited on page 10).

[71] Emmanuelle Conil et al. 'Exposure index of EU project LEXNET: principles and simulation-based computation'. In: *8th European Conference on Antennas and Propagation (EUCAP 2014)*. IEEE. 2014, pp. 3029–3032 (cited on page 10).

[72] Corentin Regrain et al. 'Design of an integrated platform for mapping residential exposure to rf-emf sources'. In: *International Journal of Environmental Research and Public Health* 17.15 (2020), p. 5339 (cited on page 10).

[73] *Evolved Universal Terrestrial Radio Access (E-UTRA); User Equipment (UE) radio transmission and reception. Technical specification (TS) 36.101. Release 8.* [Online; accessed 23. May 2021]. May 2021. URL: https://portal.3gpp.org/desktopmodules/Specifications/SpecificationDetails.aspx?specificationId=2411 (visited on 05/23/2021) (cited on pages 11, 31).

[74] Jürgen Breckenkamp et al. 'Residential characteristics and radiofrequency electromagnetic field exposures from bedroom measurements in Germany'. In: *Radiation and environmental biophysics* 51.1 (2012), pp. 85–92 (cited on page 12).

[75] Peter Gajšek et al. 'Electromagnetic field exposure assessment in Europe radiofrequency fields (10 MHz–6 GHz)'. In: *Journal of exposure science & environmental epidemiology* 25.1 (2015), pp. 37–44 (cited on page 12).

[76] John F. B. Bolte. 'Lessons learnt on biases and uncertainties in personal exposure measurement surveys of radiofrequency electromagnetic fields with exposimeters'. In: *Environ. Int.* 94 (Sept. 2016), pp. 724–735. DOI: 10.1016/j.envint.2016.06.023 (cited on pages 12, 13).

[77] Jonghyuk Choi et al. 'Assessment of radiofrequency electromagnetic field exposure from personal measurements considering the body shadowing effect in Korean children and parents'. In: *Sci. Total Environ.* 627 (June 2018), pp. 1544–1551. DOI: 10.1016/j.scitotenv.2018.01.318 (cited on page 13).

[78] John F. B. Bolte, Gerard van der Zande, and Jos Kamer. 'Calibration and uncertainties in personal exposure measurements of radiofrequency electromagnetic fields'. In: *Bioelectromagnetics* 32.8 (Dec. 2011), pp. 652–663. DOI: 10.1002/bem.20677 (cited on page 13).

[79] Sanjay Sagar et al. 'Radiofrequency electromagnetic field exposure in everyday microenvironments in Europe: A systematic literature review'. In: *J. Exposure Sci. Environ. Epidemiol.* 28 (Mar. 2018), pp. 147–160. DOI: 10.1038/jes.2017.13. (Visited on 05/07/2021) (cited on pages 13, 63).

[80] Tan Zhang et al. 'A wireless spectrum analyzer in your pocket'. In: *Proceedings of the 16th International Workshop on Mobile Computing Systems and Applications*. ACM. 2015, pp. 69–74 (cited on pages 13, 40).

[81] Ana Nika et al. 'Towards commoditized real-time spectrum monitoring'. In: *Proceedings of the 1st ACM workshop on Hot topics in wireless*. ACM. 2014, pp. 25–30 (cited on pages 13, 40).

[82] Andreas Achtzehn et al. 'CrowdREM: Harnessing the power of the mobile crowd for flexible wireless network monitoring'. In: *Proceedings of the 16th International Workshop on Mobile Computing Systems and Applications*. ACM. 2015, pp. 63–68 (cited on pages 14, 40).

[83] OpenMoko project. *OpenMoko*. 2019. URL: www.openmoko.org (cited on page 14).

[84] OsmocomBB project. *OsmocomBB*. 2019. URL: osmocom.org/projects/baseband (cited on page 14).

[85] Chenglong Li et al. 'ReLoc: Hybrid RSSI- and Phase-Based Relative UHF-RFID Tag Localization With COTS Devices'. In: *IEEE Trans. Instrum. Meas.* 69.10 (Apr. 2020), pp. 8613–8627. DOI: 10.1109/TIM.2020.2991564 (cited on page 14).

[86] Valter Pasku, Mario Luca Fravolini, and Antonio Moschitta. 'Effects of antenna directivity on RF ranging when using space diversity techniques'. In: *Measurement* 98 (Feb. 2017), pp. 429–438. DOI: 10.1016/j.measurement.2015.11.030 (cited on page 14).

[87] Narseo Vallina-Rodriguez et al. 'RILAnalyzer: A Comprehensive 3G Monitor on Your Phone'. In: *Proceedings of the 2013 Conference on Internet Measurement Conference*. IMC '13. Barcelona, Spain: Association for Computing Machinery, 2013, pp. 257–264. DOI: 10.1145/2504730.2504764 (cited on pages 14, 27, 40).

[88] Yuanjie Li et al. 'Mobileinsight: Extracting and analyzing cellular network information on smartphones'. In: *Proceedings of the 22nd Annual International Conference on Mobile Computing and Networking*. 2016, pp. 202–215 (cited on pages 14, 27, 40).

[89] OpenSignal. *Mobile Analytics and Insights | Opensignal*. [Online; accessed 31. Jan. 2020]. Jan. 2020. URL: https://www.opensignal.com (cited on pages 14, 40).

[90] Tutela. [Online; accessed 31. Jan. 2020]. Jan. 2020. URL: https://www.tutela.com (cited on pages 14, 40).

[91] T. Mazloum et al. 'XMobiSensePlus: An updated application for the assessment of human exposure to RF-EMFs'. In: *2020 XXXIIIrd General Assembly and Scientific Symposium of the International Union of Radio Science*. 2020, pp. 1–2. DOI: 10.23919/URSIGASS49373.2020.9232310 (cited on pages 15, 40, 69).

[92] *Quanta Monitor. Cellraid, making mobile well-being products for you.* [Online; accessed 9. Jun. 2021]. June 2021. URL: http://www.cellraid.com/quanta-monitor (visited on 06/09/2021) (cited on page 15).

[93] *Tawkon. Tawkon LTD.* (Cited on page 15).

[94] *EME Spy Evolution | MVG*. [Online; accessed 14. Jun. 2021]. June 2021. URL: https://www.mvg-world.com/fr/products/rf-safety/public-rf-safety/eme-spy-evolution (visited on 06/14/2021) (cited on page 15).

[95] *ExpoM – RF |Fields at Work GmbH Zurich*. [Online; accessed 14. Jun. 2021]. June 2021. URL: https://fieldsatwork.ch/products/expom-rf (visited on 06/14/2021) (cited on page 15).

[96] Lena K. Hedendahl et al. 'Measurements of Radiofrequency Radiation with a Body-Borne Exposimeter in Swedish Schools with Wi-Fi'. In: *Front. Public Health* 5 (Nov. 2017). DOI: 10.3389/fpubh.2017.00279. (Visited on 06/14/2021) (cited on page 16).

[97] Marco Zahner. 'Analysis, Methods, and Tools for Electromagnetic Field Exposure Assessment and Control'. PhD thesis. Zürich, Switzerland: ETH, 2017. DOI: 10.3929/ethz-b-000206057 (cited on page 16).

[98] *Observatoire des ondes*. [Online; accessed 1. Oct. 2021]. Sept. 2021. URL: https://www.anfr.fr/controle-des-frequences/exposition-du-public-aux-ondes/la-mesure-de-champ/observatoire-des-ondes (cited on page 17).

[99] ANFR. *Protocole de mesure*. [Online; accessed 19. Nov. 2021]. Dec. 2019. URL: https://www.anfr.fr/controle-des-frequences/exposition-du-public-aux-ondes/la-mesure-de-champ/protocole-de-mesure (cited on page 17).

[100] *Cartoradio - ANFR*. [Online; accessed 19. Nov. 2021]. Nov. 2021. URL: https://www.cartoradio.fr/# (cited on page 18).

[101] *Mobile Operating System Market Share Worldwide | StatCounter Global Stats*. [Online; accessed 1. Jul. 2021]. July 2021. URL: https://gs.statcounter.com/os-market-share/mobile/worldwide (cited on page 21).

[102] *Mobile OS market share 2021 | Statista*. [Online; accessed 1. Jul. 2021]. July 2021. URL: https://www.statista.com/statistics/272698/global-market-share-held-by-mobile-operating-systems-since-2009 (cited on page 21).

[103] Sajal Kumar Das. *Mobile Terminal Receiver Design: LTE and LTE-Advanced*. Wiley Telecom, 2017. (Visited on 04/21/2021) (cited on pages 22, 23, 27, 28, 30, 36).

[104] *Core of the matter: Is octa always better than quad? | Qualcomm*. [Online; accessed 20. Apr. 2021]. May 2019. URL: https://www.qualcomm.com/news/onq/2016/06/01/core-matter-octa-always-better-quad (visited on 04/20/2021) (cited on page 22).

[105] *Counterpoint Research*. [Online; accessed 20. Apr. 2021]. Sept. 2020. URL: https://www.counterpointresearch.com/qualcomm-leads-market-despite-losing-share-to-hisilicon-q2-2020 (visited on 04/20/2021) (cited on page 22).

[106] *Counterpoint Research*. [Online; accessed 1. Jul. 2021]. Sept. 2020. URL: https://www.counterpointresearch.com/qualcomm-leads-market-despite-losing-share-to-hisilicon-q2-2020 (cited on page 23).

[107] Bushra Aloraini et al. 'A New Covert Channel over Cellular Voice Channel in Smartphones'. In: (Apr. 2015) (cited on page 23).

[108] *Android Overview | Open Handset Alliance*. [Online; accessed 22. Apr. 2021]. Dec. 2019. URL: https://www.openhandsetalliance.com/android_overview.html (visited on 04/22/2021) (cited on page 24).

[109] Adrianne Jeffries. 'Disconnect: why Andy Rubin and Android called it quits'. In: *Verge* (Mar. 2013). (Visited on 04/21/2021) (cited on page 24).

[110] By Ben Elgin. *Google Buys Android for Its Mobile Arsenal*. [Online; accessed 21. Apr. 2021]. Apr. 2021. URL: https://web.archive.org/web/20110205190729/http://www.businessweek.com/technology/content/aug2005/tc20050817_0949_tc024.htm (visited on 04/21/2021) (cited on page 24).

[111] *Mobile OS market share 2021 | Statista*. [Online; accessed 21. Apr. 2021]. Apr. 2021. URL: https://www.statista.com/statistics/272698/global-market-share-held-by-mobile-operating-systems-since-2009 (visited on 04/21/2021) (cited on page 24).

[112] *Platform Architecture | Android Developers*. [Online; accessed 22. Apr. 2021]. Mar. 2021. URL: https://developer.android.com/guide/platform (visited on 04/22/2021) (cited on page 24).

[113] *Android Apps on Google Play*. [Online; accessed 22. Apr. 2021]. Apr. 2021. URL: https://play.google.com/store/apps (visited on 04/22/2021) (cited on page 24).

[114] *Modem – Complete History of The Modem*. [Online; accessed 22. Apr. 2021]. Apr. 2021. URL: https://history-computer.com/modem-complete-history-of-the-modem (visited on 04/22/2021) (cited on page 25).

[115] Dave Jing Tian et al. 'Attention spanned: Comprehensive vulnerability analysis of {AT} commands within the android ecosystem'. In: *27th {USENIX} Security Symposium ({USENIX} Security 18)*. 2018, pp. 273–290 (cited on pages 25, 26).

[116] *ETSI TS 102 511 V1.1.1)*. [Online; accessed 22. Apr. 2021]. (2007. URL: https://www.etsi.org/deliver/etsi_ts/102500_102599/102511/01.01.01_60/ts_102511v010101p.pdf (visited on 04/22/2021) (cited on page 25).

[117] ITU. *Serial asynchronous automatic dialling and control. Recommendation V.250*. [Online; accessed 23. Apr. 2021]. URL: https://www.itu.int/rec/T-REC-V.250/en (visited on 04/23/2021) (cited on page 25).

[118] *ETSI TS 127 007 V10.3.0*. [Online; accessed 22. Apr. 2021]. (2011. URL: https://www.etsi.org/deliver/etsi_ts/127000_127099/127007/10.03.00_60/ts_127007v100300p.pdf (visited on 04/22/2021) (cited on page 25).

[119] Collin Mulliner et al. 'Taming Mr Hayes: Mitigating signaling based attacks on smartphones'. In: *IEEE/IFIP international conference on dependable systems and networks (DSN 2012)*. IEEE. 2012, pp. 1–12 (cited on page 25).

[120] Fabien Sanglard. *Tracing the baseband*. [Online; accessed 23. Apr. 2021]. Apr. 2021. URL: https://fabiensanglard.net/cellphoneModem (visited on 04/23/2021) (cited on page 25).

[121] Fabien Sanglard. *Tracing the baseband*. [Online; accessed 23. Apr. 2021]. Apr. 2021. URL: https://fabiensanglard.net/cellphoneModem/index2.php (visited on 04/23/2021) (cited on page 25).

[122] Joshua J Drake et al. *Android hacker's handbook*. John Wiley & Sons, 2014 (cited on page 26).

[123] Navnath S Bagal and ND Kale. 'Android open-source operating System for mobile devices.' In: *IOSR Journal of Computer Engineering* 11 (2013), pp. 25–29 (cited on page 26).

[124] *Android RIL Architecture*. [Online; accessed 26. Apr. 2021]. Apr. 2021. URL: https://www.e-consystems.com/Articles/Android/Android-RIL-Architecture.asp (visited on 04/26/2021) (cited on page 26).

[125] *Radio Layer Interface | Android Open Source*. [Online; accessed 26. Apr. 2021]. Sept. 2015. URL: https://wladimir-tm4pda.github.io/porting/telephony.html (visited on 04/26/2021) (cited on page 26).

[126] AJ Singh and Akshay Bhardwaj. 'Android internals and telephony'. In: *Int. J. Emerg. Technol. Adv. Eng* 4 (2014), pp. 51–59 (cited on page 26).

[127] *Qualcomm XDM*. [Online; accessed 11. May 2021]. Apr. 2020. URL: https://www.qualcomm.com/documents/qxdm-professional-qualcomm-extensible-diagnostic-monitor (visited on 05/11/2021) (cited on page 27).

[128] *Half wave dipole antenna*. [Online; accessed 14. May 2021]. May 2021. URL: https://pt.slideshare.net/roshankattel/half-wave-dipole-antenna-64646583?smtNoRedir=1 (visited on 05/14/2021) (cited on page 28).

[129] Fraidoon Mazda. *Telecommunications Engineer's Reference Book*. Oxford, England, UK: Butterworth-Heinemann, 1993. (Visited on 05/12/2021) (cited on page 28).

[130] Thomas Norman. *Integrated Security Systems Design*. Oxford, England, UK: Butterworth-Heinemann, 2014. (Visited on 05/12/2021) (cited on page 28).

[131] Kyohei Fujimoto and J. R. James. *Mobile Antenna Systems Handbook, Third Edition*. Norwood, South Australia, Australia: Artech House Publishers, July 2008. (Visited on 05/14/2021) (cited on pages 28–30).

[132] FCC ID. 'SMG900P Multi band GSM/EDGE/UMTS/CDMA/LTE Phone with WLAN, Bluetooth, RFID, and ANT+ RF Exposure Info Samsung Electronics'. In: *FCC ID* (Feb. 2020). (Visited on 05/17/2021) (cited on page 29).

[133] Martin Sauter. *From GSM to LTE-Advanced Pro and 5G*. Aug. 2017 (cited on pages 30, 31, 33, 34, 36).

[134] IEEE Standards association. 'IEEE 802.11-1997'. In: (1997). [Online; accessed 24. Sep. 2020] (cited on page 31).

[135] IEEE Standards association. 'IEEE P802.11ax'. In: (2017). IEEE Draft Standard [Online; accessed 24. Sep. 2020] (cited on page 31).

[136] Jaidev Sharma. 'The Wi-Fi Evolution'. In: (2020). [Online; accessed 24. Sep. 2020] (cited on page 31).

[137] IEEE Standards association. 'IEEE 802.11a-1999'. In: (1999). [Online; accessed 24. Sep. 2020] (cited on page 31).

[138] IEEE Standards association. 'IEEE 802.11b-1999'. In: (1999). [Online; accessed 24. Sep. 2020] (cited on page 31).

[139] IEEE Standards association. 'IEEE 802.11g-2003'. In: (2003). [Online; accessed 24. Sep. 2020] (cited on page 31).

[140] IEEE Standards association. '802.11n-2009'. In: (2009). [Online; accessed 24. Sep. 2020] (cited on page 31).

[141] IEEE Standards association. '802.11ac-2013'. In: (2013). [Online; accessed 24. Sep. 2020] (cited on page 31).

[142] *Wi-Fi 6 adoption will outpace 5G by a wide margin, says ABI | Wi-Fi NOW Global*. [Online; accessed 16. Feb. 2021]. Dec. 2018. URL: https://wifinowglobal.com/news-and-blog/wi-fi-6-adoption-will-outpace-5g-by-a-wide-margin-says-abi-research (visited on 02/16/2021) (cited on page 31).

[143] Matthew S. Gast. *802.11ac: A Survival Guide*. O'Reilly Media, Inc., Aug. 2013 (cited on pages 32, 33).

[144] H. T. Friis. 'A Note on a Simple Transmission Formula'. In: *Proc. IRE* 34.5 (May 1946), pp. 254–256. DOI: 10.1109/JRPROC.1946.234568 (cited on pages 32, 73).

[145] Motorola. *5ghz ieee 802.11a for interference avoidance*. [Online; accessed 24. Sep. 2020]. 2009 (cited on page 32).

[146] *What is the maximum range of a Bluetooth connection? | Samsung Pakistan*. [Online; accessed 18. Feb. 2021]. Nov. 2020. URL: https://www.samsung.com/pk/support/mobile-devices/what-is-the-maximum-range-of-a-bluetooth-connection (visited on 02/18/2021) (cited on page 33).

[147] *What are passive and active scanning? | Wi-Fi Alliance*. [Online; accessed 24. May 2021]. May 2021. URL: https://www.wi-fi.org/knowledge-center/faq/what-are-passive-and-active-scanning (visited on 05/24/2021) (cited on page 34).

[148] *Voice over Wireless LAN 4.1 Design Guide*. [Online; accessed 24. May 2021]. May 2021. URL: https://www.cisco.com/c/en/us/td/docs/solutions/Enterprise/Mobility/vowlan/41dg/vowlan41dg-book.html (visited on 05/24/2021) (cited on page 34).

[149] German Castignani, Nicolas Montavont, and Andrés Arcia-Moret. 'Analysis and evaluation of wifi scanning strategies'. In: *Proceeding of IV Cibelec* (2010), pp. 3–7 (cited on page 34).

[150] German Castignani, Andrés Arcia, and Nicolas Montavont. 'A study of the discovery process in 802.11 networks'. In: *ACM SIGMOBILE Mobile Computing and Communications Review* 15.1 (2011), pp. 25–36 (cited on page 34).

[151] David Murray, Michael Dixon, and Terry Koziniec. 'Scanning delays in 802.11 networks'. In: *The 2007 International Conference on Next Generation Mobile Applications, Services and Technologies (NGMAST 2007)*. IEEE. 2007, pp. 255–260 (cited on page 34).

[152] *[802.11] Wi-Fi Connection/Disconnection process*. [Online; accessed 25. May 2021]. Oct. 2020. URL: https://community.nxp.com/t5/Wireless-Connectivity-Knowledge/802-11-Wi-Fi-Connection-Disconnection-process/ta-p/1121148 (visited on 05/25/2021) (cited on page 34).

[153] Ryan JR Thompson, Ediz Cetin, and Andrew G Dempster. 'Unknown source localization using RSS in open areas in the presence of ground reflections'. In: *Proceedings of IEEE/ION PLANS 2012*. 2012, pp. 1018–1027 (cited on page 35).

[154] *Understanding the scan modes in WiFi Explorer Pro | Intuitibits*. [Online; accessed 25. May 2021]. July 2020. URL: https://www.intuitibits.com/2017/08/11/understanding-scan-modes-wifiexplorerpro (visited on 05/25/2021) (cited on page 35).

[155] Frank Siegemund and Michael Rohs. 'Rendezvous layer protocols for Bluetooth-enabled smart devices'. In: *International Conference on Architecture of Computing Systems*. Springer. 2002, pp. 256–273 (cited on page 35).

[156] Gergely V Záruba and Vishant Gupta. 'Simplified Bluetooth device discovery-Analysis and simulation'. In: *37th Annual Hawaii International Conference on System Sciences, 2004. Proceedings of the*. IEEE. 2004, 9–pp (cited on page 35).

[157] *ETSI - TS 125 304 - Universal Mobile Telecommunications System (UMTS); User Equipment (UE) procedures in idle mode and procedures for cell reselection in connected mode | Engineering360*. [Online; accessed 26. May 2021]. May 2021. URL: https://standards.globalspec.com/std/14328923/TS%5C%20125%5C%20304 (visited on 05/26/2021) (cited on page 36).

[158] *ETSI - TS 145 008 - Digital cellular telecommunications system (Phase 2+) (GSM); GSM/EDGE Radio subsystem link control | Engineering360*. [Online; accessed 26. May 2021]. May 2021. URL: https://standards.globalspec.com/std/14343151/TS%5C%20145%5C%20008 (visited on 05/26/2021) (cited on page 36).

[159] *ETSI TS 36.304 - Evolved Universal Terrestrial Radio Access (E-UTRA); User Equipment (UE) procedures in idle mode* (cited on page 36).

[160] Yixin Wang et al. 'RSSI-based bluetooth indoor localization'. In: *2015 11th International Conference on Mobile Ad-hoc and Sensor Networks (MSN)*. IEEE. 2015, pp. 165–171 (cited on page 40).

[161] Google Apple. *Exposure Notification, Bluetooth Specification*. Tech. rep. Preliminary work, V1.2. Apr. 2020 (cited on page 40).

[162] Claude Castelluccia et al. 'ROBERT: ROBust and privacy-presERving proximity Tracing'. working paper. May 2020 (cited on page 40).

[163] Y BOUSSAD et al. *Calibration Android application - Prototype and Resources, https://github.com/Yanis-Boussad/smartphone_calibration*. URL: %5Curl%7Bhttps://github.com/Yanis-Boussad/smartphone_calibration%7D (cited on pages 40, 49, 51, 53).

[164] Y BOUSSAD et al. 'Open-Source 4G Experimental Setup'. In: *2020 IEEE International Symposium on Antennas and Propagation and North American Radio Science Meeting*. IEEE. Montreal, Canada, July 2020 (cited on page 41).

[165] Navid Nikaein et al. 'OpenAirInterface: an open LTE network in a PC'. In: *Proceedings of the 20th annual international conference on Mobile computing and networking*. ACM. 2014, pp. 305–308 (cited on page 42).

[166] Ettus. *Ettus USRP B210*. 2019. URL: www.ettus.com/product/details/UB210-KIT (cited on page 42).

[167] RedBearLab. *Blend Micro*. Web page. [Online; accessed October 2020]. URL: https://github.com/RedBearLab/Blend (cited on page 42).

[168] *Fossil, Hybrid Smartwatch Commuter, FTW1150*. Web page. [Online; accessed October 2020]. URL: https://www.fossil.com/en-gb/products/hybrid-smartwatch-commuter-dark-brown-leather/FTW1150.html (cited on page 42).

[169] Cartoradio - ANFR. [Online; accessed 3. Feb. 2020]. Jan. 2020. URL: https://www.cartoradio.fr/ (cited on page 43).

[170] Android Developers. *PhoneStateListener*. 2019. URL: https://developer.android.com/reference/android/telephony/PhoneStateListener (visited on 08/10/2019) (cited on page 44).

[171] Android Developers. *TelephonyManager*. 2019. URL: https://developer.android.com/reference/android/telephony/TelephonyManager.html#getAllCellInfo() (visited on 08/10/2019) (cited on page 44).

[172] EB Dam, M Koch, and M Lillholm. 'Quaternions Interpolation and Animation. Datalogisk Institut'. In: *Københavns Universitet* (1998) (cited on page 45).

[173] A Alaimo et al. 'Comparison between euler and quaternion parametrization in uav dynamics'. In: *AIP Conference Proceedings*. Vol. 1558. 1. AIP. 2013, pp. 1228–1231 (cited on page 45).

[174] ETSI. '3GPP TS 27.007 version 8.5.0 Release 8'. In: *ETSI TS* () (cited on page 46).

[175] Rohde&Schwarz. *FSL3 Spectrum Analyzer*. 2019. URL: www.rohde-schwarz.com/fr/produit/fsl-page-de-demarrage-produits_63493-8042.html (cited on page 47).

[176] calibrateMag. *Calibrating magnetometer sensor*. 2019. URL: ww2.mathworks.cn/help/supportpkg/beagleboneblue/ref/calibratemag.html (cited on page 47).

[177] Constantine A Balanis. *Antenna theory: analysis and design*. John wiley & sons, 2016 (cited on page 49).

[178] Carl B Dietrich et al. 'Spatial, polarization, and pattern diversity for wireless handheld terminals'. In: *IEEE transactions on antennas and propagation* 49.9 (2001), pp. 1271–1281 (cited on page 56).

[179] Sukhdeep Kaur, Jaipreet Kaur, and Manjit Sandhu. 'Antenna Diversity Techniques'. In: () (cited on page 56).

[180] Kyōhei Fujimoto. *Mobile antenna systems handbook*. Artech House, 2001 (cited on page 58).

[181] Shiwangi Gupta, Radhey Shyam Sharma, and Rajeev Singh. 'Non-ionizing radiation as possible carcinogen'. In: *International Journal of Environmental Health Research* (Sept. 2020), pp. 1–25. DOI: 10.1080/09603123.2020.1806212. (Visited on 05/07/2021) (cited on page 63).

[182] John William Frank. 'Electromagnetic fields, 5G and health: what about the precautionary principle?' In: *J. Epidemiol. Community Health* jech-2019-213595. (Jan. 2021). DOI: 10.1136/jech-2019-213595. (Visited on 05/07/2021) (cited on page 63).

[183] Lennart Hardell. 'World Health Organization, radiofrequency radiation and health - a hard nut to crack (Review)'. In: *Int. J. Oncol.* 51.2 (Aug. 2017), pp. 405–413. DOI: 10.3892/ijo.2017.4046. (Visited on 05/07/2021) (cited on page 63).

[184] Timur Saliev et al. 'Biological effects of non-ionizing electromagnetic fields: Two sides of a coin'. In: *Prog. Biophys. Mol. Biol.* 141 (Jan. 2019), pp. 25–36. DOI: 10.1016/j.pbiomolbio.2018.07.009. (Visited on 05/07/2021) (cited on page 63).

[185] Agostino Di Ciaula. 'Towards 5G communication systems: Are there health implications?' In: *Int. J. Hyg. Environ. Health* 221.3 (Apr. 2018), pp. 367–375. DOI: 10.1016/j.ijheh.2018.01.011. (Visited on 05/07/2021) (cited on page 63).

[186] International Agency for Research on Cancer et al. 'IARC classifies radiofrequency electromagnetic fields as possibly carcinogenic to humans'. In: *Press release* 208 (2011) (cited on page 63).

[187] *Standard IARC classification Glossary*. [Online; accessed 18 May 2021]. May 2021. URL: https://ec.europa.eu/health/scientific_committees/opinions_layman/en/electromagnetic-fields/glossary/ghi/iarc-classification.htm (cited on page 63).

[188] Marloes Eeftens et al. 'Personal exposure to radio-frequency electromagnetic fields in Europe: Is there a generation gap?' In: *Environment international* 121 (2018), pp. 216–226 (cited on page 63).

[189] J. Breckenkamp et al. 'Residential characteristics and radiofrequency electromagnetic field exposures from bedroom measurements in Germany'. In: *Radiat. Environ. Biophys.* 51.1 (Mar. 2012), pp. 85–92. DOI: 10.1007/s00411-011-0389-2. (Visited on 05/07/2021) (cited on page 63).

[190] *Operational Committee for the assesment of Legal and Ethical risks.* [Online; accessed 18 May 2021]. May 2021. URL: https://www.inria.fr/en/operational-committee-assesment-legal-and-ethical-risks (cited on page 66).

[191] European General Data Protection Regulation (GDPR). [Online; accessed 1. Dec. 2020]. Dec. 2020. URL: https://gdpr-info.eu/ (cited on page 66).

[192] Wikipedia: Exynos. [Online; accessed 1. Dec. 2020]. Dec. 2020. URL: https://en.wikipedia.org/wiki/Exynos/ (cited on page 69).

[193] *OpenStreetMap Nominatim*. [Online; accessed 15. Jan. 2021]. Jan. 2021. URL: https://nominatim.openstreetmap.org/ui/search.html (visited on 01/15/2021) (cited on page 71).

[194] *timezonefinder*. [Online; accessed 15. Jan. 2021]. Jan. 2021. URL: https://pypi.org/project/timezonefinder (visited on 01/15/2021) (cited on page 71).

[195] Goutam Chakraborty et al. 'Analysis of the Bluetooth Device Discovery Protocol'. In: *Wirel. Netw.* 16.2 (Feb. 2010), p. 421436. DOI: 10.1007/s11276-008-0142-1 (cited on page 72).

[196] *ISO 3166 Country Codes*. [Online; accessed 16. Jun. 2021]. June 2021. URL: https://www.iso.org/iso-3166-country-codes.html (cited on page 75).

[197] Bradley Efron and Robert J Tibshirani. *An introduction to the bootstrap*. CRC press, 1994 (cited on page 75).

[198] WHO - Global Health Observatory data repository. *Exposure limits for radio-frequency fields (public) Data by country*. [Online; accessed 22-February-2021]. 2017. URL: https://apps.who.int/gho/data/view.main.EMFLIMITSPUBCRADIOFREQUENCYv (cited on page 77).

[199] Rianne Stam. 'Comparison of international policies on electromagnetic fields:(power frequency and radiofrequency fields)'. In: (2018) (cited on page 77).

[200] Samuel Y Liao. 'Measurements and computations of electric field intensity and power density'. In: *IEEE Transactions on Instrumentation and Measurement* 26.1 (1977), pp. 53–57 (cited on page 78).

[201] Y. Boussad et al. 'Evaluating Smartphone Accuracy for RSSI Measurements'. In: *IEEE Transactions on Instrumentation and Measurement* 70 (2021), pp. 1–12. DOI: 10.1109/TIM.2020.3048776 (cited on page 81).

[202] *Wireless regulatory database for CRDA*. [Online; accessed 8. Feb. 2021]. Feb. 2021. URL: https://git.kernel.org/pub/scm/linux/kernel/git/sforshee/wireless-regdb.git/about (visited on 02/08/2021) (cited on page 82).

[203] US Census Bureau. 'Computer and Internet Use in the United States: 2016'. In: *United States Census Bureau* (Oct. 2019) (cited on pages 83, 92).

[204] *Statistics | Eurostat*. [Online; accessed 15. Sep. 2020]. Sept. 2020. URL: https://ec.europa.eu/eurostat/databrowser/view/tin00073/default/table?lang=en (cited on pages 83, 92).

[205] Martin Ester et al. 'A density-based algorithm for discovering clusters in large spatial databases with noise.' In: *Kdd*. Vol. 96. 34. 1996, pp. 226–231 (cited on page 83).

[206] Parliamentary Assembly. 'The potential dangers of electromagnetic fields and their effect on the environment'. In: Resolution 1815 (2011). Council of Europe, May 2011 (cited on page 84).

[207] *Ookla 5G Map - Tracking 5G Network Rollouts Around the World*. [Online; accessed 2. Jul. 2021]. July 2021. URL: https://www.speedtest.net/ookla-5g-map (cited on page 89).

[208] *What is 5G | Everything You Need to Know About 5G | 5G FAQ | Qualcomm*. [Online; accessed 2. Jul. 2021]. May 2021. URL: https://www.qualcomm.com/5g/what-is-5g (cited on page 89).

[209] Jonathan Rodriguez. *Fundamentals of 5G Mobile Networks*. Hoboken, NJ, USA: Wiley, June 2015 (cited on page 89).

[210] *5G technology and networks (speed, use cases, rollout)*. [Online; accessed 2. Jul. 2021]. July 2021. URL: https://www.thalesgroup.com/en/markets/digital-identity-and-security/mobile/inspired/5G (cited on page 89).

[211] Robert Falkenberg et al. 'Machine Learning Based Uplink Transmission Power Prediction for LTE and Upcoming 5G Networks Using Passive Downlink Indicators'. In: *2018 IEEE 88th Vehicular Technology Conference (VTC-Fall)*. IEEE, Aug. 2018, pp. 1–7. DOI: 10.1109/VTCFall.2018.8690629 (cited on page 90).